INVESTIGATIONS INTO OPTICAL-FIBRE RING RESONATORS

by

Rajeshkumar. K. Kadiwar

a thesis submitted to
University of London
for the degree of
Doctor of Philosophy
in Electronic and Electrical Engineering

Department of Electronic and Electrical Engineering
University College London
July 1990

ProQuest LLC.
789 East Eisenhower Parkway
P.O. Box 1346
Ann Arbor, MI 48106 – 1346

ABSTRACT

This thesis is concerned with the theoretical and experimental characterisation of the all fibre ring resonator. Active and passive versions of the ring resonator fibre optic gyroscope are examined as specific applications for the fibre ring resonator.

Firstly, the characteristics of ring resonators formed with polarisation maintaining fibre are investigated. Polarisation mode cross coupling within the fibre resonator is shown to cause the resonant polarisation eigenmodes of the device to become dependent upon the loop birefringence. Resonance splitting effects and a non-linear phase separation between the resonant eigenmodes with loop birefringence is found to follow. The effects of polarisation anisotropy within the resonator are presented in detail. Several methods to reduce this polarisation instability are evaluated theoretically and a novel method demonstrated experimentally.

The limitations of the ring resonator due to the non-linear stimulated Brillouin scattering process are then investigated. The depletion effect due to the onset of stimulated Brillouin lasing in fibre resonators is shown to lead to finesse and modulation depth variations with input power. The dependence of these effects upon resonator and material parameters is characterised. Two novel schemes for suppressing the onset of stimulated Brillouin lasing are presented.

The drift characteristics of passive ring resonator gyroscopes made with polarisation maintaining fibre are theoretically calculated. The feasibility of various polarisation stabilisation schemes are evaluated. One of the first solid-state stimulated Brillouin ring laser gyroscopes is also demonstrated. The design criteria of this gyroscope are presented. The frequency lock-in effect is shown to occur in this gyroscope and a novel scheme that avoids this effect is demonstrated.

ACKNOWLEDGMENTS

I wish to express my thanks and appreciation to:

Dr Bob Youngquist and Professor Gareth Parry for their encouragement, enthusiasm and support.
Dr Ian Giles for supervision and help of various kinds.
Zacharious Ioannidis for his fruitful collaboration and friendship during this work.
Nigel Stokes, Akis Markatos, Micheal Zervas, Mahmoud Farhadiroushan and Ali Twaij for their friendship, 'walks and talks' and many stimulating discussions.
Tony Kerr for the skillful fabrication of high quality polished components and his humor.
Darren Kreit, Sally Carr, Steve Novak, Kim Mallellue and Izumi Sakai for their many discussions and contributions.
Piyush, Nidhi and Shailesh Kadiwar for their love, encouragement and vision.
Victor Chisese, Sunjay Mehta and Abdool Karim Vakil for their continued friendship and support.

. . . and many others for adding to this work and my experience at University College.

To my loving parents
Jasvanti & Kantilal Kadiwar

TABLE OF CONTENTS.

Chapter One

INTRODUCTION

Optical fibres have made considerable inroads into the fields of communications, signal processing and sensing. An important class of optical fibre device that finds applications in all these areas is the all fibre ring resonator. This device is a resonant ring cavity in which an optical signal traverses a closed fibre loop. For coherent optical inputs, the ring resonator forms the most sensitive interferometer configuration. When the roundtrip path-length equals an integer number of optical wavelengths, constructive interference leads to a build-up of the optical intensity inside the fibre cavity, and a concurrent decrease in the intensity at the output port. The properties of this device are thus similar to those of any resonant device, such as acoustic resonators or tuned electrical circuits, where energy storage (a high amplitude circulating wave) occurs at discrete frequencies.

Extensive research has been performed over the past decade into the fabrication and application of optical fibre ring resonators. The steep variation in output intensity with loop phase about the resonance condition makes them very attractive for sensor applications, such as hydrophones and gyroscopes[1,2]. The storage nature of the resonator yields further applications such as delay lines[3], pulse generators[4] and the study of optical non-linearities (due to the high circulating intensities at resonance). The autocorrelation nature of the device can also be used to form demultiplexers and optical spectrum analysers[5,6].

A favoured configuration for the device is shown in Fig 1.1, where a single length of optical fibre is closed onto itself by means of a low loss evanescent field directional coupler. The two coupler halves are fabricated on the same strand of fibre to avoid fibre

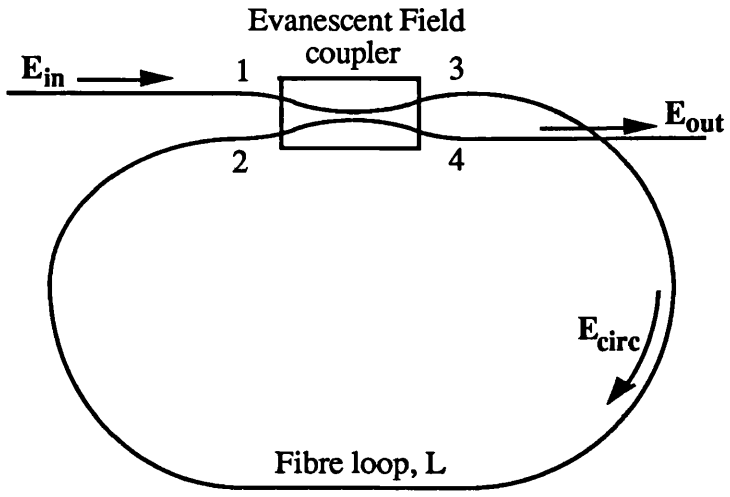

Figure 1.1 Configuration of the all fibre ring resonator. The optical fibre is closed onto itself by means of an evanescent field coupler and the transmission response is determined by the summation of the multiple transits experienced by the input light around the fibre loop, L.

splices within the loop. The response of the device may be understood in terms of the multiple passes experienced by the light around the fibre loop. Light input at port 1 is split between ports 3 and 4. The light at port 3 circulates round to port 2 and is again split between ports 3 and 4, and so on. The transmission response is then due to the interference between all the terms output at port 4. The couplers intensity coupling coefficient, κ, is optimised when it is adjusted to inject just enough light into the fibre loop to compensate for the roundtrip cavity loss. At resonance constructive interference leads to the circulating intensity within the loop building up to a level such that the fraction of the circulating intensity that exits from port 2 to port 4 (given by $1-\kappa$) is exactly matched by the intensity of light coupled directly from port 1 to port 4. Because the loop losses are typically low in all-fibre ring resonators (<2%), κ is close to unity and the circulating intensity at resonance can be considerably enhanced. The differential phase shift at resonance of $\pi/2$ (modulo 2π) between the circulating and directly coupled components, leads to complete destructive interference occurring at port 4. The output is then a series of resonance dips, and the behaviour is similar to that of a Fabry-Perot étalon, except that the all-fibre resonator has sharp output minima (not maxima) reaching zero at resonance. We can define for the fibre resonator, the finesse, F, as being the ratio of the free spectral range (separation of the resonances) to the full width at half maximum of the resonance dips. This finesse value then provides a direct measure of the quality (in terms of optical losses) of the fibre resonator.

Progress in the exploitation of optical fibre ring resonators relies heavily upon research performed to understand the fundamental properties of the device. Theoretical investigations into the dependence upon source coherence[7], polarisation[8-10] and phase noise characteristics[11] of passive single mode fibre resonators have been reported. The effects of Rayleigh scattering and the non-linear optical Kerr and Faraday effect have also been studied[12-14]. This dissertation complements that work and examines theoretically and experimentally the polarisation properties of ring resonators fabricated with polarisation maintaining fibre, and the effects of stimulated Brillouin scattering upon device performance. The results of this investigation are then used to explore a specific sensor application, namely the optical gyroscope, which increasingly forms the basis of modern navigational systems.

Single mode fibre resonators require active polarisation control to match the input polarisation state to one of the resonator polarisation eigenstates. The resonator eigenstate being simply defined as the state of polarisation that would return unchanged upon transmission through the coupler and fibre loop[10]. Ideal polarisation maintaining fibre ring resonators (PMRRs), fabricated with isotropic, zero polarisation crosstalk couplers, offer the potential of reducing system complexity by eliminating the need for polarisation controllers. Chapter 2 examines the polarisation properties of practical PMRRs, in which anisotropy and an effective misalignment of the fibre axis at the polarisation maintaining coupler occurs[15]. The eigenmodes of the resonator are found to become dependent upon the loop birefringence. This leads to strong variations in transmission response with any environmental parameters that affect the loop birefringence, such as temperature or pressure. Such variations are often unacceptable and need to be minimised. Dissimilar loop losses or coupling coefficients for the fast and slow fibre axis are also shown to lead to non-orthogonal resonator eigenmodes. Solutions for suppressing this polarisation instability are proposed, and a novel technique based upon dissimilar mode coupling due to the insertion of a nematic liquid crystal between the coupler half blocks demonstrated[16,21]. The research on this polarisation instability was performed in collaboration with Zachos Ioannidis.

Chapters 3 and 4 examine the effects of optical non-linearities in ring resonators. Continued improvements in the quality of optical fibre components[17] has led to the availability of fibre ring resonators with higher finesse and hence greater potential sensitivity. However, since the enhancement of the circulating intensity over the input intensity, is directly proportional to the finesse, the onset of these optical non-linearities

occurs at even lower input power thresholds, hence necessitating an investigation into their effects upon device performance. The optical non-linearity with the lowest threshold for coherent inputs, is stimulated Brillouin scattering (SBS). Chapter 3 presents an introduction to SBS and lays some of the groundwork necessary for the later chapters. Chapter 4 investigates the depletion effects of the SBS process upon the performance characteristics of the optical fibre ring resonator[18-21]. Theoretical and experimental investigations are presented to demonstrate the variations in resonator finesse and modulation depth with input power. The onset of SBS leads to a trade off between the input wave intensity and the resonator finesse, in order to optimise the device performance. Novel methods for suppressing the onset of SBS to increase the regime of passive operation of the ring resonator are also outlined.

In Chapter 5 some of the characterisation work of the previous chapters is applied to the optical fibre ring resonator gyroscope. The analysis of Chapter 2 is used to calculate the resonance drift due to the polarisation instability in a PMRR gyroscope. The effectiveness of the techniques proposed in Chapter 2 for suppressing the polarisation instability upon the PMRR gyroscope drift are investigated[16]. A potentially important application of SBS lasing in ring resonators is shown with one of the first demonstrations of the all fibre SBS gyroscope[22,23]. This device is the first solid state ring laser gyroscope and should offer considerable advantages over conventional ring laser gyro and passive fibre-optic gyro technologies. The basic design criteria are outlined, and a novel technique is demonstrated to suppress the occurrence of frequency lock-in in such a gyroscope.

Finally Chapter 6 presents the main conclusions of this dissertation and suggests the form of future fibre resonators based upon the work presented. Some interesting future topics of research are also proposed.

Chapter 2

POLARISATION EIGENMODES OF HIGHLY BIREFRINGENT OPTICAL FIBRE RING RESONATORS

Interest has been increasing recently in ring resonators made of polarisation maintaining fibre[24], primarily based upon their potential for reducing system complexity[25]. In an ideal polarisation maintaining fibre ring resonator (PMRR), the coupler is formed with the polarisation axes of the fibre perfectly aligned along the interaction region, and is isotropic as far as the intensity coupling and attenuation constants of the fast and slow axes are concerned. The resonant eigenstates of the ring then simply correspond to the two orthogonal (fast and slow) polarisation axes of the fibre. The incident polarised light is projected onto these two linearly polarised eigenstates, and each eigenstate independently generates its own resonance characteristics. The output is then the simple superposition of these projections onto the two resonant eigenstates, and the phase separation between the resonances formed is a direct function of the fibre birefringence. By launching on only one fibre axis a stable resonance response corresponding only to that eigenstate is formed.

In practical PMRRs the device performance deviates significantly from that of the ideal case. A finite amount of polarisation cross coupling always occurs, predominantly due to the unavoidable slight misalignment of the fibre axes at the coupler, and also to a much lesser extent because of deformations and scattering in the fibre loop. The intensity coupling and attenuation constant may also in general be slightly different for each birefringent axes. The effects of these parameters upon the resonator characteristics needs to be quantified in order to optimise the device performance. Previous related analysis was concerned only generally with the effects of fibre

birefringence in single mode fibre resonators, and no experimental results were reported[8-10]. This chapter presents a detailed theoretical and experimental examination of practical polarisation maintaining fibre ring resonators. A discussion of the fabrication and components of a PMRR is presented first, in order to give an insight into the source and magnitude of coupler anisotropy to be anticipated. The resonator is then modelled using the Jones matrix formalism and an expression that completely describes the PMRR response derived. It is shown that the eigenstates of practical PMRRs are strongly dependent upon loop birefringence, and that this leads to a polarisation instability in the device response. To examine this further the effects of misalignment, anisotropic coupling and anisotropic loss are first considered separately, and possible solutions evaluated. The experimental results obtained from several PMRRs are reported, and a scheme to stabilise the PMRR response demonstrated for the first time. An observed aging effect, and experimental investigations into the source of polarisation coupling in the devices is also presented. Finally the main results of the chapter are summarised.

2.1 Polarisation Maintaining Fibres and Fabrication of Polarisation Maintaining Fibre Ring Resonators

The characteristics of polarisation maintaining optical fibre and polarisation maintaining couplers, used for the fabrication of PMRRs are discussed in this section.

Polarisation maintaining fibres can be of either low birefringent or high birefringent type[26]. The low birefringent type polarisation maintaining fibres (eg highly circular single mode fibres and spun fibres[27]) allow any state of polarisation to be propagated with little polarisation dispersion. This class of polarisation maintaining fibre is however sensitive to environmental perturbations, such as temperature, pressure, bends, etc. Highly birefringent polarisation maintaining fibres on the other hand, ensure that a linear polarisation state is forcibly maintained, despite large environmental perturbations. In this chapter we are primarily concerned with highly birefringent polarisation maintaining fibres and from henceforth these will be referred to as PM fibres.

The PM fibres can be characterised by their modal birefringence B and the mode coupling parameter h. The modal birefringence is a measure of the difference in the effective refractive index between the orthogonal linear fibre polarisation modes. It is

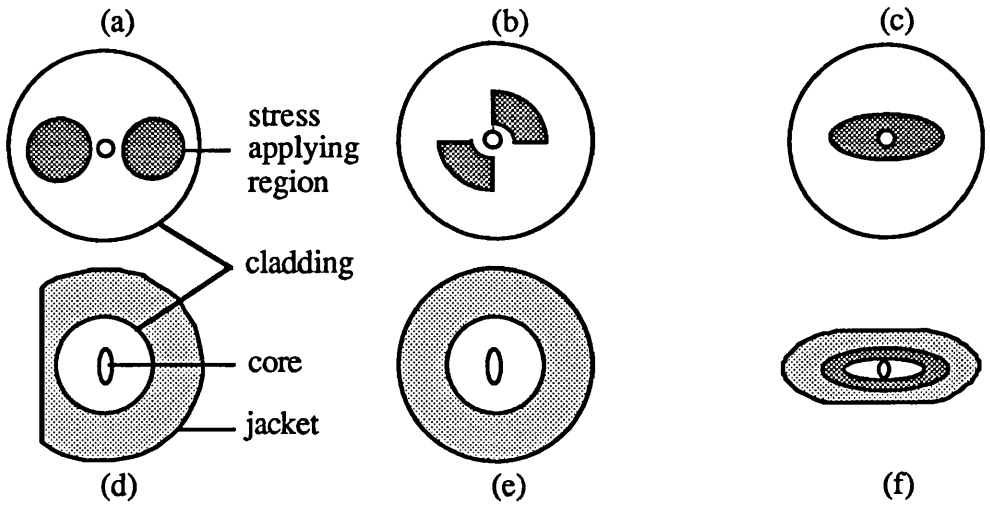

Figure 2.1. Cross-sections of several PM fibres, showing (a) Rod-stressed, (b) Bow-Tie, (c) Elliptical stressed cladding, (d) D-shaped fibre, (e) Elliptical core and (f) Rectangular stressed cladding fibres.

related to the beat length L_p by, $L_p=\lambda/B=2\pi/\Delta\beta$, where λ is the vacuum wavelength of light and $\Delta\beta$ the difference in propagation constant between the orthogonal fibre polarisation modes.

The large birefringence ($B>10^{-5}$) typical in PM fibres can be obtained by a geometrical effect of the core and/or a stress effect around the core. Elliptical core fibres[28] and D-shaped fibres[29] utilise the geometrical effect to provide their birefringence. Whilst the modal birefringence of such fibres can be quite high ($B=8.4\times 10^{-4}$ in ref.[28]), their large refractive index difference and imperfection of core shape means that their optical loss tends generally to be high. Stress induced PM fibres can be realised in the form of Bow-Tie fibres[30], elliptical cladding/jacket fibres[31] and PANDA fibres[32]. These types of PM fibre typically tend to have lower optical losses, due to the insertion of a buffer layer between the core and stress applying regions, and they also exhibit low polarisation cross-talk. The cross sections of several types of PM fibre are shown in Fig. 2.1.

The mode coupling parameter *h*, gives a measure of the cross-talk in PM fibres based upon random mode coupling[33]. It is defined by $h=(P_c/P_t)/L$ where P_c and P_t are the cross-coupled and transmitted powers respectively, in a fibre of length L. The determination of the value of *h* is found to be sensitive to the quality of fibre coatings, external stresses and bends, which need to be controlled to allow comparison between fibres. The ability to maintain a linear polarisation state is fundamentally limited in short

lengths of PM fibre by the fact that in circular waveguides the guided mode is not strictly linear but actually slightly curved (eg, the orthogonal minor field component is -40dB down from the major field component in Bow-Tie fibre[34]). In long lengths of fibre it is limited by Rayleigh scattering, which scatters the light into both polarisation modes (to -30dB in 100Km of Bow-Tie fibre[35]).

The choice of PM fibre for the fabrication of PMRRs is typically determined by the fibre loss, system application and the ease of polarisation axes alignment. The latter is important for the formation of the polarisation maintaining fibre directional coupler used to create the resonant cavity (cf: Fig.1.1). The coupler can be either of polished[36], fused[37], or etched type[38]. Whilst fused PM fibre couplers are quick to make and have good stability, polished PM fibre couplers are preferable in fibre resonators because of their lower loss, variable coupling constant, and to date better polarisation isolation[39]. The lower loss yields a greater resonator finesse, and the variable coupling ratio allows the resonance finesse and modulation depth to be readily optimised. Fabrication of etched couplers is in general difficult to control.

For the polished coupler design, the polarisation axes of the PM fibre are aligned with the surface of a glass/quartz half block and the fibre bonded into a groove of defined curvature cut into the half block surface. The half block is then polished to gain access to the evanescent field, and two such aligned half blocks overlapped to form a tunable PM coupler.

Depending upon the fibre structure, several methods can be used to align the fibre polarisation axes. For example, (1) In rectangular and D-shaped fibre the fibre structure leads to an automatic alignment of the polarisation axes when one end of the fibre is clamped and the fibre bent[40]. (2) The internal structure that provides the birefringence can be imaged to provide alignment, either by direct observation under a microscope or by examination of the diffraction pattern obtained by side illumination of the fibre[41], (3) The difference in polarisation cross coupling as a function of fibre orientation can be used to discern the fibre axis by means of an elasto-optic technique[42]. This last method was the one used within our laboratory due to its good alignment accuracy ($<0.5^{o}$).

In the elasto-optic alignment technique, linearly polarised incoherent light is launched along one of the fibre polarisation modes, by means of an input polariser, and an output analyser is aligned to transmit light in the orthogonal fibre polarisation. When a section of the fibre is laterally squeezed as shown in Fig. 2.2, the applied force results in a birefringence being created in the fibre. The vector addition of the created

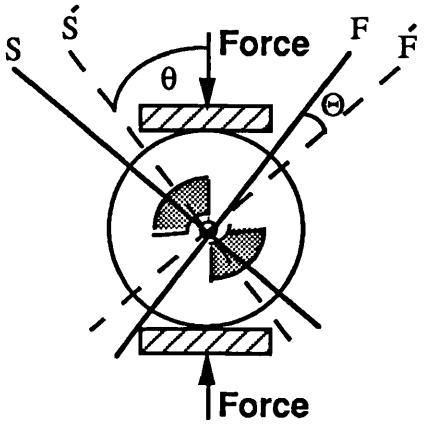

Figure 2.2. The application of a small lateral force, upon a birefringent fibre applied at an angle θ to the slow fibre polarisation axes, causes the principal polarisation axes, Ś and F́, to rotate by angle Θ to become the new principal axes S and F.

birefringence and the original internal birefringence leads to the orientation of the birefringent axes in that section being altered, and coupling between the two original fibre eigenmodes occurs in all cases, except for when the pressure is applied along one of the principal axes. The amount of cross-coupling is determined by the direction and and magnitude of the applied stress as well as the length of fibre over which the stress is applied. The output power measured by a detector after the analyser is given by [42],

$$P_{out} = P_{in}\left(\sin 2\Theta \sin\frac{\Psi}{2}\right)^2 \tag{2.1}$$

where ψ is the (constant) retardation caused by the (constant) applied stress, and Θ is the rotation of the new birefringent axes from the unperturbed orientation, given by,

$$\tan 2\Theta = \frac{B_{ext}\sin 2\theta}{B_{int} - B_{ext}\cos 2\theta} \tag{2.2}$$

θ is the angle with respect to the unperturbed slow axes, at which the force is applied. Eqs 2.1 and 2.2 show that as expected P_{out} is zero whenever $\theta=0$ or $\pi/2$. It is found that the minimum about the fast axes is broader than the minimum about the slow axes. This is because squeezing the fibre parallel to the fast axes increases the net birefringence, whereas along the slow axes the intrinsic and applied birefringences tend to cancel, resulting in a more sensitive dependence on θ. This leads to a better

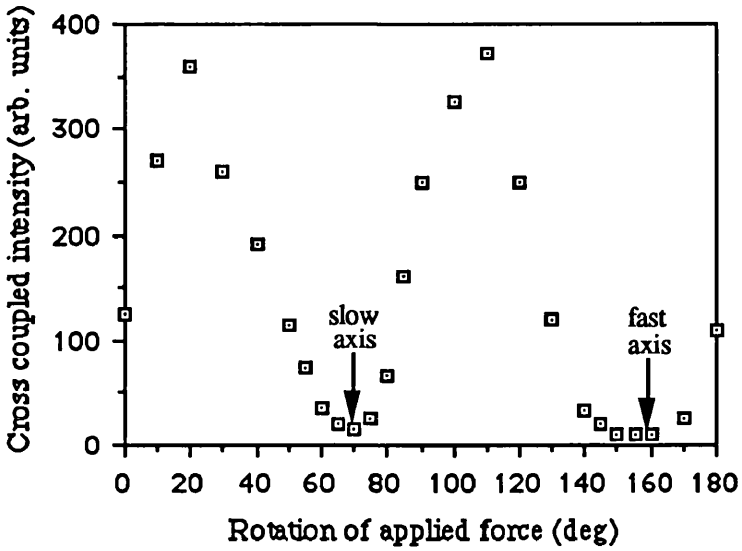

Figure 2.3 Typical experimental results obtained with York Bow-Tie HB600-1 of output signal versus rotation of applied force.

alignment resolution being achieved along the slow axes, and allows the two polarisation axes to be distinguished. This can be seen in the typical plot of output power versus angle of applied force shown in Fig.2.3. The fibre aligned was York Bow-Tie HB600-1 fibre, although similar results were obtained when aligning Andrews elliptical core fibre and Fujikura Panda fibre. It is important to ensure that the axes alignment is carried out on the section of fibre that will form the interaction region, as there may be a rotation of the birefringent axes of several degrees per cm along the length of the PM fibre[43]. This rotation can be seen in Fig. 2.4, where cross sections along a typical polished coupler half are shown.

Once the PM fibre is aligned and bonded into the coupler-half block, it is first lapped and then polished until the throughput of the fibre is attenuated by -30dB with the appropriate refractive index oil placed on the interaction region. Provided the fibre is not polished into the core the transmission of the coupler half-block is, as expected unchanged for oil indices upto the refractive index of the fibre mode. For oil indices in the vicinity of the effective index of the fibre guided mode, the velocities of the bulk optical wave in the oil and guided wave in the fibre are nearly identical and the guided wave is strongly coupled out of the fibre. For higher indices the oil still acts as a mode stripper, but with reduced efficiency. The oil drop test on a York Bow-Tie 633nm half-block, for both the fast and slow axis is shown in Fig. 2.5, and as can be seen the

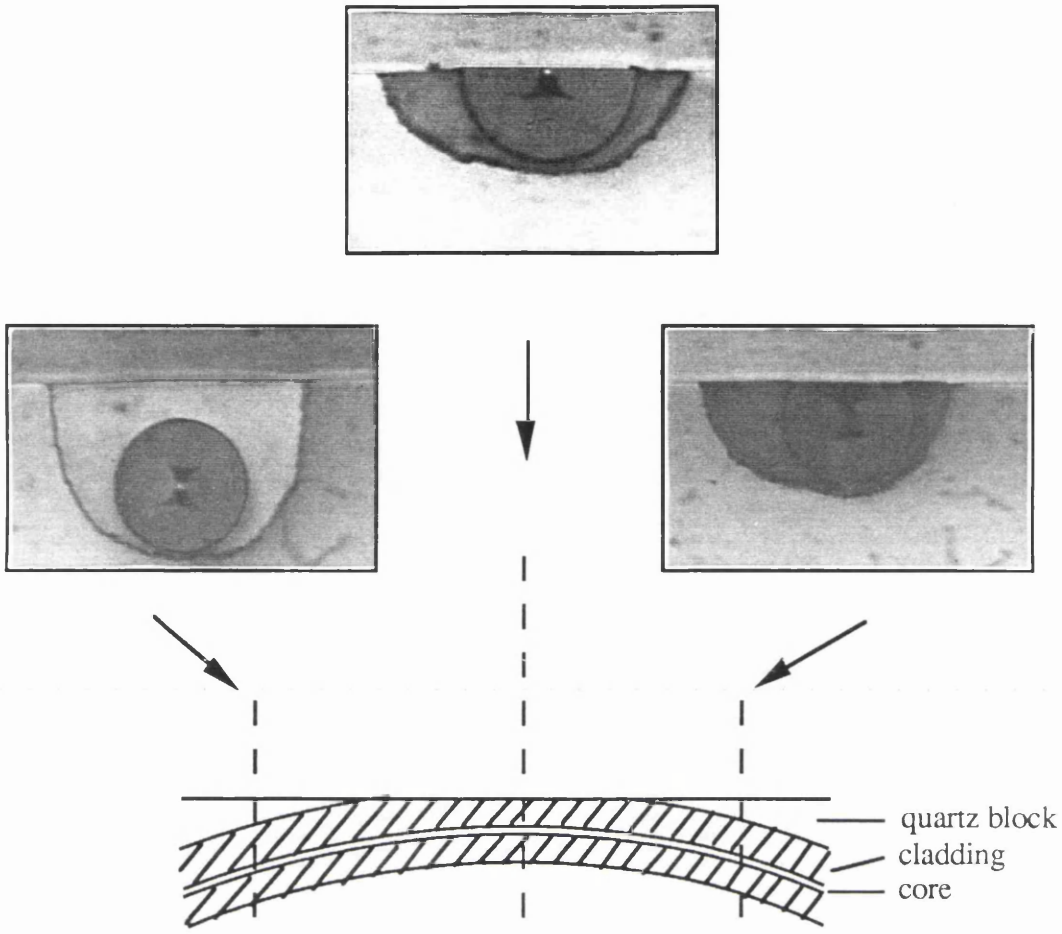

Figure 2.4. Cross section of York Bow-Tie half coupler block. Note the slight rotation of Bow along the length of the block, and the slightly raised height of the fibre in the interaction region.

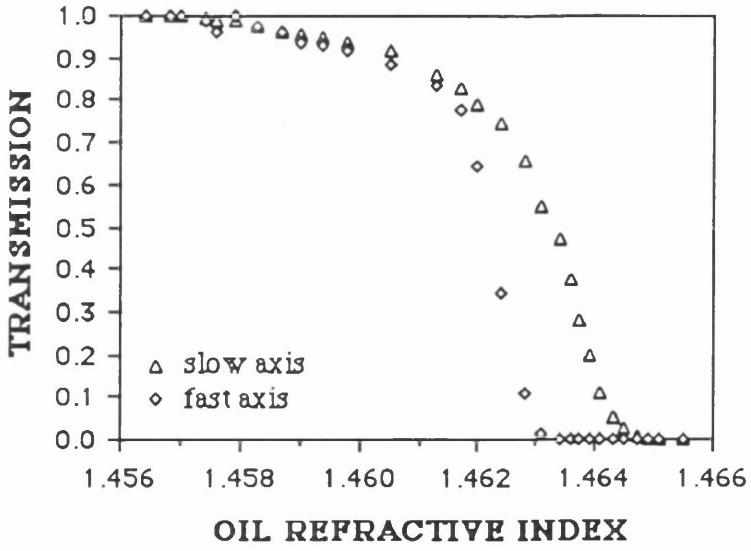

Figure 2.5 Typical plot of transmission for a York Bow-Tie HB600-1 polished half coupler block versus refractive index of oil overlay for fast and slow axis.

efficiency of light coupled out of the fibre can be quite different for certain oil refractive indices. This demonstrates a potential source of coupling constant anisotropy in the PM coupler.

Two such polished half-blocks can be put together to form a directional PM fibre coupler suitable for high finesse PMRR operation. The PM coupler is in itself an important component for coherent communication and sensor systems and has received increasing attention[44-45]. The theories of fused and polished PM fibre couplers are different. The fused coupler relies upon the form birefringence due to the non-circular air-cladding interface, and the polished coupler upon the fibre anisotropy. Polished PM fibre couplers can be characterised by four parameters. (1) The physical alignment accuracy between the principal axis of the individual coupler fibres. (2) A conceptual coupling length, $L_c=\pi/C$, where C is the maximum coupling coefficient calculated in the absence of fibre birefringence. It can be described by the beating of the odd and even coupler modes and gives the distance required to couple all the light from one fibre to the other and back again. (3) The isolated fibre beat length L_p, defined previously, and (4) the effective interaction length, L_i. This is not necessarily the same as the coupling length and is controlled by the radius of curvature of the fibre groove.

The evanescent coupling length L_c is different for light launched on either the fast or slow axis of the input fibre, and for PM couplers designed for use in fabricating a PMRR it is important to ensure that the interaction length is not long enough to allow the dispersion in these coupling lengths to lead to polarisation splitting[46-48], although this effect is small for PM polished couplers with fibres polished along the same axis. The misalignment angle has the effect of altering the effective coupler anisotropy and hence changing the coupling lengths for each polarisation. A parameter Q, equal to the ratio of L_c to L_p is also defined[45]. When Q=0 the modes are those of the well known isotropic coupler, and when Q>>1 (eg. due to weak coupling compared to fibre birefringence) the modes closely resemble those of the isolated birefringent fibres. For intermediate values of Q, both the evanescent coupling and fibre birefringence are significant and the modes lie in between those described above. Clearly large Q values are desirable for polarisation maintaining coupler applications, and it has been suggested that since increasing the fibre birefringence increases the modal mismatch, the constraints on fibre alignment in such couplers can be relaxed[40,45]. In analysing the polarisation maintaining ability of polished PM couplers Shafir *et. al.*[49] theoretically

predicted the possibility of more than one polarisation isolation ratio, for a given coupling constant. This is due to the fact that in slightly overpolished couplers the same coupling constant can be achieved for different lateral offsets (corresponding to over or undercoupling) between the two coupler fibres, whilst the amount of light coupled to the "unwanted" fibre axis decreases monotonically with fibre offset.

The final PM fibre coupler polarisation isolation ratio results from a complex combination of the above parameters, and for the purposes of analysis it is convenient to combine these contributions into an effective misalignment angle α. The York Bow-Tie PM fibre couplers fabricated in our laboratory, typically had Q values close to unity, physical alignment accuracies between the polarisation axes of repeatedly better than 1^{o}, and measured polarisation isolation ratios, defined by CIR=20log(tanα), better than -25dB (α=3.22°). The effects of the coupling constant and loss anisotropy, discussed in this section, upon the operation of PMRRs is now analysed in detail in the next section.

2.2 Theoretical Investigation of Polarisation Maintaining Fibre Ring Resonators.

In the following sections we model the PMRR of Fig.2.6, in which there exists a physical misalignment angle, ϕ, between the fibre birefringence axis at the coupler, and

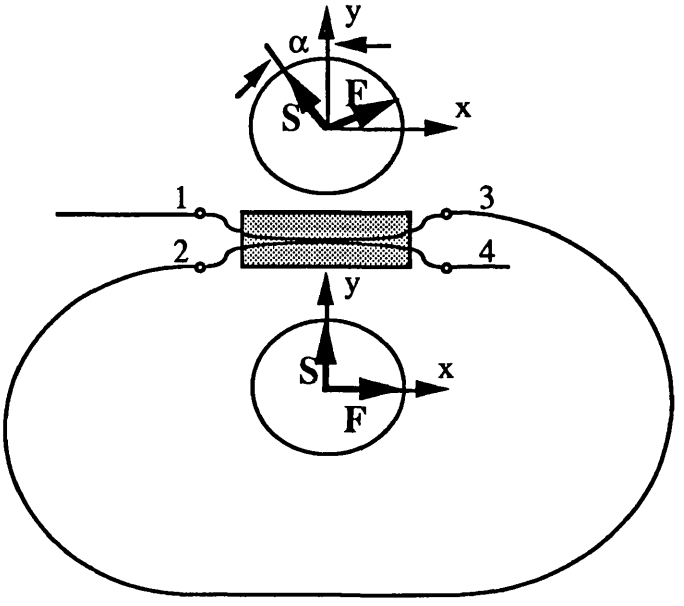

Figure 2.6. Highly birefringent fibre ring resonator. S and F denote slow and fast axis respectively, the cross talk between the slow and fast axis is described by an equivalent misalignment angle α.

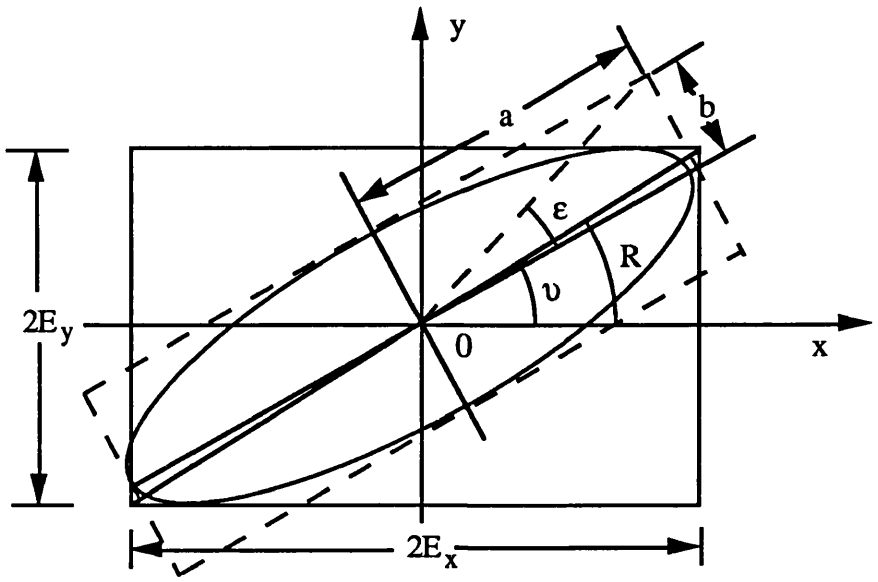

Figure 2.7 Parameters of an elliptical polarisation state, having components of amplitude E_x and E_y along the x and y axes respectively. The major and minor axes of the ellipse are 2a and 2b respectively.

an anisotropic loss and coupling constant within the coupler. The resonator components are described by Jones vectors[50], and these are used to derive a matrix equation to describe the PMRR response. The corresponding loop eigenvalues and eigenvectors[8,10] of the system are then calculated to help analyse the response.

The general polarisation state of a monochromatic beam is the elliptical state, which is represented in Fig.2.7, and may be described by means of its azimuth angle υ, its ellipticity, ξ, and by the angle R defined below. Referring to Fig.2.7, a general elliptical polarisation state is given by the Jones matrix $[\ |E_x|\exp(j\varphi_x),\ |E_y|\exp(j\varphi_y)\ ]^T$ where T denotes a transpose and we have[51],

$$\tan R = \frac{E_y}{E_x} \tag{2.3}$$

$$\tan 2\upsilon = \tan 2R \cos(\varphi_y - \varphi_x) \tag{2.4}$$

$$\xi = \tan\varepsilon = \frac{b}{a} \tag{2.5}$$

where,

$$\pm \sin 2\varepsilon = \sin 2R \sin(\varphi_y - \varphi_x) \tag{2.6}$$

The ellipse is termed right handed or left handed according to the direction of rotation of

the electric field vector. By convention it is defined as right handed if the vector is seen to revolve clockwise when looking into the beam, ie when $\varphi_y-\varphi_x<0$, and as left handed otherwise. In Eq.2.6 the upper and lower sign hold for whether the ellipse is left or right handed respectively. Two elliptical polarisations (of which circular and linear polarisation are ofcourse simply special cases with $\xi=1$ and 0 respectively) are said to be orthogonal when the azimuths of their major axes differ by $\pi/2$, their handedness are opposite and their ellipticities identical.

2.2.1 Analytical Model of the Polarisation Maintaining Fibre Ring Resonator.

The electric field at port j of the coupler (j=1,2,3,4) can be expressed by its Jones vector $\mathbf{E}_j = [\, E_s, E_f \,]^T$, where E_s and E_f are the complex amplitudes of the electric field along the slow and fast axis respectively. For simplicity we shall assume that the most significant cross-talk between the fibre polarisation modes occurs only in the coupler. As discussed above there generally exists a differential coupling constant and a differential loss in a PM coupler, and hence these shall be taken into account in the following analysis.

The coupler intensity coupling $\mathbf{C}_c$ and transmission $\mathbf{C}_t$ matrices are given in general form by,

$$\mathbf{C}_{c,t}=\begin{bmatrix} C_{11} & C_{12} \\ C_{21} & C_{22} \end{bmatrix} \tag{2.7}$$

where the symbols in bold type represent matrices and $C_{j,k}$ are the relevant coupling or transmission coefficients between the coupler ports. The matrices $\mathbf{C}_{c,t}$ take into account the possible differential coupler intensity loss γ_f and γ_s and differential intensity coupling constants K_f and K_s for the fast and slow axes respectively. For the slow fibre axes j,k=1 and for the fast fibre axes j,k=2. The off-diagonal coefficients ($j\neq k$) represent the effect of polarisation cross coupling.

To incorporate the presence of an effective misalignment at the PM coupler all the Jones vectors are analysed in the co-ordinate system of the coupler. This may be achieved, with reference to Fig.2.6, by setting the off-diagonal elements of C to zero

and using another matrix, **A**, to describe the necessary coordinate rotation on coupling from port 1 to port 4,

$$\mathbf{A} = \begin{bmatrix} \cos\alpha & \sin\alpha \\ -\sin\alpha & \cos\alpha \end{bmatrix} \tag{2.8}$$

The matrix $\mathbf{A}^{-1}$ is used to describe the necessary reverse transform, ie to describe coupling from port 2 to port 3. The only difference is that the off-diagonal terms of the matrix reverse signs. It should be emphasised again, that α is not necessarily equal to the physical misalignment angle between the fibre birefringence axis, ϕ. The matrix combination $\mathbf{AC_c}$ now describes the coupling of light across the coupler from port 1 to port 4.

The Jones matrix for the fibre loop can be expressed by the 2x2 diagonal matrix, **F**,

$$\mathbf{F} = \exp[(-\alpha_0 + i\beta)L] \begin{bmatrix} e^{i\Delta\beta L/2} & 0 \\ 0 & e^{-i\Delta\beta L/2} \end{bmatrix} \tag{2.9}$$

α_o is the linear fibre amplitude attenuation coefficient (assumed initially to be constant for both fibre principal axis), L is the loop length, $\beta=(\beta_s+\beta_f)/2$, and $\Delta\beta=\beta_s-\beta_f$, where β_s and β_f are the propagation constants of the slow and fast axis.

By considering the loop by loop buildup of the PMRR response we can see that the electric fields at ports 3 and 2 are given by,

$$\mathbf{E_3} = \mathbf{SC_t E_1} \tag{2.10}$$

$$\mathbf{E_2} = \mathbf{FE_3} = \mathbf{FSC_t E_1} \tag{2.11}$$

where,

$$\mathbf{S} = \sum_{n=0}^{\infty} (\bar{\mathbf{S}})^n = \sum_{n=0}^{\infty} (\mathbf{A}^{-1}\mathbf{C_c F})^n \tag{2.12}$$

$\bar{\mathbf{S}}$ is the matrix representing a single transit around the fibre loop and coupler. Hence,

the matrix S represents the effect of multiple transits around the resonant loop. Now, the intensity of light attenuated by the coupler, is ofcourse equal to $\gamma_s|E_{1x}|^2+\gamma_f|E_{1y}|^2$. We can rewrite this as being equal to $\gamma_s|E_1|^2+\Delta\gamma\,|E_{1y}|^2$, where $\Delta\gamma=(\gamma_f - \gamma_s)$. Then, in order to derive an expression for the PMRR response we apply conservation of energy to the PM coupler to obtain the following relation,

$$(1-\gamma_s)\,|E_1|^2 - \Delta\gamma\,|E_{1y}|^2 + (1-\gamma_s)\,|E_2|^2 - \Delta\gamma\,|E_{2y}|^2 = |E_3|^2 + |E_4|^2 \qquad (2.13)$$

Substituting Eqs 2.10 and 2.11 into Eq. 2.13, and noting from Eq. 2.11 that,

$$\Delta\gamma|E_{2y}|^2 \equiv \mathbf{E}_1^t\mathbf{C}_t^t\mathbf{S}^t\mathbf{F}^t\begin{bmatrix}0 & 0\\ 0 & \Delta\gamma\end{bmatrix}\mathbf{F}\mathbf{S}\mathbf{C}_t\mathbf{E}_1 \qquad (2.14)$$

we obtain after some simple manipulation,

$$|\mathbf{E}_4|^2=\mathbf{E}_1^t\left\{\left(1-\gamma_s-\Delta\gamma\left|\frac{E_{1y}}{E_1}\right|^2\right)\mathbf{I}- \mathbf{C}_t^t\mathbf{S}^t\left[\mathbf{I}-(1-\gamma_s)\mathbf{F}^t\mathbf{F}+\mathbf{F}^t\begin{bmatrix}0 & 0\\ 0 & \Delta\gamma\end{bmatrix}\mathbf{F}\right]\mathbf{S}\mathbf{C}_t\right\}\mathbf{E}_1 \qquad (2.15)$$

where **I** is the identity matrix and the superscript t denotes complex conjugate transpose. In an ideal fibre, with no differential loss or polarisation cross-talk, $\mathbf{F}^t\mathbf{F}=\exp(-2\alpha_o L)\mathbf{I}$, and Eq.2.15 becomes,

$$|\mathbf{E}_4|^2=\mathbf{E}_1^t\left\{(1-\gamma_{eq})\mathbf{I}-(1-d)\mathbf{C}_t^t\mathbf{S}^t\mathbf{S}\mathbf{C}_t- d\mathbf{C}_t^t\mathbf{S}^t\begin{bmatrix}0 & 0\\ 0 & \frac{\Delta\gamma}{1-\gamma_s}\end{bmatrix}\mathbf{S}\mathbf{C}_t\right\}\mathbf{E}_1 \qquad (2.16)$$

where $\gamma_{eq}=\gamma_s+\Delta\gamma\,|E_{1y}/E_1|^2$ and $d=(1-\gamma_S)\exp(-2\alpha_o L)$. γ_{eq} is the equivalent coupler attenuation and d is the roundtrip intensity attenuation for light propagating in the slow axis.

2.2.2 Eigenvalues and Eigenvectors

Whilst Eq.2.16 describes the intensity transmission response of the PMRR, it is more instructive to re-write this in terms of the system eigenvalues and eigenvectors. The matrix $\bar{S}$ defined by Eq. 2.12 describes a single transit around the resonator ring, and can thus be used to determine the eigenvalues and polarisation eigenvectors of the ring. These completely characterise the resonator. The eigenvalue of the system defines the resonance characteristics of a particular resonator eigenmode. The corresponding eigenvector defines the polarisation state required to be input at port 1 in order to fully excite that resonance. Now, taking into account the possible coupler anisotropy, the coupling matrix C_C is given by,

$$C_c = j\begin{bmatrix} \sqrt{K_s(1-\gamma_s)} & 0 \\ 0 & \sqrt{K_f(1-\gamma_f)} \end{bmatrix} \tag{2.17}$$

Thus,

$$\bar{S} = A^{-1}C_cF = \lambda_0\begin{bmatrix} \cos\alpha\, e^{j\frac{\Delta\beta L}{2}} & -\sqrt{h}\sin\alpha\, e^{-j\frac{\Delta\beta L}{2}} \\ \sin\alpha\, e^{j\frac{\Delta\beta L}{2}} & \sqrt{h}\cos\alpha\, e^{-j\frac{\Delta\beta L}{2}} \end{bmatrix} = \lambda_0\begin{bmatrix} a_{11} & a_{12} \\ a_{21} & a_{22} \end{bmatrix} \tag{2.18}$$

where,

$$\lambda_0 = \sqrt{K_s(1-\gamma_s)}\exp(-\alpha_o L)\exp j(\beta L + \pi/2) \tag{2.19}$$

$$h = \frac{K_f(1-\gamma_f)}{K_s(1-\gamma_s)} \tag{2.20}$$

h is a measure of the anisotropy of the coupler. The eigenvalues λ_j (j=1,2) of Eq.2.18 can be found by using the relation,

$$\det(A - \lambda I) = 0 \tag{2.21}$$

which leads to the ratio of the eigenvalues λ_1, λ_2, to λ_j being given by the solutions of

the quadratic equation,

$$\lambda^2 - \lambda(a_{11}+a_{22}) + (a_{11}a_{22} - a_{12}a_{21}) = 0 \tag{2.22}$$

The corresponding eigenvectors $\mathbf{V}_j$ (j=1,2) of $\tilde{\mathbf{S}}$ can be determined by noting that,

$$(\tilde{\mathbf{S}} - \lambda_j \mathbf{I})\mathbf{V}_j = 0 \tag{2.23}$$

Thus the non-normalised eigenvectors of Eq. 2.18 are given by,

$$\mathbf{V}_j = \left[1 , \frac{\lambda_j - a_{11}}{a_{12}} \right]^T \tag{2.24}$$

Any polarisation state input at port 1 of the resonator can be resolved into the two resonator ring eigenvectors, thus we can write $\mathbf{C_t E_1} = e_1\mathbf{V}_1 + e_2\mathbf{V}_2$. Substituting this into Eq. 2.16 for a normalised input, ($\mathbf{E_1}^t\mathbf{E_1} = 1$) and noting that since $\mathbf{S}$ is a summation, $\mathbf{SV}_j = 1/(1-\lambda_j)$, gives,

$$\begin{aligned} |\mathbf{E_4}|^2 = (1-\gamma_{eq}) - (1-d)\left\{ \frac{|e_1|^2}{|1-\lambda_1|^2} + \frac{|e_2|^2}{|1-\lambda_2|^2} + \frac{e_1^* e_2 \mathbf{V}_1^t \mathbf{V}_2}{(1-\lambda_1)^*(1-\lambda_2)} + \frac{e_1 e_2^* \mathbf{V}_2^t \mathbf{V}_1}{(1-\lambda_1)(1-\lambda_2)^*} \right\} \\ - d\left(\frac{e_1^* \mathbf{V}_1^t}{1-\lambda_1^*} + \frac{e_2^* \mathbf{V}_2^t}{1-\lambda_2^*} \right) \begin{bmatrix} 0 & 0 \\ 0 & \frac{\Delta\gamma}{1-\gamma_s} \end{bmatrix} \left(\frac{e_1 \mathbf{V}_1}{1-\lambda_1} + \frac{e_2 \mathbf{V}_2}{1-\lambda_2} \right) \end{aligned} \tag{2.25}$$

where $*$ represents complex conjugate. Eq. 2.25 yields after some simple manipulation,

$$|\mathbf{E_4}|^2 = (1-\gamma_{eq}) - \left[(1-d_1)\frac{|e_1|^2}{|1-\lambda_1|^2} + (1-d_2)\frac{|e_2|^2}{|1-\lambda_2|^2} \right] - 2\,\mathcal{R}e\left\{ \frac{(1-d_3)e_1^* e_2 \mathbf{V}_1^t \mathbf{V}_2}{(1-\lambda_1^*)(1-\lambda_2)} \right\} \tag{2.26}$$

where,

$$d_1 = \left(1 - \frac{\Delta\gamma\,|V_{1y}|^2}{(1-\gamma_s)} \right) d \tag{2.27}$$

$$d_2 = \left(1 - \frac{\Delta\gamma|V_{2y}|^2}{(1-\gamma_s)} \right) d \tag{2.28}$$

$$d_3 = \left(1 - \frac{\Delta\gamma V_{1y}^* V_{2y}}{(1-\gamma_s)\mathbf{V}_1^t\mathbf{V}_2} \right) d \tag{2.29}$$

$\mathcal{R}e\{z\}$, means the real part of the complex number z. Eq. 2.26 is completely general and defines the response of a PMRR with polarisation cross-talk and differential coupling constant and/or loss at the PM coupler. The first term on the RHS of Eq.2.26 is a constant that represents the constant throughput of the resonator, away from resonance. The second and third terms independently define the two resonator resonances (as shown below). The last term corresponds to the interaction between the two resonator eigenmodes in determining the overall response of the device. This last term only comes into significance when the eigenmodes of the ring resonator become non-orthogonal, since otherwise $\mathbf{V}_1^t\mathbf{V}_2=0$. It is also equal to zero if only one eigenstate is excited ($e_1^* e_2=0$).

Before directly investigating some special conditions with Eq.2.26, it is worth examining the relationship between the eigenvalues of $\bar{\mathbf{S}}$ and the resonator response. We shall assume for the time being that the two resonator responses are independent, ie that the two eigenvectors are orthogonal. We may express λ_j/λ_o as $\sqrt{Q_j}e^{j\theta_j}$ and hence $\lambda_j = \sqrt{Q_j dK_s}\,e^{j(\beta L + \pi/2 + \theta_j)}$. Thus we may write,

$$\frac{1}{|1-\lambda_j|^2} = \frac{1}{|1-\sqrt{Q_j dK_s}\,e^{j(\beta L + \pi/2 + \theta_j)}|^2}$$

$$= \frac{1/(1-\sqrt{Q_j dK_s})^2}{1 + \dfrac{4\sqrt{Q_j dK_s}}{(1-\sqrt{Q_j dK_s})^2}\sin^2\left(\dfrac{\beta L + \pi/2 + \theta_j}{2}\right)} \tag{2.30}$$

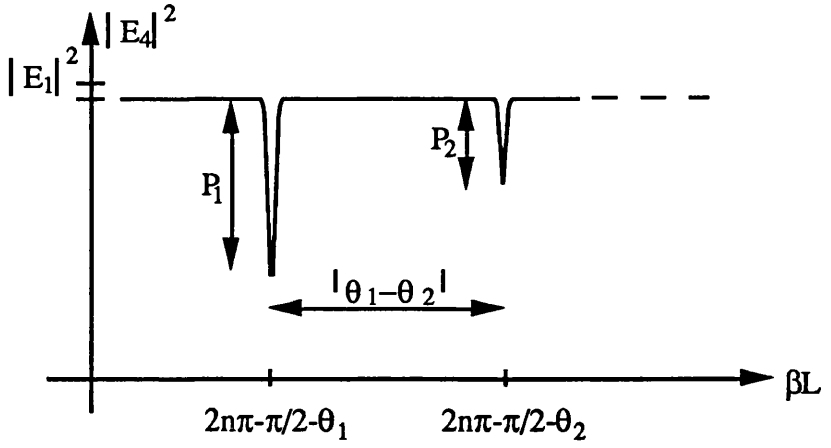

Figure 2.8 Outline of resonance curves of PMRR eigenstates, showing level of excitation of eigenstates for arbitrary input polarisation and separation between their resonance points.

Substituting Eq.2.30 into Eq. 2.26 yields (for orthogonal eigenvectors),

$$|E_4|^2 = (1-\gamma_{eq}) - P_1\frac{1}{1+A_1\sin^2\left(\frac{\beta L+\pi/2+\theta_1}{2}\right)} - P_2\frac{1}{1+A_2\sin^2\left(\frac{\beta L+\pi/2+\theta_2}{2}\right)} \qquad (2.31)$$

where,

$$P_j = \frac{(1-d_j)\,e_j^2}{(1-\sqrt{Q_jK_sd_j})^2} \quad \text{and} \quad A_j = \frac{4\sqrt{Q_jK_sd_j}}{(1-\sqrt{Q_jK_sd_j})^2} \qquad (2.32)$$

Eq. 2.31 corresponds to two resonances in the transmission response of the resonator, each corresponding to a particular eigenvalue/eigenvector pair. The depths of the resonances are equal to P_j, and the separation between the two resonances is given by the differences in the arguments of the two eigenvalues, ie by $\theta_1-\theta_2$. This is summarised in Fig. 2.8.

The finesse, F, of each resonance can be determined in the following manner. If we plot individually any of the latter terms in Eq.2.31, we find that they give rise to resonance peaks of height P_j. Now, the linewidth Δf of the resonator (FWHM) can be found by equating each of these resonance terms of Eq. 2.31 with half the peak height, $^1/_2P_j$. If we let $\omega_{1/2}$ be the angular frequency at which the response reaches half its peak value, and writing $\beta L=n\omega_{1/2}L/c$, we have,

$$\frac{1}{2}P_j = \frac{P_j}{1+A_j\sin^2\left(\frac{n\omega_{1/2}L/c+\pi/2+\theta_j}{2}\right)} \tag{2.33}$$

and hence,

$$\sin\left(\frac{n\omega_{1/2}L}{2c}+\frac{\pi}{4}+\frac{\theta_j}{2}\right) = \pm\frac{1}{\sqrt{A_j}} \tag{2.34}$$

The angular frequency at the q^{th} resonance mode is given by, $\omega_q=(c/nL)(q2\pi-\pi/2-\theta_j)$, and the solution of Eq. 2.34 corresponding to this q^{th} resonance is denoted by $\omega_{q1/2}$

$$\omega_{q1/2} = \frac{c}{nL}\left[q2\pi - \frac{\pi}{2} - \theta_j - 2\sin^{-1}\left(\frac{1}{\sqrt{A_j}}\right)\right] \tag{2.35}$$

Therefore, the linewidth is given by,

$$\Delta f_j \equiv 2\left|\frac{\omega_q - \omega_{q1/2}}{2\pi}\right| = \frac{c}{nL}\frac{2}{\pi}\sin^{-1}\left(\frac{1}{\sqrt{A_j}}\right) \tag{2.36}$$

The free spectral range (FSR) of the resonator is defined as the frequency spacing between two adjacent resonances of the same eigenmode, thus FSR=c/nL. The resonator finesse F, is therefore,

$$F_j = \frac{FSR}{\Delta f_j} = \frac{\pi}{2\sin^{-1}\left(\frac{1}{\sqrt{A_j}}\right)} = \frac{\pi}{2\sin^{-1}\left(\frac{(1-\sqrt{Q_jK_sd_j})}{2\sqrt[4]{Q_jK_sd_j}}\right)} \tag{2.37}$$

By comparing Eq.2.37 with equivalent formulas derived for ordinary single mode fibre resonators[52], we find that the term $\sqrt{Q_jK_sd_j}$ is equal to the effective resonant coupling constant, κ of the resonator for that eigenmode. We also note that Eq.2.37 demonstrates the possibility of the two resonance eigenmodes having different finesses.

We are now in a position to further investigate Eq.2.26 and some of its consequences. It is instructive to consider the effects of the effective misalignment, anisotropic coupling and anisotropic loss separately.

2.2.3 PMRR with Misalignment and Zero Differential Loss / Coupling.

In this case the PM coupler anisotropy parameter, h=1, and either K_S or K_f may be used in Eq.2.20. Eqs. 2.27-2.29 reduce to $d_1=d_2=d_3=d=(1-\gamma s)\exp(-2\alpha_o L)$. The eigenvalues for the resonator are then found to be,

$$\lambda_1/\lambda_0 = \cos\varphi + j\sin\varphi \tag{2.38}$$

$$\lambda_2/\lambda_0 = \cos\varphi - j\sin\varphi \tag{2.39}$$

where $\varphi=\cos^{-1}[\cos\alpha.\cos(\Delta\beta L/2)]$. The corresponding non-normalised eigenvectors are

$$V_1 = \left[1, \frac{\cos\alpha\, e^{j\Delta\beta L/2} - e^{j\varphi}}{\sin\alpha\, e^{j\Delta\beta L/2}}\right]^T \tag{2.40}$$

$$V_2 = \left[1, \frac{\cos\alpha\, e^{j\Delta\beta L/2} - e^{-j\varphi}}{\sin\alpha\, e^{j\Delta\beta L/2}}\right]^T \tag{2.41}$$

The eigenvectors are found to be orthogonal, so $V_2^t V_1=0$, and the last term in Eq.2.26 disappears. Thus the above analysis on the PMRR response and finesse is applicable here.

Examining the eigenvalues and eigenvectors shows that they are dependent upon the PM fibre birefringence $\Delta\beta$. This dependence on $\Delta\beta$ has severe effects upon the transmission response of the resonator. We can easily show that when $\Delta\beta L/2=(2m+1/2)\pi$ that λ_1/λ_o and λ_2/λ_0, the eigenvalues of ring become +j and -j, with the corresponding eigenvectors being,

$$\mathbf{V}_1 = \left[1, \frac{\cos\alpha+1}{\sin\alpha}\right]^T \quad \text{and,} \quad \mathbf{V}_2 = \left[1, \frac{\cos\alpha-1}{\sin\alpha}\right]^T \tag{2.42}$$

This means that for small α, the resonant eigenvectors are a pair of orthogonal nearly linearly polarised input, almost identical to the fibre linear polarisation modes. The resonance dips of the response are separated as outlined above by $|\arg(\lambda_1)-\arg(\lambda_2)|$, which for this case is equal to π. However, as $\Delta\beta L$ varies and approaches $2m\pi$ (m=0,1,2...), the eigenstates rapidly become elliptically polarised, and finally at $\Delta\beta L=2m\pi$ the eigenvalues become $\lambda_1/\lambda_0=\cos\alpha+j\sin\alpha$ and $\lambda_2/\lambda_0=\cos\alpha-j\sin\alpha$, with eigenvectors,

$$\mathbf{V}_1 = \begin{bmatrix} 1 \\ -j \end{bmatrix} \quad \text{and,} \quad \mathbf{V}_2 = \begin{bmatrix} 1 \\ j \end{bmatrix} \tag{2.43}$$

corresponding to left and right handed circular polarisation states. It is important to notice that even for exceptionally low cross-talk levels ($\alpha\approx 0$), the polarisation eigenstates still become circular as $\Delta\beta L$ approaches $2m\pi$. However, the resonance points are then separated by an angle 2α rad, which is often very small, and except in the case of very high finesses ($F>2\pi/\alpha$) the two resonator modes almost completely overlap. This minimum phase separation has also been reported independently by Takahashi *et. al.*[53]. However, they have mistakenly attributed this phase separation solely to the physical misalignment angle and not the effective misalignment angle.

When the PM coupler is perfectly aligned, $\alpha=0$ and the eigenvectors are linear polarisation states corresponding to the fibre polarisation axes. Under normal operation of a ring resonator, the input polarisation is adjusted so as to properly match only one of the polarisation eigenvectors of the system. However, when this is done with a PMRR with misalignment as described above, one finds that the variation in resonator eigenvalues and eigenvectors with loop birefringence leads to the (originally matched) input polarisation state being projected onto both of the new eigenvectors leading to a strong variation in the transmission characteristics of the resonator.

Fig. 2.9 shows the variation in (a) the ellipticity, (b) azimuth angle and (c) phase separation of the resonator eigenvectors with loop birefringence for a resonator with an

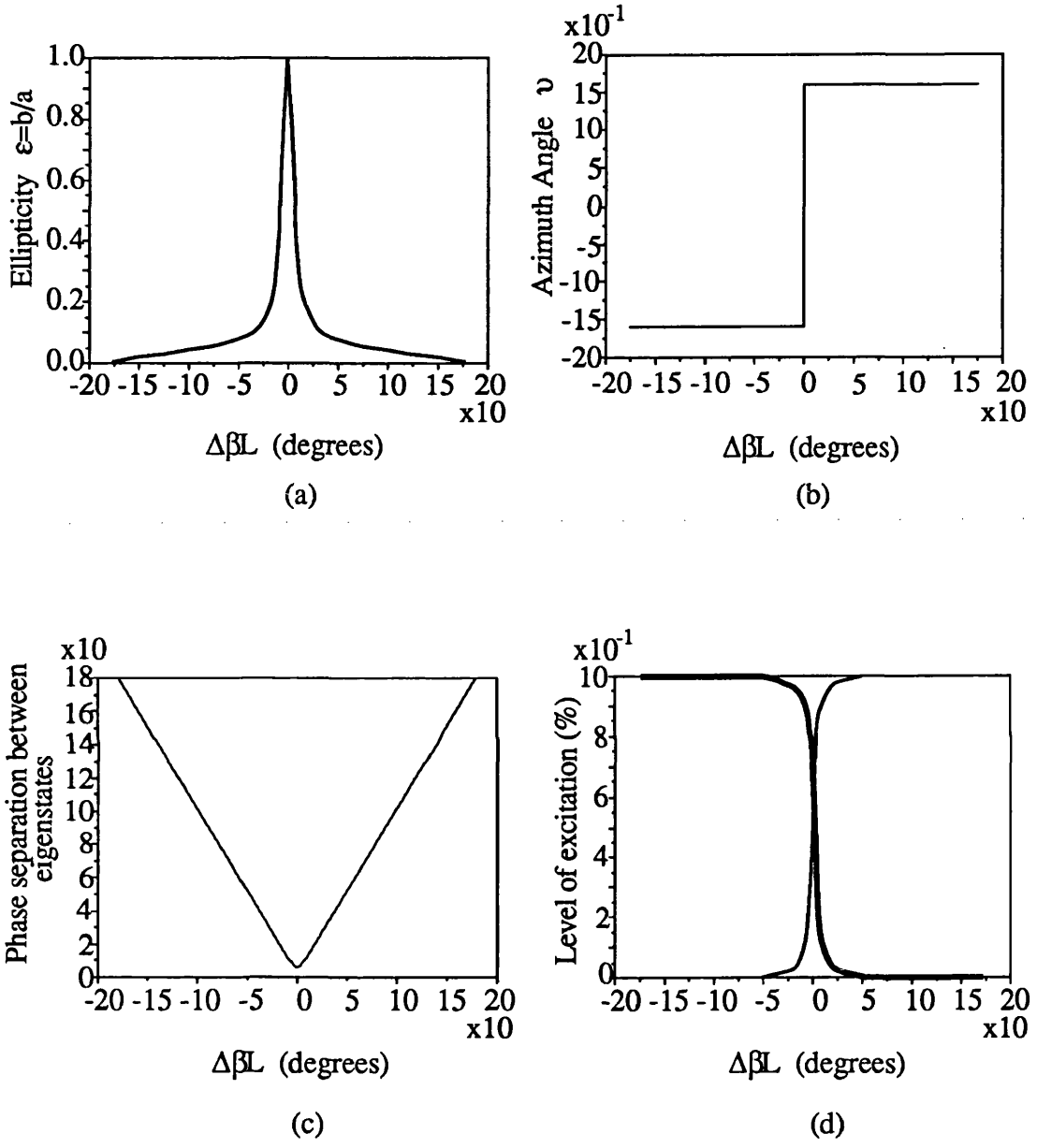

Figure 2.9 Variation in (a) Ellipticity, (b) azimuth angle, (c) phase separation and (d) level of excitation of resonator eigenstates with loop birefringence.

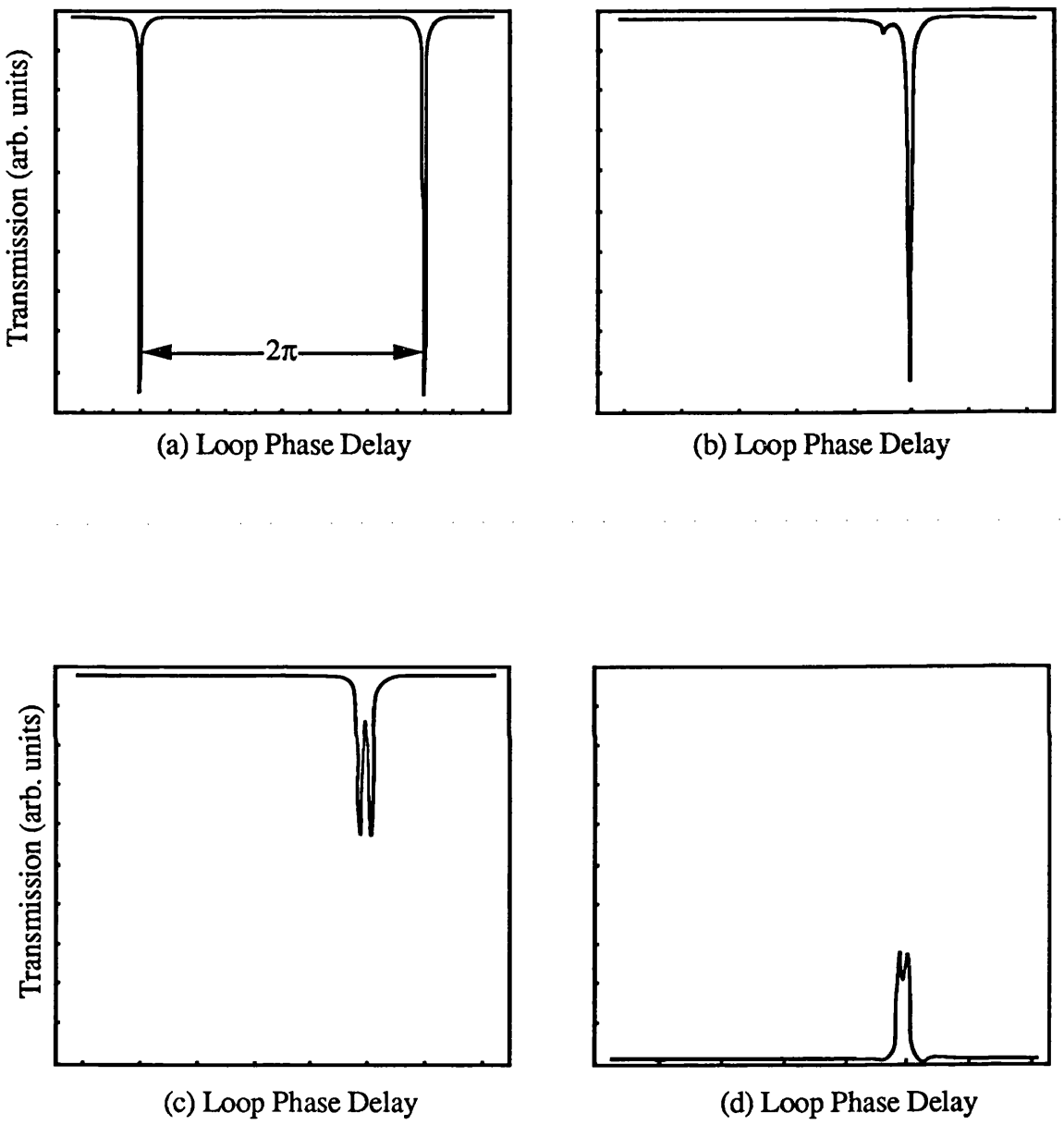

Figure 2.10 Theoretical plot of resonator transmission, for resonator of finesse 100, and polarisation isolation -25dB, as a function of $\Delta\beta L$. Linear polarisation launched on slow axis. (a) $\Delta\beta L=\pi$, (b) $\Delta\beta L$ close to $2m\pi$ and (c) $\Delta\beta L=2m\pi$. (d) level of power in fast axis at output.

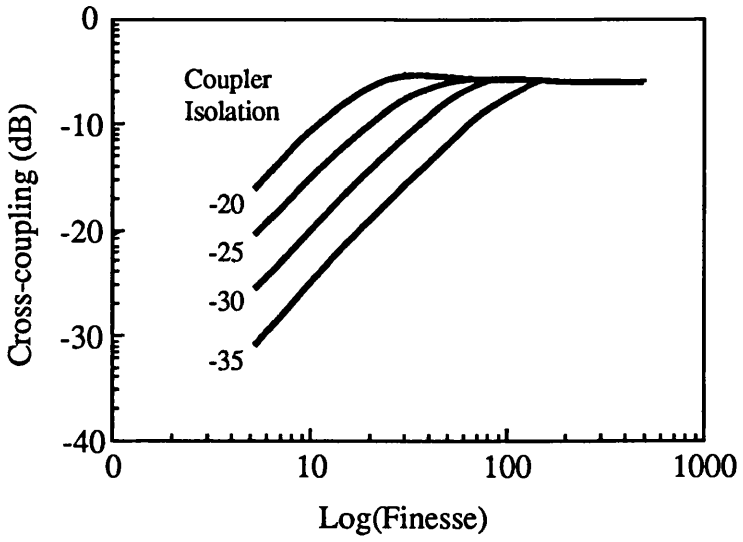

Figure 2.11. Level of polarisation cross coupling in a PMRR as a function of finesse for different values of isolation ratio in the coupler at $\Delta\beta L=2m\pi$

effective misalignment angle of 3.22°. Fig. 2.9 (d) shows the level of excitation of each of the resonator eigenstates for a linear input polarisation state with loop birefringence. The relationship between $\Delta\beta L$ and the phase separation is not linear and it becomes more parabolic as α increases. Notice that as $\Delta\beta L$ approaches $2m\pi$ the resonance modes come to within 2α rad of each other, but never actually cross. As $\Delta\beta L$ increases the separation again increases, but now the orthogonal eigenvector is mainly exited.

Fig. 2.10 shows the expected transmission response of a resonator of finesse 100, with a polarisation isolation of -25dB for various loop birefringences, when the input is a linear polarisation state aligned with the slow axes of the fibre. Fig. 2.10 (a) shows that when $\Delta\beta L=\pi$ the resonator response is the one normally expected, with the second eigenstate hardly exited. However, as shown in fig. 2.10 (c) when $\Delta\beta L=2m\pi$, the eigenvectors are circular and the linear input polarisation state excites both equally, leading to the observed resonance splitting. Fig. 2.10 (b) represents an intermediate stage where the minor eigenstate begins to be more strongly exited and the major eigenstate is no longer fully exited. This excitation of the "unwanted" resonator eigenstate leads to power being coupled into the orthogonal fibre mode, and the level of power coupled is found to be dependent upon both the PMRR polarisation isolation level and the finesse. Fig.2.10 (d) shows the level of power in the fast axis at the output of the resonator.

Fig. 2.11 shows the theoretically calculated values of the resonant power level in

the orthogonal polarisation axes for optimised coupler adjustment (100% resonance notch depth), at $\Delta\beta L=2m\pi$. It demonstrates that even for very precise alignment giving better than -35dB isolation, a large transfer of power between the fibre polarisation modes occurs when $\Delta\beta L=2m\pi$, if the finesse is high enough.

If the input polarisation is a circular polarisation then at mutual resonance the resonator response becomes a single resonance notch of 100% depth, since one of the resonator eigenmodes is now fully matched. Away from mutual resonance the resonator response splits and at $\Delta\beta L=\pi$, the response becomes two equally excited resonance curves of 50% resonance notch depth separated by π. This is because the eigenvectors of the PMRR are now linear, and the circular input polarisation excites them both equally.

2.2.3.1 PMRR with Large Misalignment and Zero Differential Loss or Coupling.

It is interesting to consider the response of a PMRR with the half blocks misaligned by nearly 90^0. In this case it is convenient to define the angle α', such that $\alpha'=\pi/2-\alpha$. This is obviously now a measure of how misaligned the coupler fibre axes are from the desired $\pi/2$ value. The matrices $\mathbf{A}^{-1}$ and $\bar{\mathbf{S}}$ then become,

$$\mathbf{A}^{-1}=\begin{bmatrix} \sin\alpha & -\cos\alpha \\ \cos\alpha & \sin\alpha \end{bmatrix} \quad \text{and} \quad \bar{\mathbf{S}}=\mathbf{A}^{-1}\mathbf{C}_c\mathbf{F}=\lambda_0\begin{bmatrix} \sin\alpha\, e^{j\Delta\beta L/2} & -\cos\alpha\, e^{-j\Delta\beta L/2} \\ \cos\alpha\, e^{j\Delta\beta L/2} & \sin\alpha\, e^{-j\Delta\beta L/2} \end{bmatrix} \quad (2.44)$$

The eigenvalues are, $\lambda_1=j\lambda_0 e^{-j\theta}$ and $\lambda_2=j\lambda_0 e^{j(\theta-\pi)}$, where $\sin\theta=\sin\alpha\cos(\Delta\beta L/2)$, {note: for small α, $\sin\alpha \approx \alpha$}. The phase separation between the two resonances is again the difference in the arguments of both eigenvalues, which in this case is given by $\pi-2\alpha$

Table 2.1 shows the important result that in this configuration the PMRR resonances are separated by a mean value of π and only vary with loop birefringence about their mean positions by at most 2α.

TABLE 2.1

$\Delta\beta L$	0	$\frac{2\pi}{3}$	π	$\frac{4\pi}{3}$	2π
Phase seperation $\pi-2\theta$	$\pi-2\alpha$	$\pi-\alpha$	π	$\pi+\alpha$	$\pi+2\alpha$

Variation in seperation between resonances with loop birefringence for a PMRR with approximately 90 degrees misalignment.

The corresponding eigenvectors of the system are,

$$V_1 = \left[1, \frac{\sin\alpha - je^{-j(\Delta\beta L/2+\theta)}}{\cos\alpha} \right]^T \tag{2.45}$$

$$V_2 = \left[1, \frac{\sin\alpha + je^{-j(\Delta\beta L/2-\theta)}}{\cos\alpha} \right]^T \tag{2.46}$$

The eigenvectors are again orthogonal ($V_2{}^tV_1=0$). In the ideal case of $\alpha=0$ the phase separation is fixed at π and the eigenvectors are always inclined at +/- $\pi/4$ to the birefringence axis and hence an input linear polarisation state launched on axis is always analysed equally onto the two eigenvectors, regardless of the loop birefringence. Some physical insight can be drawn from this by considering that the situation modelled in this section represents (at the coupler) the fast axis coupling to the slow axis and the slow axis coupling to the fast axis. Since the resonator response is made of multiple passes through the coupler+loop this can be thought of as scrambling the loop birefringence, in a manner analogous to the operation of spun low birefringence fibres, thus leading to the resonator response loosing its sensitivity to birefringence.

A similar case occurs when the misalignment is now caused by a 90^0 splice, within the fibre loop, a distance L_a away from port 3 and L_b from port 2. Assuming (for ease of analysis) the coupler to be perfectly aligned, we find that the eigenvalues of the system are the same as above leading to the same dependence on loop birefringence. The eigenvectors are found to be,

$$V_1 = \left[1, \ \frac{\sin\alpha\, e^{j\phi_a} - je^{-j(\Delta\phi/2+\theta)}}{\cos\alpha} \right]^T \qquad (2.47)$$

$$V_2 = \left[1, \ \frac{\sin\alpha\, e^{j\phi_a} + je^{-j(\Delta\phi/2-\theta)}}{\cos\alpha} \right]^T \qquad (2.48)$$

where $\phi_a=\Delta\beta L_a$, $\phi_b=\Delta\beta L_b$ and $\Delta\phi=\phi_a-\phi_b$. These are found to vary with ϕ_a, $\Delta\phi$ in essentially the same manner as in the previous configuration. The difference is that $\Delta\phi$ appears instead of $\Delta\beta L$ (which is equivalent to the splice being at the coupler), and there is an additional term $e^{j\phi_a}$, which represents the effect of the length of fibre L_a on the input polarisation state. A related analysis upon PMRRs formed by closing the fibre loop by means of a splice, has also been recently reported by Hotate, *et. al.*[54]. Their results concentrated upon small effective misalignment operation of the device, and its gyroscope drift characteristics.

2.2.4 PMRR with Misalignment and Anisotropic Loss and/or Coupling.

The cases outlined in §2.23 whilst instructive are not completely accurate for real PMRRs in which there will generally exist a differential coupling constant and a differential loss. The anisotropy parameter h, given by Eq.2.20 is thus no longer equal to 1. For the case of differential coupling but zero differential loss, the coupler anisotropy parameter $h=K_f / K_s$, and the coefficients are $d_1=d_2=d_3=d$ as in the case above. For the case of the PM coupler with differential loss (and no differential coupling) the anisotropy parameter becomes $h=(1-\gamma_f)/(1-\gamma_s)$ and the coefficients d_1, d_2, and d_3 are the same as those given in Eqs.2.27-2.29.

The introduction of the coupler anisotropy parameter $h\neq1$ leads to some interesting observations. The eigenvalues of the new system, whilst now difficult to solve analytically can still be computed numerically and written in terms of magnitude and phase. The corresponding eigenvectors of such a system are now found generally to be non-orthogonal ($V_2{}^tV_1\neq0$). Whereas, in the previous cases the eigenvectors were orthogonal and each eigenstate of polarisation independently generated the resonance

characteristics, with the overall response simply being the superposition of the two eigenvalues, this is no longer the case here and the effects of this are related by the final term of Eq.2.26 which is no longer zero. That the response of the PMRR is no longer the simple superposition of the two eigenvalues is so because the two eigenstates can no longer carry the power in the ring independently. Thus each resonance observed in the transmission response of such a PMRR is not due solely to a single eigenvector, but has a component of the other eigenvector in it as well.

This non-orthogonality term is found to be more significant close to the resonance points and can effectively be neglected away from them. If the level of excitation of the unwanted eigenstate is small, then the magnitude of this term is very small, and it may still be neglected for most considerations, except those in which extreme phase sensitivity is required, such as the gyroscope, and is considered further in chapter 5.

As in the previous case the relationship between the separation of the resonance points and the differential loop phase is not perfectly linear, but this is more pronounced in the case of the anisotropic PM coupler

Fig. 2.12 uses the Poincare' sphere representation of polarisation states[55] to illustrate the drift of V_1,V_2 of a PMRR with $\Delta\beta L$, as calculated from Eq.2.18. Any polarisation state can be defined by a point on the sphere. The points H and V on the equator represent orthogonal linearly polarised light, and the points R and L on the poles represent right and left circularly polarised light respectively. Points on the same circle of longitude represent light of the same azimuth, but varying ellipticity, and points on the same circle of latitude represent light of the same ellipticity but varying azimuth. In an ideal PMRR with no cross-coupling (α=0), the eigenstates are fixed at points H and V (fibre birefringence axes). Curve 2.12 (a) shows the drift of V_1, V_2 assuming CIR=25dB, which is a typical value obtained in the polarisation preserving couplers examined. When $\Delta\beta L=\pi$, the eigenstates are linear, very close to points H and V. A linear input polarisation state along a fibre axis excites the unwanted resonance at a level of -28dB; however as $\Delta\beta L$ approaches zero, the eigenstates drift quickly to the poles R and L (right and left circular polarisation states) and the same input state excites them now at equal levels. At $\Delta\beta L=-\pi$ the eigenstates exchange positions on the sphere. Curve 2.12 (b) shows that similar drift takes place even when a small anisotropy ($|h|<<1$dB) is present. It is easy to verify in this case that V_1,V_2 do not follow orthogonal trajectories on the sphere any more.

Let us now consider a PMRR that exhibits significant anisotropy. For the same

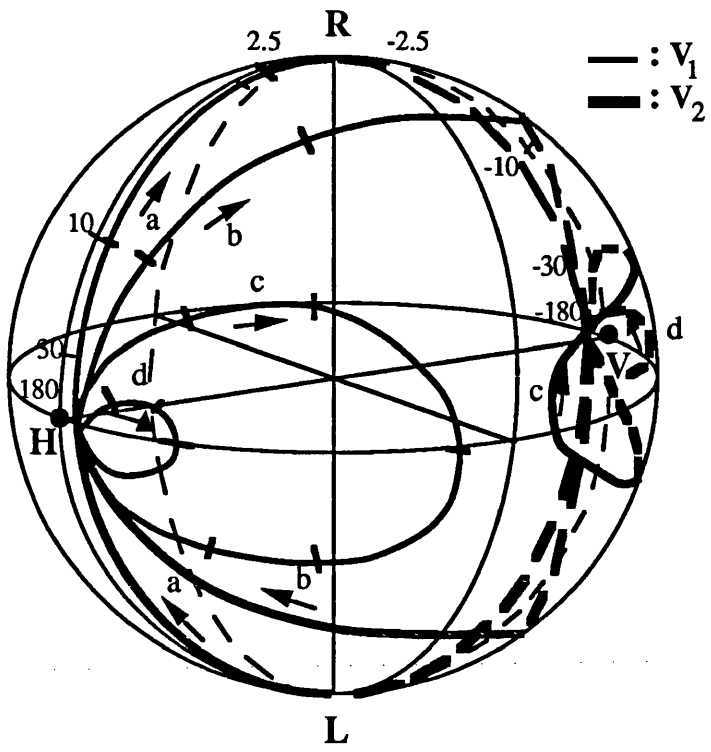

Figure 2.12. Poincare' sphere representation of the drift of the polarisation eigenstates of a PMRR with $\Delta\beta L$. Parameter h is : (a) 0dB, (b) 0.5dB, (c) 1dB, and (d) 3dB.

isolation level of 25dB, curves 2.12 (c) and 2.12 (d) on the Poincare' sphere show that as |h| increases, the trajectories of V_1, V_2 become closed loops of decaying size, lying on the locus of H and V, thus reducing the drift in the excitation of the unwanted resonance. The second effect of introducing a significant anisotropy is that the finesse of the unwanted eigenstate will also be greatly reduced, as the coupling constants will no longer properly match the loop losses. This further suppresses the effect of the unwanted eigenmode upon the performance of the resonator. As an example, consider a typical PMRR that exhibits differential coupling constant in the coupler and has k_x=0.97, k_y=0.1 (h=-10dB), $\gamma_x=\gamma_y$=0.03, L=1m, 8.5dB/Km loss at λ=633nm and CIR=25dB. For a linear input polarisation state aligned with axis x, as $\Delta\beta L$ drifts between $-\pi$ and π, the minor resonance shows a finesse of only F_2=3.25 and its level is now kept below -48dB, while the finesse and modulation depth of the major resonance vary only 4% around the values F_1=94 and ρ_1=0.86.

In practice such a resonator could be realized using a coupler that exhibits polarisation splitting properties or anisotropic loss, or inserting an in-line polariser[9,15] in the fibre loop (alternatively, a resonator made of polarising fibre[56] could serve the

same purpose).

In both the isotropic and anisotropic resonator ring, the trajectories of the eigenvectors around the Poincare sphere do not cross, because of the phase in the eigenvalues.

We shall consider briefly the effect upon the transmission response caused by either differential coupling or loss. In the case of an ideal polarisation selective PM coupler, with $K_f = 0$ the $\tilde{S}$ matrix becomes,

$$\tilde{S} = \sqrt{(1-\gamma)K_s}\, e^{-\alpha_o L}.e^{j(\beta L+\pi/2+\Delta\beta L/2)}\begin{bmatrix} \cos\alpha & 0 \\ \sin\alpha & 0 \end{bmatrix} \qquad (2.49)$$

The eigenvalues and eigenvectors are,

$$\frac{\lambda_2}{\lambda_0} = 0 \qquad \text{and} \qquad \frac{\lambda_1}{\lambda_0} = \cos\alpha \qquad (2.50)$$

$$V_2 = \begin{bmatrix} 0 \\ 1 \end{bmatrix} \qquad \text{and} \qquad V_1 = \begin{bmatrix} \cos\alpha \\ \sin\alpha \end{bmatrix} \qquad (2.51)$$

where λ_0 is the term representing the products outside the matrix in $\tilde{S}$. V_1 is a linear polarisation inclined at an angle α to the slow axis. V_2 is the degenerate eigenvector that corresponds to light coupled perfectly onto the non-coupled state. The intensity response is given by,

$$|E_4|^2 = (1-\gamma_{eq}) - (1-d)\frac{|e_1|^2}{|1-\lambda_1|} - (1-d)|e_2|^2 - 2(1-d)\sin\alpha\, \mathcal{R}e\left\{\frac{e_1^* e_2}{(1-\lambda_1^*)}\right\} \qquad (2.52)$$

The first two terms on the RHS of this equation represents the generation of resonances at $\Delta\beta L = 2n\pi - \pi/2$. The finesse of the response is reduced because of the $\cos\alpha$ attenuation in the eigenvalue. The third term, which normally corresponds to the second eigenvector is here a constant and does not create a resonance. The final term is the

non-orthogonality term. The eigenvalues and eigenvectors are now seen to be completely independent of loop birefringence.

Now consider the PMRR with differential loss, but isotropic coupling. We examine the case in which this differential loss within the PMRR originates from an in-line polariser, of insertion loss g and extinction ratio ER=10log(1-b), where b is the normalised intensity loss of the unwanted polarisation. Following the procedure outlined from Eq.2.10 to 2.29 we obtain a similar equation to Eq.2.26, except that the coefficients defined in Eqs.2.27-2.29 are slightly different. The term $\Delta\gamma/(1-\gamma_s)$ is replaced by the term b, and all the coefficients have an additional factor of (1-g).

For an ideal in line polariser, the extinction ratio is infinite and b=1. The eigenvalues and eigenvectors are exactly the same as the previous case of perfect anisotropic coupling and the same comments on these values apply. However, the intensity transmission is now given by,

$$|E_4|^2 = (1-\gamma_{eq}) - (1-d_1)\frac{|e_1|^2}{|1-\lambda_1|} - |e_2|^2 - 2\sin\alpha\, \mathcal{R}e\left\{\frac{e_1^* e_2}{(1-\lambda_1)^*}\right\} \qquad (2.53)$$

where $d_1=(1-g)d\cos^2\alpha$. The first two terms of the above equation again represent the generation of resonances at $\Delta\beta L=2n\pi-\pi/2$. The finesse of the response is however further reduced as a consequence of the polariser insertion loss, as well as by the $\cos\alpha$ attenuation in the eigenvalue. The third term is again a constant, however we see that now the effect of exiting the unwanted eigenstate in such a PMRR is to directly reduce the intensity of the output because of the action of the polariser, which now absorbs the light (as opposed to the previous case where the the light in the unwanted eigenstate was coupled straight out of the resonator). The final non-orthogonality term in this resonator is found to be larger than in the previous case because of the lack of the (1-d) term. Since d is often close to 1, this difference can be quite large. Again, the response of such an ideal PMRR is completely independent of the loop birefringence.

Infact to be useful as a technique for reducing the polarisation drift problem of real PMRRs, the extinction ratio of the in-line polariser does not have to be very high as it will experience multiple passes through it. As shown in Fig. 2.13 a 10dB in-line polariser aligned with one of the fibre axis was found theoretically to be sufficient to reduce the effect of the polarisation drift to negligible levels. The PMRR modelled prior to the addition of the in-line polariser, has a PM coupler polarisation isolation ratio of

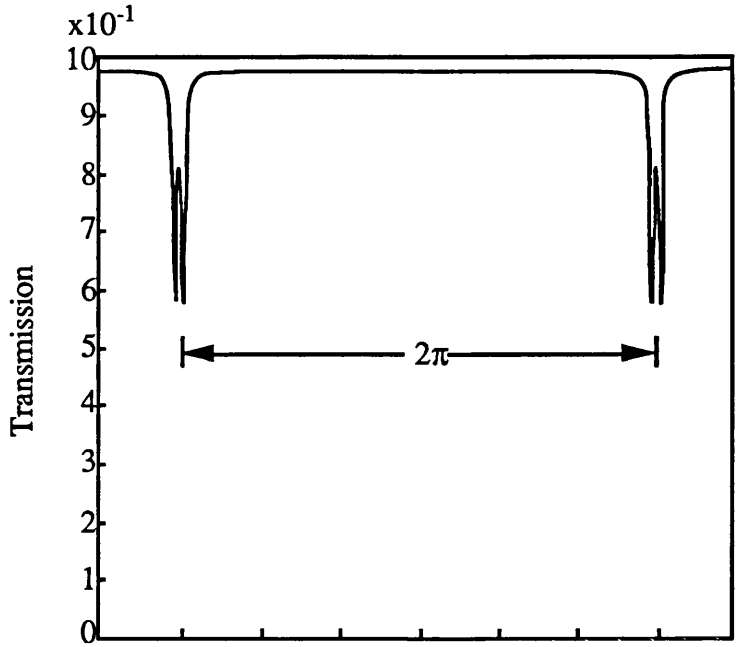

(a) Loop Phase Delay

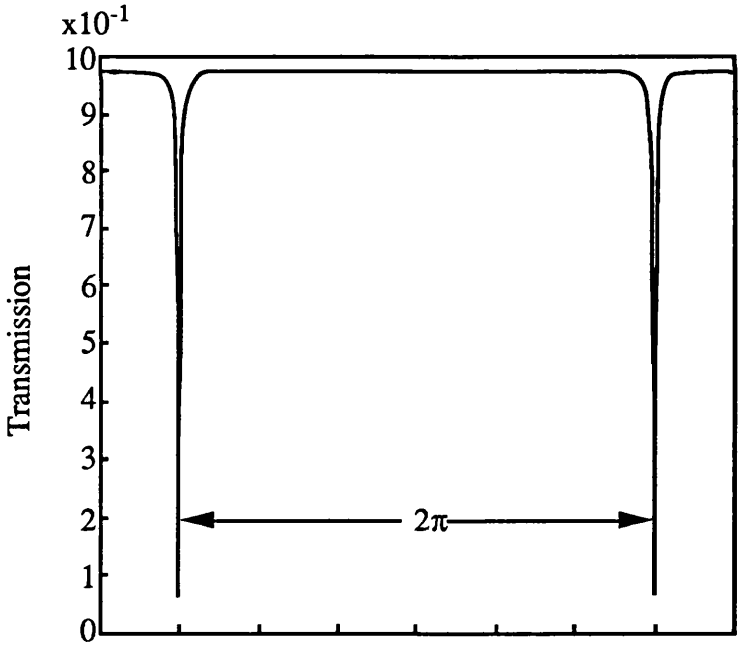

(b) Loop Phase Delay

Figure 2.13 response of PMRR described in text for $\Delta\beta L=2m\pi$, with h=-0.05dB and CIR=24dB (a) before insertion of in-line polariser and (b) after insertion of a 10db in-line polariser.

-24dB, and differential coupling and loss, which yield well away from mutual resonance, a finesse 120 and a resonance notch depth of 97.1% for light launched along one fibre axis and a finesse of 115 and resonance notch depth of 91.4% when the input polarisation was aligned with the orthogonal fibre axis. This leads to an anisotropy parameter h=-0.05dB. Fig. 2.13 demonstrates the transmission response of the PMRR at mutual resonance (a) before and (b) after the insertion of the 10dB polariser.

When considering the combined effect of differential loss, and differential coupling, in a real PMRR, with a view to reducing the polarisation drift, the main consideration is to ensure that as far as possible the coupling constant and loss of the unwanted eigenstate are not matched, in order to avoid the finesse and modulation depth of that eigenmode being optimised.

2.3 Experimental Investigations of Polarisation Maintaining Fibre Ring Resonators.

Several high quality PMRRs were successfully fabricated for operation at 633nm, 830nm and 1.3μm. The PMRRs were all fabricated with York V.S.O.P Bow-Tie fibre. Only the PMRRs fabricated for 633nm operation were used primarily to investigate the polarisation instability in these devices, although all the resonators showed the same basic operational characteristics. The resonators fabricated include (1) a 1m PMRR with a demonstrated finesse of over 600[17(a)], which was at the time of fabrication the highest value of finesse reported, (2) a 4.15m PMRR with a finesse of over 250, and (3) a 3m PMRR with a finesse of over 180. Care was taken when measuring the above finesse values to avoid the effects of optical non-linear phenomenon, particularly stimulated Brillouin scattering, upon the measurements. This is discussed further in chapter 4.

The basic schematic of the experimental system used to investigate the polarisation instability is shown in Fig. 2.14. A 633nm stabilised single longitudinal mode HeNe laser was used as the source. As outlined above, the transmission response of a PMRR is found to be extremely sensitive to fibre birefringence, and in the type of PM fibre used the birefringence is strongly temperature sensitive[57]. To reduce the effects of random environmental temperature variation the PMRR to be investigated was placed within a temperature shield. A linear polarisation state was defined at the input of the

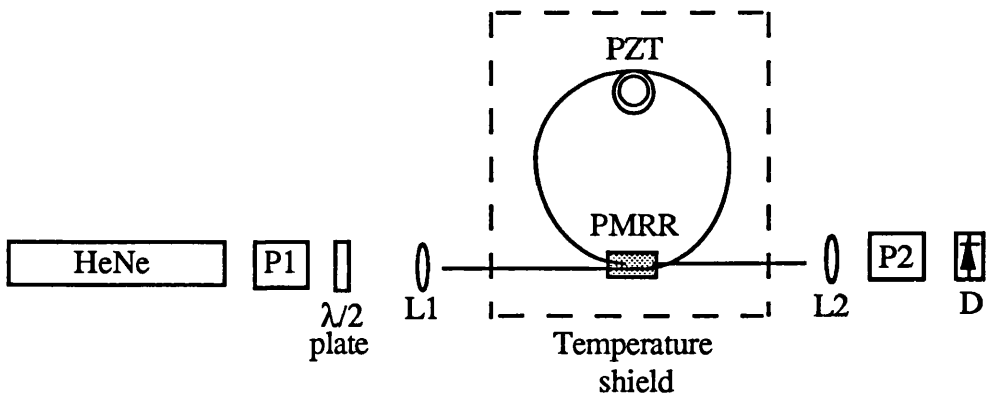

Figure 2.14 Schematic of experimental setup used to investigate polarisation instability in PMRRs. P1, P2 : polarisers, L1, L2 : x30 objective lenses, D : detector, PZT : piezoelectric cylinder.

fibre by means of a 50dB Glan-Thomson polariser and a rotatable half wave plate. Care was taken to try and enclose as much of the input fibre within the temperature shield as possible, as when light is present upon both the fibre principal axis, the polarisation state that reaches the PM coupler will be dependent upon the (environmentally sensitive) input lead birefringence. When required the light present on the orthogonal fibre axes at the output of the PMRR could be investigated by means of an output analyser aligned with the fibre principal axis, as shown in the diagram, or by means of an aligned polarising beamsplitter, and detector pair. Care must be taken to ensure that any polarisation selective components at the output of the PMRR are carefully aligned, with the output fibre axis, as any misalignment causes selective filtering of the polarisation components of the output and this can again lead to significant changes in the transmission characteristics of the PMRR[58], sometimes resulting in the resonance notches becoming resonance peaks. It was important to ensure that the collimated output of the PMRR fell on the center of the detector, to allow the output of each polarisation axis to excite the detector equally. Strong polarisation filtering was found to occur when only the edge of the output beam was used to excite the detector.

The input and output polarisers was aligned with the fibre principal axis by one of several means. The simplest method was to temporarily replace the HeNe laser with a low coherence source, then by iteratively varying the output polariser for a fixed position of the input polariser, both polarisers could be aligned with the fibre axis by noting the position at which the extinction ratio of the two cross polarisers with the PMRR in between was maximised. Extinction ratios of 30dB with the two 50dB polarisers could typically be achieved. The disadvantage of this technique is that the

HeNe laser then needs to be re-aligned into the system.

The same technique can be used again directly with the HeNe laser source, however the long coherence length of the source leads to interference effects which also give output minima. By varying the birefringence of the fibre (eg, by heating it) it is possible to determine whether the output minimum is due to interference effects or the successful alignment of the output polariser with the output fibre principal axis. Once the output polariser is aligned, the input polariser can be readily aligned by rotating it until the output is maximised (or minimised). Generally care had to be taken to ensure that the PMRR was kept well off resonance, or if the coupler was dismantled, to ensure that the coupler halfs and intermediate fibre were kept within the temperature shield, as the small cross coupling at the half blocks leads to a Mach-Zender interferometer being formed between the blocks.

An imaging technique can also be used to determine the orientation of the fibre polarisation axis, by observing the fibre ends under a microscope and fixing them in special holders and marking the axis alignment on the holders. Whilst this technique, unlike the previous methods allows the fast and slow axes to be discriminated, it only allows rough alignment.

A novel method that also allows the axis to be discriminated is based upon the fact that the output of the York Bow-Tie PM fibre is elliptical in shape. Two factors play upon the shape of the output. First is that the fibre core was actually slightly elliptical, with its major axis along the fast axis, and second is the differential refractive index along the fast and slow axis (see table 2.2 for the data on a typical length of HB600 Bow tie fibre). These two effects combine to form an output ellipse, with its major axis aligned along the slow fibre axis. This was checked experimentally by comparing it with markings made on the fibre holder by the above method. The orientation of the ellipse was found to be

TABLE 2.2

	Cladding Index	Peak Core Index	Core Diameter (μm)
Fast axis	1.4585	1.4648	4.36
Slow axis	1.4497	1.4653	3.30

Table 2.2 refractive index and core diameter data on typical length of York Bow-Tie HB600 fibre [ref.59].

independent of the input polarisation. Thus it is now a simple matter of aligning the output fibre with the output polariser, and consequently the input polariser.

The loop phase was varied by modulating the loop length. This was achieved by wrapping a length of fibre around a PZT and applying a saw-tooth voltage. The frequency of the applied modulation had to be kept below 40Hz for the high finesse resonators, to avoid undesirable ringing effects[60]. This is because the ring resonator is essentially a storage device that requires a characteristic build-up time to properly generate its output response.

2.3.1 Variations in Transmission Response with Loop Birefringence.

When the experimental schematic of Fig. 2.14 was set-up, resonance splitting effects similar to those described by Fig. 2.10 were observed. The loop coupler was adjusted in the 3m PMRR to give a finesse of 115 with resonance notch depth of 91.4% for linearly polarised light launched along fibre axis (1), and a finesse of 120 with resonance notch depth of 97.1% for light launched along fibre axis (2). This corresponds to an anisotropy parameter h of -0.05dB, and is the same as the resonator that was modelled in the case of the in-line polariser. The polarisation isolation ratio was estimated by monitoring the minimum phase separation between the resonances as outlined in §2.2.3 to be approximately -24dB. Given the low coupler anisotropy, this measurement is still a good approximation of the coupler polarisation isolation. The intensity transfer function of the resonator for input on axis (2) is shown in Fig.2.15. Fig.2.15(a) shows the transmission response over a single free spectral range. The main resonance dip corresponding to resonance of the launched linear polarisation mode can be observed and a second notch can barely be discerned, separated from the first dip by approximately half a free spectral range. A variation in temperature of a few degrees (^{o}C) is found to alter the birefringence enough for the separation of the two resonance dips to scan a free spectral range. Fig.2.15(b) shows the intensity transmission when a thermal drift causes the two resonance dips to approach each other. The depth of the major resonance decreases while the minor one increases to a more distinguishable level. Fig.2.15(c) shows that at $\Delta\beta L=2m\pi$ the response consists of a pair of dips of virtually equal size. After the two dips have "crossed" each other the response takes the normal form of Fig.2.15(a).

Further measurements were taken to assess the observed effect by placing a

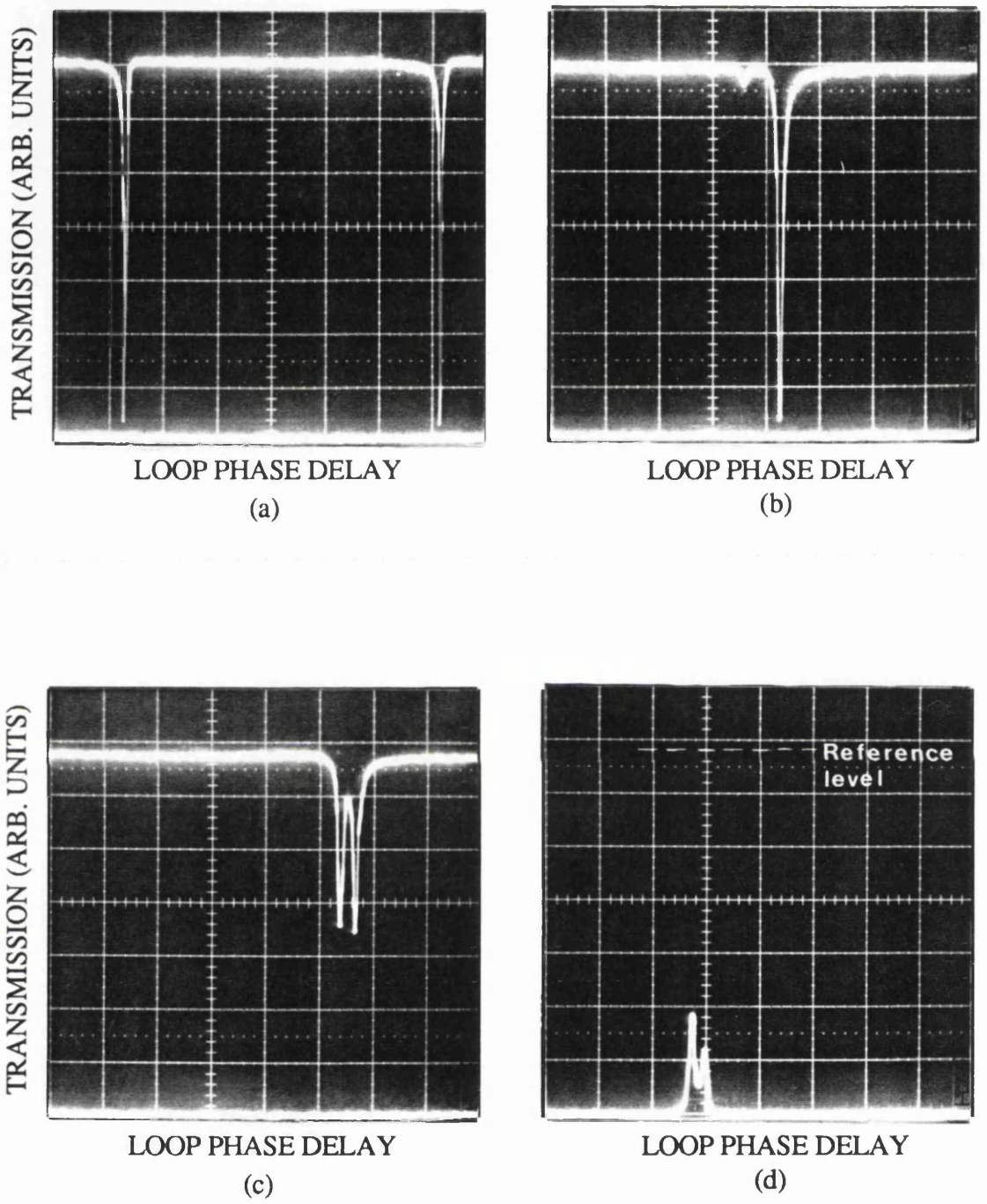

Figure 2.15 Variations in experimentally observed transmission response of PMRR with finesse 100, and isolation -25dB, as a function of $\Delta\beta L$.Linear polarisation launched on slow axis. (a) $\Delta\beta L=\pi$, (b) $\Delta\beta L$ close to $2m\pi$ and (c) $\Delta\beta L=2m\pi$. (d) level of power in fast axis at output.

polariser at the output of the resonator aligned orthogonally to the input polarisation state. When the two resonance dips were well separated, the level on the unwanted fibre mode was minimal, as expected from the low residual cross coupling. When the temperature of the loop was changed to attain resonance splitting ($\Delta\beta L=2m\pi$) the level in this orthogonal fibre mode reached a peak value as shown in Fig.2.15(d), indicating a substantial level of power conversion between the fibre polarisation modes. This peak value was found to be slightly dependent on the precise coupler adjustment and was up to 40% of the launched power. An excellent agreement is found between these experimental results and those predicted from the use of Eq.2.26 with the experimental parameters applied. Because of the low value of coupler anisotropy, h, the results are also in good quantitative agreement with the theoretical plots of Figs. 2.10 and 2.11, which demonstrate the expected transmission response and power coupling in the absence of coupler anisotropy.

2.3.2 Non-Orthogonality of Eigenvectors.

Variations in the coupler anisotropy parameter h, and polarisation isolation with relative half block alignment has been observed experimentally for the first time in our experiments. With the input polarisation aligned along one of the fibre axis, the PM coupler could be aligned to give good polarisation isolation and a high extinction ratio between the two eigenstates (ie low coupler anisotropy). With the input polarisation state maintained constant, slight coupler adjustments were found to be sufficient to alter the transmission response of the PMRR to that shown in Fig. 2.16. A large component of the other PMRR eigenmode is now excited. That the eigenmodes are now significantly non-orthogonal can be deduced by the fact that the summation of the normalised resonance notch depths is greater than 1, and it is no longer possible to excite only one eigenstate. The finesses of the 'major' and 'minor' resonances shown in Fig. 2.16 are 196 and 220 respectively. The most extreme variation observed was in the 4.15m PMRR with the one of the eigenstates having a finesse of 137 and a resonance notch depth of 90% and the other eigenstate having a finesse of 87 and a resonance notch depth also of 90%, for a fixed coupler adjustment.

For large polarisation isolation ratios (and $\Delta\beta L=\pi$), the finesse of the PMRR was determined for linearly polarised input launched along either the slow or fast axis, with

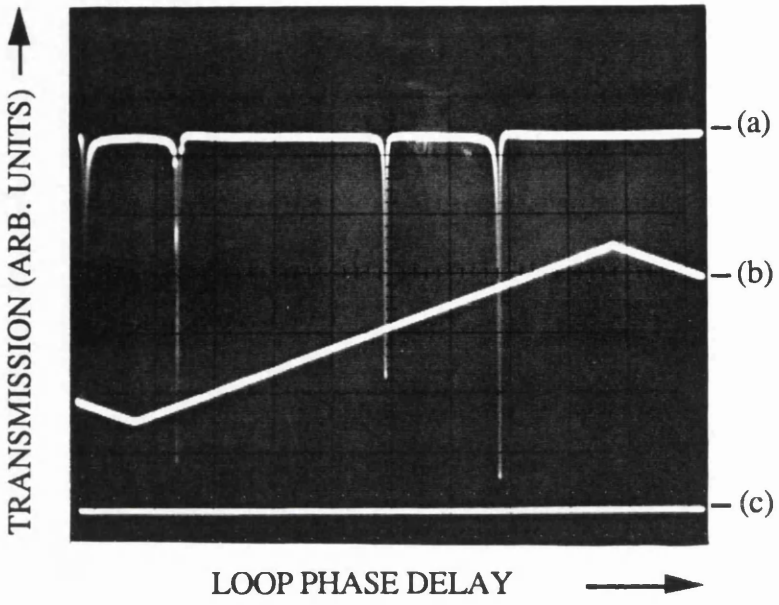

Figure 2.16 (a) PMRR transmission response demonstrating strongly anisotropic PM coupler behaviour, (b) PZT driving voltage and (c) zero detector response. The same coupler demonstrated negligible anisotropy when its half blocks were adjusted to another position.

the coupling constant optimised for each case. The finesse was found to be consistently higher for light launched along the fast axis, and hence the PM couplers have a lower loss along their fast axis.

2.3.3 Reduction of Polarisation Instability in PMRRs.

The non-linear drift in the separation of the eigenvectors and the consequent resonance splitting at mutual resonance due to the dependence of the PMRR transmission response upon the loop birefringence is unacceptable in all applications in which the ring resonator is required to be immune to environmental perturbations. The theoretical analysis developed above gives some useful clues as to how the PMRR can be made insensitive to the loop birefringence. This includes the effect of 90° misalignment at the coupler, but this has the disadvantage of the difficulty in achieving good isotropic coupling between the orthogonally aligned polished coupler half blocks. The PMRR with a 90^0 splice in the fibre loop would overcome these problems to some extent, but the splice loss would lead to a reduction in finesse. Strong differential coupling at the coupler, or strong differential loss in the fibre and coupler (the effects of the latter may be lumped together to represent an equivalent anisotropic loss at the

coupler) can also be used to reduce the polarisation instability. The latter case can be achieved either by the insertion of a low loss, relatively low isolation polariser in the loop, as outlined above (cf. Fig. 2.13) or by means of a single polarisation fibre. The important parameter is the loss of the loop formed by either method, as this will determine the finesse of the PMRR. The in-line polariser could either be of evanescent type (eg plasmon polarisers[61]) or of coiled birefringent fibre type[62]. Preliminary attempts to fabricate a PMRR with an in-line evanescent type polariser proved unsuccessful, because of the difficulty in polishing three half blocks on the same strand of optical fibre, all with the required coupling and polarisation isolation ratios.

A PMRR with large differential coupling constant could be achieved, without the need for external components by suitably polishing the coupler halves to give the necessary polarisation dispersion, in the manner outlined in §2.1. However, this effect is small for polishing along the same fibre axis as is required here. Another method is to introduce some anisotropic material between the coupler half block interaction regions, and this method was also chosen to be investigated experimentally.

A thin film of nematic liquid crystal (NLC) was placed in between the two polished fibre blocks of the 4.15m PMRR, instead of the usual refractive index matching liquid. The NLC consists of rod shaped molecules, which can in macroscopic terms be aligned on average in one direction, called the director. The cylindrical shape of the molecules gives the NLC its birefringent properties. Linearly polarised light propagating along the director experiences a higher (extraordinary) refractive index n_e, while linearly polarised light propagating in a direction normal to the director experiences a lower (ordinary) refractive index, n_o. The choice of NLC was determined by the suitability of the values of these indices for good PMRR performance. The NLC used in the experiments was BDH mixture 14616, which demonstrates refractive index values of n_o=1.452 and n_e=1.5 at λ=633nm over a wide temperature range. The molecules of the NLC were aligned homogeneously (ie with the director lying on the plane of the coupler half block surface), perpendicular to the fibre axes; thus a TM-like field faces the lower (ordinary) refractive index, while a TE-like field experiences the higher (extraordinary) one. The NLC was aligned by means of first rubbing the surface of the coupler blocks with a soft tissue. This creates micro-grooves along which the NLC molecules can align. Care was taken not to adjust the coupler blocks too excessively as this would misalign the NLC. Due to this anisotropic interlayer the coupler exhibits vastly different coupling constants and loss for the two fibre polarisation modes; the

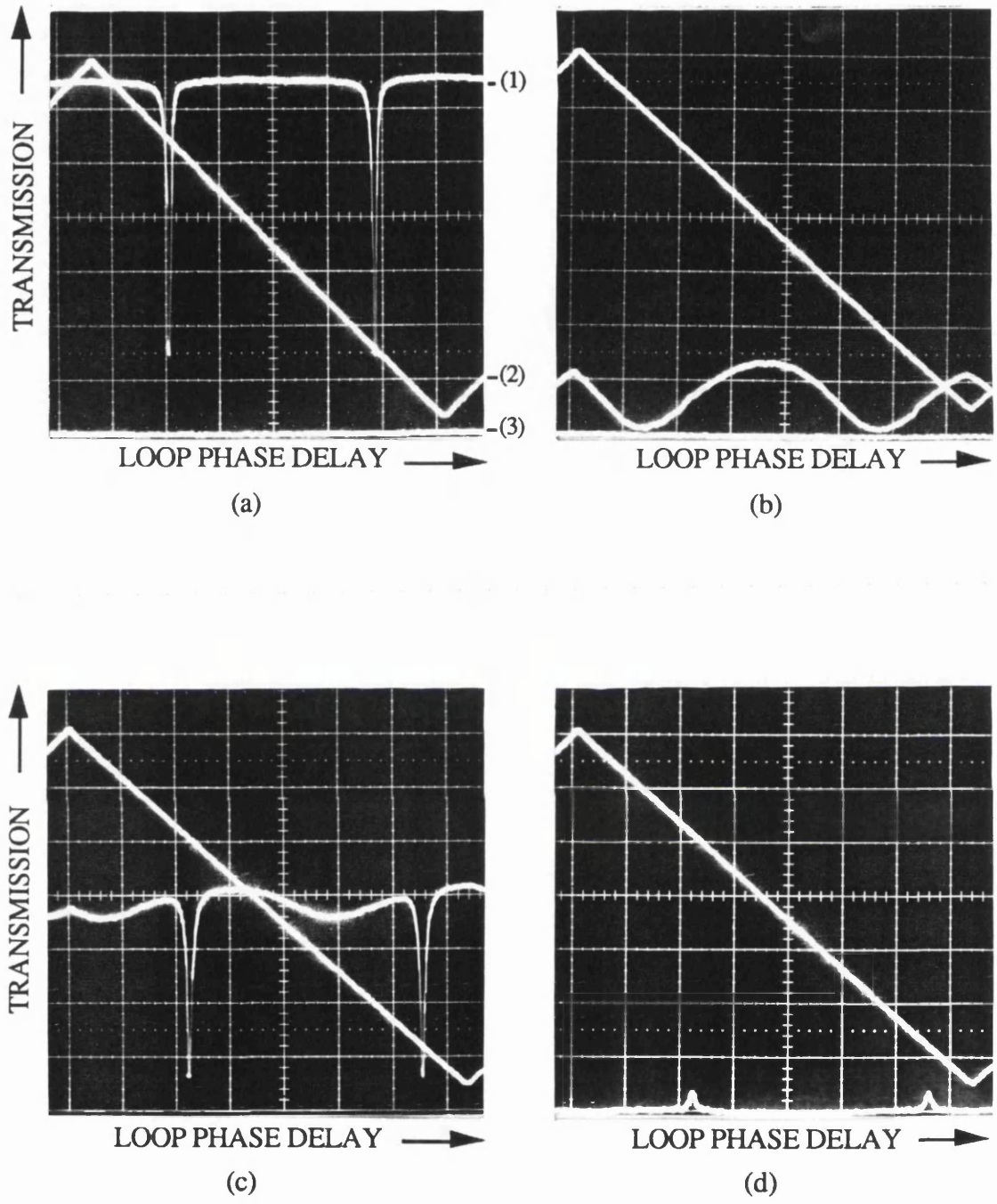

Fig.2.17 Intensity response of resonator with nematic liquid crystal for linear input polarisation state (a) launched along the slow axis, (b) the fast axis and (c) along both fibre axis. (d) amount of light coupled over to the orthogonal fibre axis (note: this photograph is magnified by a factor of 4 compared to the other photographs on this page). Curves (1), (2) and (3) are the intensity response, PZT driving voltage and zero transmission response, respectively.

anisotropy parameter was estimated to be h=-10dB. Fig.2.17 shows the intensity response of this resonator for a linear input polarisation state (a) launched along the slow axis, (b) the fast axis and (c) along both fibre axes. The polarisation state of the input was varied by means of fibre polarisation controllers spliced onto the input of the PMRR. This helped to ensure a constant launch power as the polarisation state was adjusted. Fig. 2.17 (d) demonstrates that now the amount of light coupled over to the orthogonal fibre axis is greatly reduced. Clearly the two polarisation eigenstates exhibit vastly different finesses (F_1=70, F_2: almost sinusoidal modulation). When the input was aligned with the fibre axis that creates the higher finesse, the response consisted of a single resonance dip and was not noticeably affected by normal external perturbations. To our knowledge this is the first demonstration of a resonator that exhibits vastly different finesses and a polarisation stabilized response. The finesse in this resonator was limited by the scattering the NLC. Lower NLC scattering loss should be possible by the application of production techniques used in liquid crystal display technology.

2.3.4 Determination of Coupling Regions in a PMRR.

The analysis of §2.2 assumed that all the polarisation coupling in the PMRR occurred at the PM coupler, and it is of interest to experimentally determine the validity of this, and to compare the strength of cross-coupling at the coupler compared to the other sources, such as along the fibre in the loop and especially at the fibre wrapped tightly around the PZT cylinder.

This was achieved by means of the coherence matching technique of Fig. 2.18. It

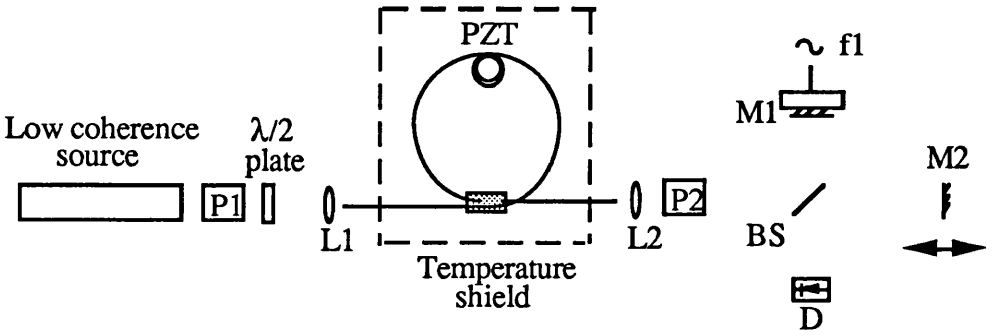

Figure 2.18. Coherence scanning experiment to locate points of cross-coupling in PMRR. P1, P2 : polarisers, L1, L2 : x30 objective lenses, D : detector, PZT : piezoelectric cylinder, M1,M2 : mirrors, BS : 50/50 beamsplitter, f1 : applied modulation.

consists of a low coherence input, launched on axis into a PMRR with a polariser aligned at 45° to the output fibre axis, followed by a Michelson interferometer. Light that is coupled from the launched axis over to the orthogonal fibre axis may either propagate to the output end after n fibre loop transits (n=0,1,2..), or recouple back to the launched fibre axis. Either way it will suffer a differential delay from light that has propagated only in the launched axis, and this delay will depend upon the point at which the light was coupled and the distance it has had to travel (ie how many loop transits) before it reaches the output of the PMRR. If the differential phase delay is greater than the coherence length of the source then the signals after the output polariser will not interfere. The purpose of the Michelson is then to form a matched filter for the output light. As the length of one of the arms of the Michelson interferometer is varied a coherent signal will only be achieved when the differential delay of the Michelson interferometer equals (within the source coherence length) the delay between the polarisation components. To aid signal recovery, a sinusoidal modulation is also applied to one of the Michelson interferometer arms.

The system was first calibrated with just the low coherence source and Michelson interferometer to determine the position of any signal peaks due to the lasers own coherence function. Then using a single length of York HB600 fibre, similar to the one used to make the PMRR, the resolution of the Michelson to cross-coupling was found to be ΔL=11cm, for a $\Delta\beta$ of 5×10^{-4}. The experimental schematic of Fig. 2.18 was then set-up with the 1m PMRR and the path imbalance of the Michelson varied, and the corresponding signal levels noted. This procedure was repeated several times for accuracy.

The results shown in Fig. 2.19 can be explained in terms of the light cross coupled at the coupler experiencing an integer number (n=0,1,2,..) of transits around the fibre loop (Loop=1m), and either zero or one (m=0,1) transit through the output lead (Lead=30cm). m=0 corresponds to the light that had been previously cross-coupled coupling back into the launched polarisation axis. Thus signal peaks are expected at path imbalances on the Michelson corresponding to a differential distance nLoop+mLead travelled in the PMRR. Only the 8^{th} signal peak cannot be explained by this argument, and may be due to a spurious laser line being formed by end-reflections into the laser by the PMRR input. Also the term corresponding to n=1, m=0 is absent, possibly because it is below the system noise floor level (-110dB). We note that as

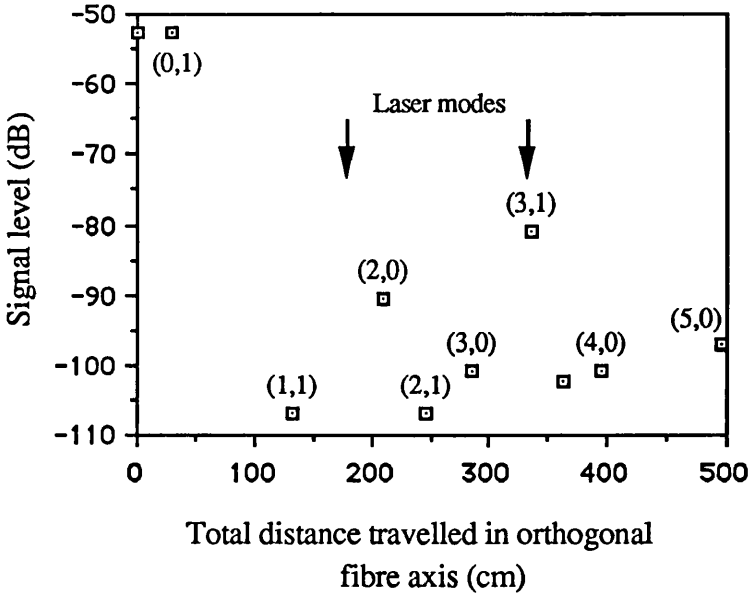

Figure 2.19 Signal peaks detected as path imbalance of Michelson interferometer is scanned. The terms (n,m) indicate the combination of differential loop (n) and output fibre (m) transits experienced by the cross coupled light.

expected, almost all the cross-coupling occurs at the coupler and that the coupling effects of the fibre length and PZT windings are not apparent in this experiment.

2.3.5 Aging Effects in Bow-Tie PMRRs.

Anomalous effects where observed in the 3m and 4.15m PMRRs when the PM couplers had been left assembled and clamped for an extended period of time (over 1month). The originally low loss couplers became very lossy and began to glow very strongly, and the transmission response of the device became severely altered. Fig. 2.20 (a) and (c) show the resonator response for the two new eigenstates of the device.

One of the eigenstates exhibits resonance peaks, similar to the response expected if the portion of light that couples straight through the coupler (without entering the ring) is missing, and the other eigenstate is similar to the response of a resonator with extreme differential losses between the coupler symmetric and asymmetric modes[63]. Fig. 2.20(b) shows the response when both eigenstates are excited. These two resonances still drifted with respect to each other, and suffered resonance splitting at $\Delta\beta L=2n\pi$. The effect was found to disappear once the pressure on the PM couplers was relieved and the couplers re-aligned. The glow of the coupler block was also found to be significantly reduced. These observed effects are similar to the effects expected if

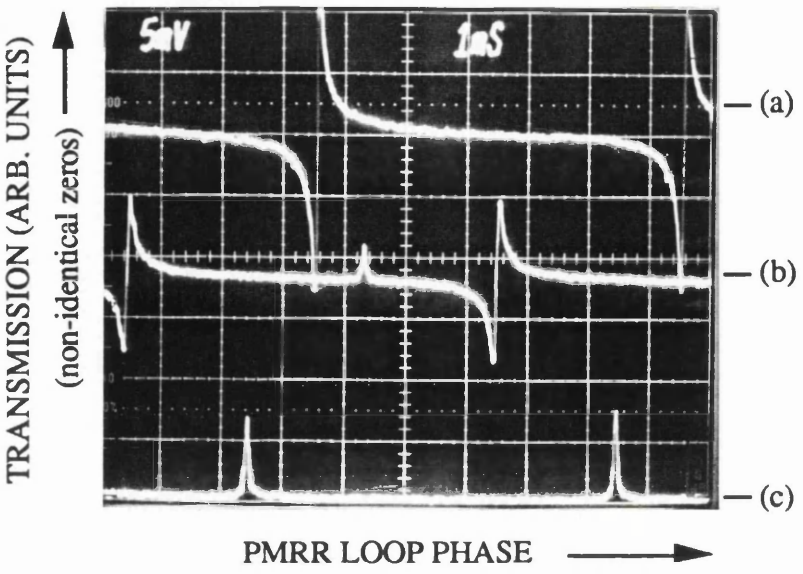

Figure 2.20 Aging effect in PMRR.(a) and (c) resonator response for the two new eigenstates of the device, (b) intermediate response of both eigenstates excited.

there is a form of polarisation filtering at the output of the PMRR. The cause of this effect is uncertain, but it seems to be related to the creation of an intercoupler polarisation selective planar waveguide by the applied pressure. This could be formed as the fibres become slightly raised relative to the coupler half block surface (cf Fig. 2.4), with aging, because the matching refractive index oil seeps into the epoxy, and each coupler half presses against each other changing the local refractive indices, leading to the planar waveguide being formed[64]. This would explain the increased loss of the coupler block. In order for this effect to explain the observed response it is necessary that there is also a longitudinal offset between the coupler half blocks, such that the majority of the polariser action of the intercoupler planar waveguide affected primarily the output port.

2.4 Conclusions.

The behaviour of practical PMRRs was investigated experimentally and theoretically. The inevitable occurrence of a finite amount of polarisation cross coupling and coupler anisotropy within real PMRRs is shown to lead to severe deviations, in device performance, from the desired stable resonance response. The Jones matrix formalism is used to develop an expression in terms of eigenvalues and eigenvectors,

device performance, from the desired stable resonance response. The Jones matrix formalism is used to develop an expression in terms of eigenvalues and eigenvectors, that fully describes the PMRR response. The agreement between this expression and the experimental results is found to be very good. Polarisation cross coupling is shown to lead to the eigenmodes of the ring resonator becoming strongly dependent upon cavity birefringence. For stable input polarisation states, this leads to strong variations in the transmission response of the device. The separation between the resonance points of the two resonator eigenmodes is no longer a linear function of cavity birefringence, and the minimum phase separation between the resonance points is shown to be equal to twice the effective misalignment angle. The effective misalignment angle being a complex function of fibre axis misalignment, coupler geometry and fibre birefringence. In the absence of significant coupler anisotropy this minimum resonance separation provides a simple means of measuring the polarisation isolation in a PMRR. The addition of coupler anisotropy in terms of loss or coupling constant generally causes the resonator eigenmodes to become non-orthogonal. This means that the two resonance dips formed are now interdependent, and the characteristics of the PMRR response depends upon the magnitude of the anisotropy. For large cavity anisotropies the PMRR eigenvectors exhibit a reduced dependence upon loop birefringence.

The occurrence of this polarisation instability in PMRRs renders the device unsuitable for any applications that require a stable device response. This instability was shown theoretically to be reduced by several methods, including (1) the introduction of a $\pi/2$ effective misalignment point within the cavity, (2) the use of an intra-cavity polariser or polarising fibre to form the cavity, (3) strongly anisotropic coupler loss, (4) strongly anisotropic coupler coupling constant. The use of coupler anisotropy to suppress the polarisation instability was also successfully demonstrated experimentally for the first time by the introduction of a nematic liquid crystal between the coupler half blocks.

Chapter 3

REVIEW OF STIMULATED BRILLOUIN SCATTERING IN FIBRE SYSTEMS

The large coherence length of many contemporary cw lasers, coupled with the small cross sectional areas and low losses of optical fibres, can result in very high intensities of light propagating over long interaction lengths. Thus even fused silica fibres, which have typically small non-linear susceptibilities, exhibit many types of optical non-linearity at relatively low input powers.

The enhancement of the circulating intensity over that of the input intensity afforded by the geometry of all-fibre ring resonators, leads to such non-linear effects becoming even more prominent in these devices, especially as the continual advance in the quality of optical fibre components leads to improvements in their achievable finesses.

One of the most pronounced optical non-linear processes in coherent fibre-optic systems is stimulated Brillouin scattering. In this effect, an intense forward propagating optical wave gives rise, via electrostriction, to a forward propagating coherent hypersonic acoustic wave, and a backward propagating frequency shifted optical wave.

For passive operation of the fibre ring resonator, as is required in most sensor applications, the onset of stimulated Brillouin scattering within the fibre loop can have deleterious effects upon device performance, and hence these effects need to be characterised. The purpose of this chapter is to present an introduction to the field of stimulated Brillouin scattering, and to provide some of the necessary theory required in Chapters 4 and 5. Chapter 4 characterises the effects of the process upon ring resonator performance and investigates methods to reduce these effects. The stimulated Brillouin process may however also be put to use, to form for example, active cavities that can

emit either stable narrowband radiation, or mode locked pulses[65,66]. Such stimulated Brillouin lasing cavities suggest the possibility of forming all fibre stimulated Brillouin ring laser gyroscopes[67]. This is investigated further Chapter 5.

The theory of stimulated Brillouin scattering is first presented, and its dependence upon pump bandwidth and material characteristics outlined. The effects of competing optical non-linear phenomenon are noted, and finally an overview of stimulated Brillouin scattering applications presented.

3.1 Non-linear optics.

When an electromagnetic field propagates through a medium, it exerts a force upon the loosely bound outer or valance electrons. Typically these forces are relatively small and at low electric field strengths, the resulting electric polarisation is parallel with and directly proportional to the applied electric field. The proportionality constant is the electric susceptibility, χ, a material constant. At high electric field strengths, the electric polarisation is no longer directly proportional to the electric field and this gives rise to non-linear optical phenomena. In this case the polarisation can be written in terms of the following power series[68],

$$\mathcal{P}_i = \sum_j \chi_{ij}^{(1)} E_j + \sum_{j,k} \chi_{ijk}^{(2)} E_j E_k + \sum_{j,k,l} \chi_{ijkl}^{(3)} E_j E_k E_l + \cdots\cdots. \qquad (3.1)$$

In centrosymmetric materials, (such as the silica based glass used in communications grade optical fibre), only the odd terms in the power series of Eq.3.1 exist and the second term of the series which gives rise to such phenomena as second harmonic generation and optical rectification does not occur. (Special optical fibres that do exhibit large second order non-linear susceptibilities can be formed by poling the fibre with a strong dc electric field to permanently align defect centers within the core[69]). Thus, in conventional optical fibres the third term of the series is the most dominant contributor to optical non-linearities. This third order term can give rise to a range of non-linear effects, such as Four Wave Mixing (FWM), self focusing, the Kerr effect, stimulated Raman and stimulated Brillouin scattering.

The stimulated Raman and Brillouin effects are associated with the generation of high frequency phonons in the material. Each of these stimulated scatterings have their

corresponding spontaneous scatterings as well. Raman scattering is from molecular vibrations on the optical branch of the dispersion curve that describes the material vibrations, and Brillouin scattering is from the acoustic branch of the dispersion curve. An excellent review of the spontaneous and stimulated scattering processes is given by Kaiser & Mair[70].

3.2 Stimulated Brillouin Scattering.

Since the first observation of stimulated Brillouin scattering by Chiao, Townes and Stoicheff[71], of intense laser light in quartz and sapphire, the effect has been studied extensively in solids, liquids and gases under a variety of conditions. Stimulated Brillouin scattering often occurs at power densities several orders of magnitude below that required for the other stimulated scattering processes and is thus of primary importance in coherent systems.

It is worth first commenting on nomenclature. In the western literature Stimulated Brillouin scattering (due to electrostriction) is often abbreviated as SBS, and stimulated Brillouin scattering (due to thermal waves via light absorption) is abbreviated as STBS. Because of the low light absorption in optical fibres, STBS can readily be ignored from the present treatise. In the Soviet literature SBS (via electrostriction) is known as stimulated Mandelshtam-Brillouin scattering (SMBS), or sometimes more confusingly as STBS. We shall adopt the western convention in this thesis.

SBS can be described entirely classically[72-74] as a coupled three wave interaction involving the incident light wave (which from parametric interaction theory is often called the pump), a generated acoustic wave and the scattered Stokes (idler) wave. Quantum mechanical representations of the process have also been made[75,76]. The only notable difference in the predictions of the two theories is that the quantum mechanical theory predicts that the SBS process can be initiated even in the absence of an initial acoustic or Stokes wave, due to zero field fluctuations.

In the classical picture an electromagnetic field in a body produces an electrostrictive force density linearly dependent upon the product $(\partial\varepsilon/\partial\rho)E_iE_j$, where $\partial\varepsilon$ and $\partial\rho$ are respectively the change in the dielectric constant and density of the material. In the case of a single plane wave propagating through the medium, this force can be resolved into a static component and a component propagating with the velocity of light. The elastic deformation that can be produced by this electrostrictive force is greatly inhibited by the

mismatch between the propagation velocities of light and acoustic waves, and hence the propagation of the pump wave alone through the medium is not enough to generate an intense acoustic wave. However, if there exists in addition to the pump wave a secondary (Stokes) light wave of the appropriate frequency and direction, then by virtue of the cross terms generated in the electrostrictive force, a force propagating at an acoustic velocity may now be generated, thus leading to strong excitation of an acoustic wave. The acoustic vibrations lead to a time and space variation of the dielectric constant of the medium, which under the action of the pump wave produces a polarisation current that acts as the source of the secondary light wave. The acoustic wave thus couples the two electromagnetic waves. There now exists an amplification process, whereby energy is coupled from the pump wave to an acoustic wave and the Stokes wave. In optical fibres the intensity of the Stokes wave can build up to such large values that it can lead to 'cratering' of the input fibre end[77].

The source of the initial secondary wave is assumed to be from elastic scattering off thermal noise in the medium, and this is known as spontaneous Brillouin scattering. A competing process as the initiator for SBS is given by quantum mechanical considerations, where the spontaneous conversion of a pump photon into an acoustic phonon and Stokes photon can occur. This in fact would be the initiating process in the absence of any acoustic or Stokes wave in the medium.

The three waves obey the energy conservation law, which relates the three frequencies,

$$\omega_A = \omega_P - \omega_S \tag{3.2}$$

and maximum power transfer occurs when the wave-vector phase matching condition is achieved,

$$K_P = K_S + K_A \tag{3.3}$$

The subscripts A, P and S in Eq.3.2 & 3.3, refer to the acoustic, pump and Stokes waves respectively.

The vector relationship of Eq.3.3 is shown in Fig.3.1(a). Since the velocity of sound is smaller than the velocity of light, typically by a factor of approximately 10^5, it

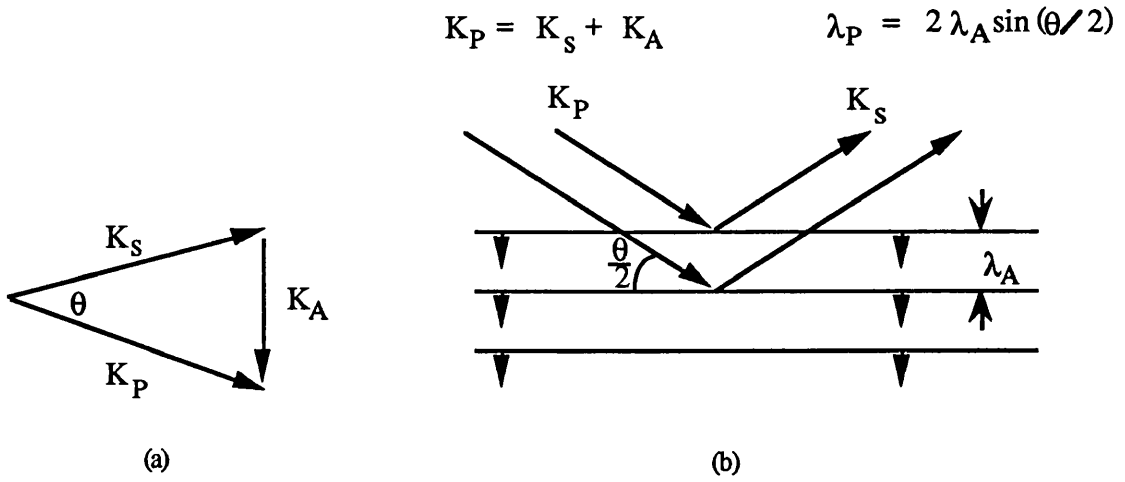

Figure 3.1 (a) The phase matching vector diagram for SBS. (b) The Bragg diagram equivalent of (a).

follows that the maximum sound frequency that can be generated, i.e., the maximum frequency shift, is approximately $10^{-5}\omega_P$. We can consequently assume to the same degree of accuracy that $K_P=K_S$ and obtain the following equation,

$$\omega_P - \omega_S = \omega_A = 2\omega_P\left(\frac{\upsilon_A n}{c}\right)\sin\frac{\theta}{2} \tag{3.4}$$

In Eq.3.4, θ is the angle between the incident and scattered wave vector, υ_A is the sound velocity of the scattering medium, and n is the refractive index. This equation was first derived by Brillouin in 1922[78] and independently by Mandelshtam in 1926[79]. As diagrammed in Fig. 3.1(b) the frequency shift given by Eq.3.4 is consistent with the Doppler shift experienced by a light wave incident at the Bragg angle $\theta/2$ on a sound wave receding at a velocity υ_A.

In single mode optical fibres the only allowable values of θ are 0 and π. Since, from the Bragg scattering model $\omega_A=0$ for $\theta=0$, forward Brillouin scattering is usually ignored, and the maximum frequency shift occurs in the backward direction with $\theta=\pi$. The frequency shift of the backscattered Stokes wave in pure silica is 13.2 GHz at 1.3μm. Such high frequency phonons are often known as hypersound in the literature. It should be noted however, that the actual propagation mode in single mode fibre has a finite angular width due to diffraction, and hence there may be a contribution of Brillouin scattering to the forward propagating light[80]. The phonon frequency of such a forward scattered component is below 1 GHz at 1.3μm. Since the amplification of the

Stokes wave is dependent upon the intensity of the pump wave, any depletion of this pump wave will effect the forward scatter much more than it will the backscatter, which will continue to experience an undepleted pump. Hence the forward scattered field components are many orders of magnitude down on the backscattered wave can thus often be ignored.

In optical fibres the anti-Stokes scattered component (where, $\omega_{AS} = \omega_p + \omega_A$ and which together with the Stokes makes up the Brillouin doublet) is not phase matched and so cannot occur due to SBS alone. However, end reflections and the process of four-wave-mixing can lead to the generation of anti-Stokes[81,82]. The properties of SBS in optical fibres are rather different in comparison to SBS in bulk optics. In bulk experiments θ can take any value, however because of the lack of the guiding nature of optical fibres, the interaction region is relatively small and focused geometries have to be used in order to achieve suitable intensities. Because the phonon wavelength is comparable to the dimensions of the fibre structure, it is possible that the acoustic waves may become guided within the fibre. This leads to a change in the phase matching conditions, as compared to the bulk optics case due to the dispersion in the guided acoustic modes.

3.2.1 Coupled non-linear wave equations.

In this section we review the coupled wave equations that can be used to describe the SBS process in optical fibres and that will be used in Chapter 4. The set of three coupled non-linear wave equations that completely characterise the SBS process are given by[72],

$$\left[\frac{\partial^2}{\partial z^2} - \frac{i\alpha_A}{K_P}\frac{\partial^2}{\partial z^2} + K_P^2\right]P(z) = \frac{\eta}{8\pi}\frac{\partial^2}{\partial z^2}[E_P(z)E_S^*(z)] \tag{3.9}$$

$$\left[\frac{\partial^2}{\partial z^2} - iK_S\alpha_o + K_S^2\right]E_S(z) = -\frac{\mu\omega_S^2\eta}{2\kappa}P^*(z)E_P(z) \tag{3.10}$$

$$\left[\frac{\partial^2}{\partial z^2} - iK_P\alpha_o + K_P^2\right]E_P(z) = -\frac{\mu\omega_P^2\eta}{2\kappa}P(z)E_S(z) \tag{3.11}$$

where P(z,t) is the acoustic amplitude, E_S and E_p are the Stokes and pump amplitude. α_A is the acoustic attenuation, α_o is the optical attenuation, μ is the permeability of the unstrained medium, η is equal to the product of the Pockel's elasto-optic constant and the square of the permittivity, ε, of the unstrained medium, and κ is a material constant. These coupled equations are derived by finding the solution to the non-linear wave equations describing the Stokes and pump waves, and the Navier-Stokes equation used to describe the acoustic wave.

Whilst these three coupled wave equations are completely general, they are often intractable analytically, and need lengthy numerical solutions. In cases where the attenuation of the acoustic wave is very large, as is the case of hypersound in most materials at room temperature, and where the slowly varying field approximations apply, the equations describing the process can be reduced to two greatly simplified coupled equations,

$$\frac{\partial I_S(z)}{\partial z} = -g(\omega_S)I_P(z)I_S(z) + \alpha_o I_S(z) \tag{3.12}$$

$$\frac{\partial I_P(z)}{\partial z} = -g(\omega_S)I_P(z)I_S(z) - \alpha_o I_p(z) \tag{3.13}$$

where,

$$g(\omega_S) = \frac{\mu h \omega_A \omega_S \gamma^2 K_A \upsilon_A^2 \alpha_A}{4\pi\kappa[4(\omega_S - \bar{\omega}_S)^2 + \alpha_A^2 \upsilon_A^2]} \tag{3.14}$$

I_p, I_s are the intensities of the pump and Stokes waves respectively, $g(\omega_s)$ is the gain of the process, and z is the distance travelled in the fibre with z=0 at the pump input end and z=L at the pump output end, where L is the length of the fibre and $\alpha_A \upsilon_A$ = acoustic damping constant Γ. Γ^{-1} is the characteristic phonon damping time. γ is the electrostrictive coefficient given by, $\gamma = \rho_o(\partial\varepsilon/\partial\rho)$, ρ_o being the material density.

Eq.3.12 shows that the rate of change of the Stokes photon flux in the -z direction contains an optical loss term and a gain term. The gain, which is due to stimulated Brillouin scattering, is proportional to the product of the intensities of the pump and Stokes waves, $I_p(z)I_s(z)$. The resonance denominator in the gain coefficient of Eq.3.14, shows the effect of the wave vectors not necessarily being perfectly matched,

and by measuring the full-width at half-maximum of the scattered Brillouin line we can have a direct measure of Γ.

Eqs.3.12 and 3.13 show that the rate of decrease of pump intensity in the +z direction, due to SBS, is exactly matched by the rate of increase of the Stokes intensity in the -z direction. Thus every pump photon scattered in the stimulated process leads to a backscattered Stokes photon. However, because of the large acoustic loss, every pump photon scattered does not also lead to a forward propagating phonon.

The presence of the optical loss terms in the coupled Eqs. 3.12 and 3.13 greatly complicates the solutions. Now, α_0 is often small compared to the other terms, and so except in threshold considerations, it is often neglected, and the exact solutions are given by,

$$I_P(z) = I_S(z) + I_P(0) - I_S(0) \tag{3.15}$$

with,

$$I_S(z) = \frac{I_S(0)[1 - I_S(0)/I_P(0)]}{\exp\{[1 - I_S(0)/I_P(0)]g(\omega_S)I_P(0)z\} - I_S(0)/I_P(0)} \tag{3.16}$$

In the limit of insignificant pump depletion with $I_S(0)/I_P(0) << 1$, Eq.3.16 can be re-written to give the output Stokes intensity after traversing the fibre of length L,

$$I_S(0) = I_S(L)\exp\{g(\omega_S)I_P(0)L\} \tag{3.17}$$

We can also define an effective length L_{eff}, different from the actual fibre length because the effective length for the gain is less than the actual length, due to attenuation, and is given by,

$$L_{eff} = \frac{1 - \exp(-2\alpha_0 L)}{2\alpha_0} \tag{3.18}$$

The main difficulty now is in determining the value for $I_S(L)$. One can see that there is clearly a difference between the case when SBS is being investigated in an amplifier-type configuration (where the Stokes wave is input externally), or a generator-type configuration (where the Stokes wave is built up from thermal noise). In the generator configuration we are guaranteed that the Stokes wave which is best correlated to the ideal phase matching condition will be the one that will experience the maximum gain

and hence survive the competition between modes at threshold. On the other hand, in the amplifier configuration, correlation of the Stokes wave to the pump is fairly arbitrary, and in the low-gain amplifier, the broadband gain may be substantially smaller than the narrowband steady-state gain. In the high-gain amplifier, the waves become correlated by the SBS process, irrespective of input conditions and the gain approaches the narrowband steady-state value. The rate equations 3.12 and 3.13 only apply to coherent pump and Stokes waves. However it can be shown that for the generator configuration where the initial Stokes is essentially noise distributed along the fibre, we can obtain an equivalent Stokes photon density per unit frequency that is input at a distance given by the reciprocal of the linear gain $[I_P(0)g(\omega_S)]^{-1}$, to represent the initial thermal noise[72]. Also the Landau-Plazeck material constant can give the ratio of Rayleigh to Brillouin backscatter at a particular temperature[83].

The linewidth of the Stokes line is found to be spectrally sharpened with increasing overall gain product, $I_Pg(\omega_S)L$, as is characteristic of all thermally exited maser type amplifiers. In the low gain limit ($I_Pg(\omega_S)L<<1$) the Stokes linewidth is equal to the acoustic damping constant Γ, and in the high gain limit ($I_Pg(\omega_S)L>>1$) the linewidth is found to vary as $\Gamma[In2/I_Pg(\omega_S)L]^{1/2}$.

The solutions to the rate equations also demonstrate that the backward propagating Stokes wave cannot continue to grow indefinitely, because of the finite intensity of the pump, and saturates whenever the Stokes intensity reaches within a few percent of the pump intensity, regardless of whether this is due to a long interaction length or high input Stokes intensity[72].

3.2.2 Dependence of SBS upon pump bandwidth.

In the above analysis the pump bandwidth was assumed to be narrow relative to the Brillouin linewidth. The effect upon the SBS gain of using a broadband pump (with a pump linewidth greater than the Brillouin linewidth) has also been extensively investigated[84-86]. Broadband pumping of the SBS generator configuration is found to affect the gain whenever the pump consists of two or more temporal modes separated by more than the SBS linewidth, or when the coherence length of the pump is shorter than the gain length of the SBS medium. Broadband pumping of the SBS amplifier configuration in the high gain limit is found to have little affect upon the gain. However in the low gain limit the broadband SBS gain is found to be much lower than the steady

state (narrowband pump) gain and is given by,

$$G_{BB} = G_{SS}\frac{\Gamma}{\Gamma \otimes \Delta V_L} \tag{3.19}$$

where G_{BB} is the broadband gain, G_{SS} is the steady state narrow band gain, ΔV_L is the linewidth of the pump (FWHM) and $\otimes$ denotes the convolution of the spectral densities of the pump and Stokes.

For the case where the pump wave is made up of two (or more) spectral lines there has been some controversy in the literature as to the exact nature of the response. Cotter[87] has suggested that a laser field consisting of two optical frequencies separated by Δv_m undergoes a phase change of π at a rate equal to Δv_m via a mode beating effect, and that providing the phase reversals occur at a rate faster than the spontaneous acoustic dephasing time Δv_B^{-1}, the acoustic wave is unable to build up to a significant amplitude and hence the gain is reduced. Cotter's results where later repeated, with slight modification by Tsubokawa *et. al*[88].

Lichtman *et. al.*[89] have also analysed the case of SBS exited by two pump waves in single mode fibre. Their model suggests that there can be interaction between the two pump laser frequencies provided that their separation is not much greater than the Brillouin bandwidth, after which the two pump waves act independently.

Following the model proposed in their paper, both pump waves, separated in frequency by Ω, interact with their corresponding Stokes mode and this is accompanied by the generation of a pressure wave at the frequency $\omega_0=\omega_p-\omega_s$. Besides these direct interactions are also the cross interactions (i.e. the interactions between pump m and stokes n, for $n \neq m$). These cross interactions generate two sidebands for the pressure wave at frequencies $\omega_0 \pm \Omega$. The intensities of these two sidebands are shown to be proportional to $1/(\Gamma^2 + \Omega^2)$, and hence when $\Omega >> \Gamma$, the two sidebands become negligible compared to the central pressure mode at ω_0. The physical meaning of this is that when the frequency separation is larger than the SBS linewidth, there are no cross interactions between the pump and Stokes waves, thus SBS is limited to interactions between the corresponding modes only. The intensity of the main central pressure wave is found to be composed of three terms, two corresponding to the direct interactions and also an oscillating third term due to the wave vector mismatch of the cross

interactions. This third term can lead to an enhancement or a suppression of the intensity of this pressure wave (and hence the SBS gain) and is determined by the relative phase between the two optical waves. This term oscillates with a spatial frequency of $\pi c/\Omega$. Since the characteristic gain length is typically much longer than this spatial period for the cases that we are considering, this term averages to zero. Hence, when the frequency separation of the two pump beams is much greater than the SBS linewidth, each beam interacts only with its corresponding Stokes beam and there are no cross terms. However, as expected for small values of Ω/Γ both direct and cross interactions contribute to the gain. Modifying the result given by Lichtman et. al. to encompass the real situation of non equal dual pump beam intensity, the normalised SBS gain is given by,

$$\frac{G_{\text{dual beam}}}{G_{\text{single beam}}} = \delta_1 + \delta_2 \frac{\Gamma^2}{\Gamma^2 + \Omega^2} \qquad (3.20)$$

where δ_1 and δ_2 are the normalised beam intensities.

The theoretical and experimental results of Cotter and Shibata are in direct contradiction with other reported observations that support Lichtman's model[90], where the gain of the SBS process is found to be independent of the number of longitudinal modes present in the pump laser, once the pump laser mode spacing exceeds the Brillouin linewidth (typically just by a factor of 5) and provided the laser coherence length exceeds the characteristic Brillouin gain length[89-91]. As the reported experimental results in Cotter's and Shibata's investigations where made in multi-kilometer length fibres with dual frequency inputs it is possible that the SBS suppression reported actually occurred because of competition with another non-linear effect[92], specifically Four Wave Mixing (FWM)[93]. The SBS process is found to be the more dominant process in systems where there is feedback (such as end reflections, or in a cavity) as was the case in Lichtman's experiment with relatively short lengths of fibre. Our own experimental investigations upon the effect of dual frequency pump beams also support Lichtman's model (cf.§.4.5).

The effects upon the SBS gain of various modulation schemes has also been extensively studied[94,95]. As one would expect, the gain decreases for increased modulation bandwidth. However, examination of the spectrum of the signals demonstrates that because of the fixed carrier component present in the spectrum of

frequency shift keying (FSK) and amplitude shift keying (ASK) schemes, the reduction in gain (with respect to the steady state gain) is limited to a factor of 2 for FSK modulation and a factor of 4 for ASK (with 100% modulation depth). For the phase shift keying (PSK) scheme, the gain is minimised when the phase shift is $(2n+1)\pi$ and the gain converges to zero as the modulation bandwidth increases. Thus PSK can be used to suppress undesired SBS effects in longhaul coherent communications systems[96]

3.2.3 Material considerations.

Writing Eq.3.14 in terms of material characteristics one obtains for the peak Brillouin gain in solids the following expression[97],

$$G_0 = (2\pi n^7 p_{12}^2 K/c\lambda^2 \rho_0 v_A \Gamma)(P/A)L_{eff} \qquad (3.21)$$

where p_{12} is the elasto-optic coefficient, λ is the optical wavelength, and K is a factor introduced to take into account the polarisation state of the pump. K=1 for identically polarised pump and Stokes wave along the interaction length, as would be found by launching linear polarisation in a polarisation preserving fibre. K=1/2 for a completely scrambled pump and Stokes wave, as one would find in a length of single mode non-polarisation preserving fibre[98,99]. P is the pump power and A is the effective core area, which is slightly different to the actual core area due to the Gaussian nature of the guided beam. When a fibre is operated near its cut-off frequency, the effective and actual core areas are nearly equal. For example for a V-number (normalised frequency) of 2.0 and 2.5, the effective area is larger than the actual area by a factor of 1.47 and 1.10 respectively. There exists a basic trade-off between the length of the interaction region (and hence also fibre attenuation), the effective area, and the power required for stimulated emission.

Core materials can be suitably chosen that maximise or minimise the SBS gain. For example Andrews germanium doped fibre has a gain approximately an order of magnitude larger than for York LB-600 fused silica fibres, however, it also suffers permanent damage at high field intensities[100]. On the other hand some of the heavy metal flouride glasses demonstrate low SBS gain and low attenuation. The halide glasses with molecules of greatest molecular weight and larger elastic constants tend to

show lower SBS gains. For example the halide glass, HBLA[101], demonstrates a reduction in the SBS gain by a factor 4 and an increase in threshold by a factor of 30 at attenuation of 0.318dB/km when operated at 2.55μm, when compared to a silicate fibre operated at 1.55μm with an attenuation of 0.114dB/km[102].

Γ is found to vary with wavelength as λ^{-2} thus, even though the gain tends to decrease with longer wavelengths, this decrease is offset by the narrowing Brillouin linewidth[103]. More significantly though, in fused silica, especially at the popular communication bands of 1.3μm and 1.55μm the fibre attenuation is greatly reduced leading to an increase in the effective length, so we can typically expect a lower SBS threshold at these wavelengths.

Stolen[98] has noted that it may be possible to artificially broaden the intrinsic SBS gain bandwidth of optical fibres by using suitable dopant materials in the core and cladding to grade the acoustic velocity across the effective core area. In this manner he was able to demonstrate an order of magnitude reduction in the peak Brillouin gain.

The temperature dependence of SBS has also been investigated for quartz and borosilicate glasses from 1.5 K to 300 K [104,105]. The variation in the phonon lifetimes, Γ^{-1} of the two glasses are very similar, being governed by a broad minimum at temperatures higher than 80 K (this minimum, being only 10% lower than the value at 300 K), due to a thermally activated structural relaxation process, and then increasing fairly linearly to approximately an order of magnitude higher at 4 K. In crystalline quartz, the phonon lifetimes vary by several orders of magnitude over the same temperature range.

In optical fibres, another important criterion to consider is whether the core and cladding material parameters can lead to the fibre acting as an acoustic waveguide. The basic criterion that needs to be satisfied to avoid guidance of acoustic waves within the optical fibre is that the longitudinal acoustic velocity within the core should be greater than that within the cladding. The discussion of this is deferred to §4.3.

3.3 Competing non-linear effects.

Determining which non-linear processes are active depends upon a number of factors. The non-linear process with the highest gain is the one that will dominate. Because of the narrow-band nature of SBS, under narrow-band or long pulse pumping it often has a gain typically a couple of orders of magnitude larger than the other non-

linear processes. Under conditions of broad-band, or short pulse pumping the SBS gain can be dramatically reduced[106], as described in §3.2.2 and stimulated Raman scattering (SRS), which benefits from a broadband pump due to its large bandwidth (approximately 400 cm^{-1} in fused silica) dominates. SRS generally also benefits from the suppression of SBS as this often depletes the pump.

Another competing non-linear process is as mentioned in §3.2.2, four wave mixing. FWM is a non-linear process whereby light of frequency ω_1 can be generated by mixing three waves of frequency ω_2, ω_3, and ω_4 that obey the relationship $\omega_1 + \omega_2 = \omega_3 + \omega_4$ (conservation of energy). ω_j (j=2,3,4) can be all the same frequency or different frequencies. The gain of the FWM process can be comparable to that of SBS in long lengths of fibre. FWM occurs along the entire length of the fibre and depletes the pump wave(s). If the depletion is significant and the frequency difference between the two waves much greater than the SBS linewidth, then this would lead to increased SBS threshold powers. Alternatively, if the SBS threshold is reached before FWM depletion occurs, then excess power is backscattered and the FWM process is frustrated. In all-fibre ring resonators where a lasing mechanism is established SBS becomes the only significant non-linear effect and hence initially SBS is the dominant effect. In straight lengths of optical fibre pumped with a broadband source or by pulses, FWM is found to be the dominant non-linearity in short lengths of fibre, but for longer fibre lengths SRS demonstrates more gain than FWM[107].

Once well above threshold, it is possible to have a combination of the various non-linear effects operating simultaneously. For example, if SBS is initially the dominant effect then the Stokes power can increase to such a level that it acts as a pump for the next Stokes order, and thus many Stokes orders can be obtained by such cascading. The presence of multiple frequencies of high intensity can then lead to FWM also becoming significant and leading to anti-Stokes generation and spectral broadening. The broad-band of signals generated can now act as a pump source for stimulated Raman scattering, and so on. In bulk systems self-focusing may also be present, further complicating the situation. In optical fibres, where the waves are already fairly tightly confined, the action of self-focussing is unlikely to have any significant effect. However, the phase matching between of the non-linear processes can be better controlled in optical fibres by such effects as fibre dispersion or birefringence over long interaction lengths[107,108]. This is more important for FWM, as this requires more

control to achieve phase matching, whereas stimulated Brillouin and Raman scattering may be viewed as self phasematching. Intensity dependent refractive index effects, such as self phase modulation and Kerr instabilities[109,110], can lead to further modulation of the signals.

3.4 Applications of SBS.

Stimulated Brillouin scattering is often the only possible method for exciting a strong hypersonic wave within a material, and the frequency shift and linewidth of the stimulated Brillouin Stokes line can yield valuable information about material characteristics. The frequency shift is a sensitive function of material composition, and in optical fibres has been used to provide precise information about the level of dopant concentration and power distribution[111]. The frequency shift also enables elastic and photoelastic constants of the material to be determined[112-114]. The Stokes linewidth, provides data on scattering loss and attenuation at hypersonic frequencies. This has proved to be a powerful tool for investigating structural changes within the material with temperature change[105].

Zel'dovich et. al.[115], were the first to demonstrate that under certain conditions the Stokes wave generated by the SBS process is the phase conjugate of the pump wave. Phase conjugation (or wave front reversal) in multimode waveguide structures was found to require small amounts of added aberration to produce better fidelity of the phase conjugated beam. Fidelity is the term used to describe the accuracy of the wave front reversal, and can be defined as the fraction of the backscattered light that is diffraction limited after passing twice through an aberrator. Phase conjugation opens up many applications for SBS, and has been used successfully to combine the output of several laser amplifiers, as well as correcting for the phase distortions due to the inhomogeneities within the amplifiers[116,117]. Since the phase of the scattered (reflected) light in SBS has no temporal reference, the phase difference between conjugated beams from different interaction volumes will be random. This can be avoided by utilising the same interaction volume or, by backinjection of a Stokes seed[118]. We can consider that the scattering by SBS makes the active material act as a Brillouin mirror. The directionality, high reflectivity and threshold nature of the effect have also been used to isolate the output of laser amplifiers from the master laser oscillators, and this has been particularly beneficial for the study of laser mediated

thermonuclear fusion[119]. The major disadvantage of phase conjugation via SBS is the frequency shift of the Stokes, which can cause problems for narrowband laser amplifiers or transmission over long distances. Another non-linear process that can be used for phase conjugation is four wave mixing.

Olsson and van der Ziel were the first to show that the SBS process can be utilised to make in-line fibre amplifiers[120]. The narrowband nature of SBS can be put to advantage by using it to selectively amplify the carrier prior to photodetection and allow quantum limited detection, or to allow channel selection in densely packed wavelength division multiplexed systems[121,122]. The bandwidth of the gain can be artificially expanded by the addition of suitable dopant gradients or by dithering the pump frequency[123].

If the length of the interaction region is finite then strong relaxation oscillations of the the pump and Stokes frequency, that decay down to the steady state value are found to occur[124]. The period of the oscillations is equal to the roundtrip time of the interaction region. This is because strong depletion of the pump by the Stokes wave chokes off the generation of more SBS. The relaxation oscillations occur at a period equal to the roundtrip time through the fibre, as this is the time required for the Stokes to completely sweep through the interaction region. Full analysis of this effect requires the use of the coupled SBS Eqs. 3.9 to 3.11, which shows that relaxation and steady oscillations are also found to occur whenever there is external feedback of the Stokes wave[125].

In fibre ring resonators pumped with cw light such relaxation oscillations have been shown to lead the generation of periodic trains of short pulses[66,125]. This can be attributed to phase synchronisation (mode locking) of the longitudinal modes in the first order Stokes components that fall under the Brillouin gain bandwidth by the oscillations. This can cause problems in the operation of fibre ring Brillouin lasers, as the output can become spontaneously noisy, because of the mode-locking. The best way to avoid this is to ensure that the cavity length of the ring resonator is such that only one cavity mode overlaps with the SBS gain bandwidth.

Phase conjugated pulse compression and pulse shaping by means of SBS with high efficiencies has also been demonstrated[126]. The interaction region should be approximately half the input pulse length, then the incident pump energy is swept up and turned around within a distance equal to the thickness of the bulk grating SBS mirror, which is the leading edge of the phonon envelope that sweeps backward at the speed c/n. In such a fashion a 20ns pulse has been compressed to a 2ns pulse.

Chapter 4

EFFECTS OF STIMULATED BRILLOUIN SCATTERING ON THE PERFORMANCE OF POLARISATION MAINTAINING ALL-FIBRE RING RESONATORS

The all fibre ring resonator can be used to form an interferometric sensor of any parameter (such as pressure or temperature) that affects the propagation constants of the light guided within the fibre cavity. The response of the device can be optimised by adjusting several resonator parameters. The sensitivity of the device to a particular measurand can be increased by applying suitable coatings to the fibre loop[127]. Lower fibre optic component losses and hence higher resonator finesse values, can greatly enhance the resonators phase sensitivity, and longer cavity loop lengths can improve the scale factor between this loop phase and the measurand. High launch powers are also desirable, in order to reduce shot noise and hence maximise signal to noise ratios.

Developments in optical fibre technology have already led to the realisation of high finesse fibre ring resonators. We have reported upon resonators made with 633nm polarisation maintaining fibre with a finesse of 600[17], and have also fabricated a single mode (633nm, non-polarisation preserving) fibre resonator with a finesse of 1000. It seems likely that these values will readily be surpassed in the near future.

Most sensor applications require the ring resonator to behave in a passive manner. Thus, the onset of optical non-linear phenomena can place an upper limit upon the allowable increases in resonator loop length, finesse and input power. The principal non-linearity in coherent fibre systems with feedback is as outlined in Chapter 3, stimulated Brillouin scattering (SBS). The onset of SBS in ring resonators can occur at relatively low input powers. In high finesse polarisation maintaining optical fibre ring

resonators (PMRRs) the threshold input pump power levels for SBS are greatly reduced for three main reasons. First, the ring resonator geometry affords a significant circulating pump power enhancement factor. Second, the polarisation maintaining nature of the fibre ensures that both the pump wave and the scattered wave have the same polarisation state, thus maximising the SBS gain factor. Third, because of the low loss nature of the device the round trip non-linear gain need be only a few percent. Circulating loop powers can thus often be above SBS threshold, even for very low input powers.

Previously with moderate finesse and loop length combinations, the limitation upon the maximum allowable input power was not too unreasonable. However, with input SBS threshold levels now in the μW level for state of the art fibre resonators[18], the effects of the onset of SBS upon the transmission characteristics of the fibre ring resonator need to be investigated. This chapter presents a detailed theoretical and experimental study of these effects. The dependence of the SBS process upon resonator parameters, such as coupling constant and loop length is investigated, and the effects of fibre parameters also discussed. Solutions to suppress SBS in ring resonators are then investigated, with a view to increasing the regime of passive operation of the device.

4.1 SBS Depletion Effects in Ring Resonators.

Coherent operation of the passive ring resonator leads to a very versatile and sensitive device. However, once the threshold for stimulated Brillouin scattering within the all-fibre ring resonator is exceeded, the resonator is no longer passive and one may consider the device as a stimulated Brillouin ring laser, being pumped by the input wave and lasing at the Stokes frequency. The consequent depletion of the input wave (pump) via the SBS process leads to the transmission characteristics of the device being altered. The nature of these variations is investigated in this section.

From Fig. 4.1, we can see that in propagating through the fibre loop of length L, the pump wave input at port (1), suffers a linear fibre attenuation given by $\exp(-2\alpha_0 L)$ and an additional attenuation given by $\exp(-gP_S L/A)$ (from Eqs.3.12 and 3.13) due to depletion via the generation of SBS in the opposite direction. The backward scattered Brillouin frequency shifted wave is amplified by a factor given from Eq.3.17, by $\exp(gP_C L/A)$, where P_C is the circulating pump power. A small fraction of the backwards travelling Stokes wave is tapped out at port (1) and adds coherently on each

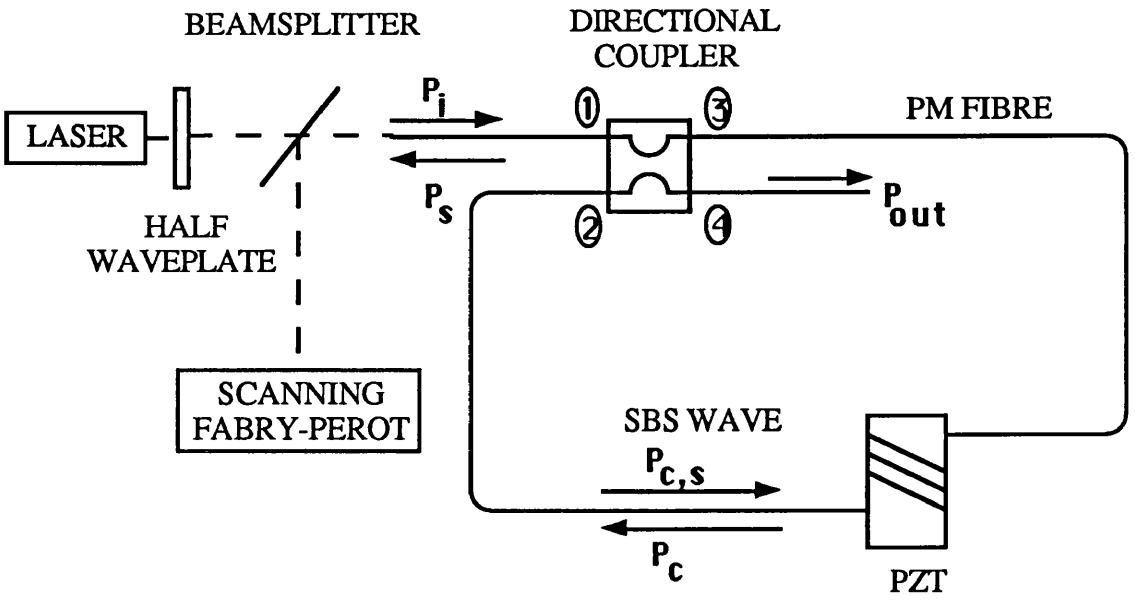

Figure 4.1 Experimental schematic for monitoring SBS in a PMRR. PZT, piezoelectric transducer; $P_{c,s}$, circulating Stokes power; P_i, input pump power; P_s, Stokes power; P_c, circulating pump power.

circulation to give an output power from port (1).

In order to estimate the enhancement of the circulating pump power to the input power, in the absence of non-linear effects, we refer back to Eq.2.31, and recall that the second term of this equation represents the component of the circulating intensity that is coupled out at port 4. The case of an isotropic PM coupler with perfect projection, e, of an input wave onto one of the resonator eigenstates yields $e=\sqrt{(1-\gamma)(1-\kappa_r)}$, where γ and κ_r are the isotropic coupler intensity loss and resonant coupling constant respectively. Thus the enhancement of the circulating power at resonance over the input is given by,

$$\left|\frac{E_3}{E_1}\right|^2 = \frac{(1-\gamma)}{(1-\kappa_r)} \tag{4.1}$$

Also for κ_r near unity, Eq.2.37 can be easily approximated by letting $\sin\left[(1-\kappa_r)/2\sqrt{\kappa_r}\right] \approx (1-\kappa_r)/2\sqrt{\kappa_r}$. The finesse can then be written as,

$$F \approx \frac{\pi\sqrt{\kappa_r}}{1-\kappa_r} \tag{4.2}$$

Now, for high finesse devices, since γ_0 is small and $\kappa_r^{1/2} \approx 1$, combining Eqs. 4.1 and 4.2 yields the desired result,

$$\left|\frac{E_3}{E_1}\right|^2 = \frac{P_c}{P_i} \approx \frac{F}{\pi} \tag{4.3}$$

Eq.4.3 demonstrates that for high finesse values the enhancement of the circulating pump power over that of the input pump power is correspondingly large.

4.1.1 Saturation of Circulating Pump Power.

For the condition of negligible pump-power depletion via the SBS process, the threshold value for the circulating power $P_{c,th}$ occurs when the SBS gain is equal to the loop losses and is obtained when the product of the roundtrip gain, $\exp(gP_{c,th}L_{eff}/A)$ and the transmission $(1 - \gamma_0)\kappa_r.\exp(-2\alpha_0 L)$ round the loop is unity[128]. Thus,

$$(1 - \gamma_0)\kappa_r.\exp(-2\alpha_0 L).\exp(gP_{c,th}L_{eff}/A) = 1 \tag{4.4}$$

To good approximation we have $1-\gamma_0 \approx e^{-\gamma_0}$ and $1-2\alpha_0 L \approx e^{-2\alpha_0 L}$ (therefore from Eq.3.18, $L_{eff} \approx L$), and the threshold for the circulating pump power is found to be,

$$P_{c,th} = \frac{2A}{gL}(\gamma_0 + 2\alpha_0 L) \approx \frac{2A}{gL}\frac{\pi}{F} \tag{4.5}$$

Combining Eq.4.5 with 4.3 gives the threshold input pump power,

$$P_{i,th} \approx \frac{2A}{gL}\frac{\pi^2}{F^2} \tag{4.6}$$

This equation demonstrates that the SBS threshold is strongly influenced by the resonator finesse and that in high finesse ring resonators, the threshold for the onset of SBS can occur at the μW input pump level. For example in a 10m loop length resonator with a finesse of 200, fibre core diameter of 5μm and an SBS gain of $4.2\text{x}10^{-11}$ mW^{-1},

the input threshold from Eq.4.6 is found to be 46μW. This low threshold level is readily surpassed in most systems.

Eq.4.4 also gives the maximum steady state level of circulating pump power in the ring. If the circulating pump power level is greater than the threshold value, the product exceeds unity and more SBS is generated and the pump further depleted, essentially experiencing an additional loss in power level. Therefore the recirculating pump power remains constant for increase of input power, but the generated SBS power increases. Hence, the depletion effect of the SBS process saturates the circulating pump power to the circulating pump threshold level and Eq.4.3 is no longer valid.

The generation of the backscattered Stokes wave (and hence the depletion of the pump wave), is transient in nature during the resonance buildup of the circulating powers. This situation can be modelled on a computer, by considering the loop transit by transit build-up of the circulating pump power, the corresponding generation of Stokes power and the consequent pump depletion. The governing equations for the output Stokes level, $P_{Sn_{out}}$, and the circulating pump power P_{Cn} after n transits are,

$$P_{S(n)_{out}} = P_{S(n-1)}(1-\kappa)(1-\gamma_o)\exp(-2\alpha_o L)\exp(gLP_{c(n)}/A) \tag{4.7}$$

$$P_{c(n)} = [E_1(1-\kappa)^{1/2}(1-\gamma_o)^{1/2} + E^{1/2}_{c(n-1)_{dep}}\kappa^{1/2}(1-\gamma_o)^{1/2}]^2 \tag{4.8}$$

$$P_{c(n)_{dep}} = P_{c(n)}\exp(-gLP_{S(n-1)}/A - 2\alpha_o L) \tag{4.9}$$

Eq.4.7 represents the output component of the circulating Stokes wave. Eq.4.8 is the pump amplitude at port 3 at resonance, where use is made of the fact that at resonance the field amplitudes within the ring can simply be added. Eq.4.9 is the single transit attenuation (linear and non-linear) experienced by the pump once it reaches port 2.

Fig. 4.2 illustrates the transient build up of the pump and Stokes waves, for a step function input. The response is modelled for a 1m PM resonator, with coupler intensity loss of γ=0.008, fibre attenuation of 8.5dB (F=308), SBS gain $g=4.2\times10^{-11}mW^{-1}$ and core area $1.49\times10^{-11}m^2$, when an input pump power of 208μW is launched. Curve 4.2(a) represents the build-up in circulating pump power when the effects of SBS depletion are not taken into account, demonstrating that approximately 21mW of steady state circulating pump power would be expected. However, curve 4.2(b) demonstrates that when SBS depletion effects are taken into account, the circulating pump power is

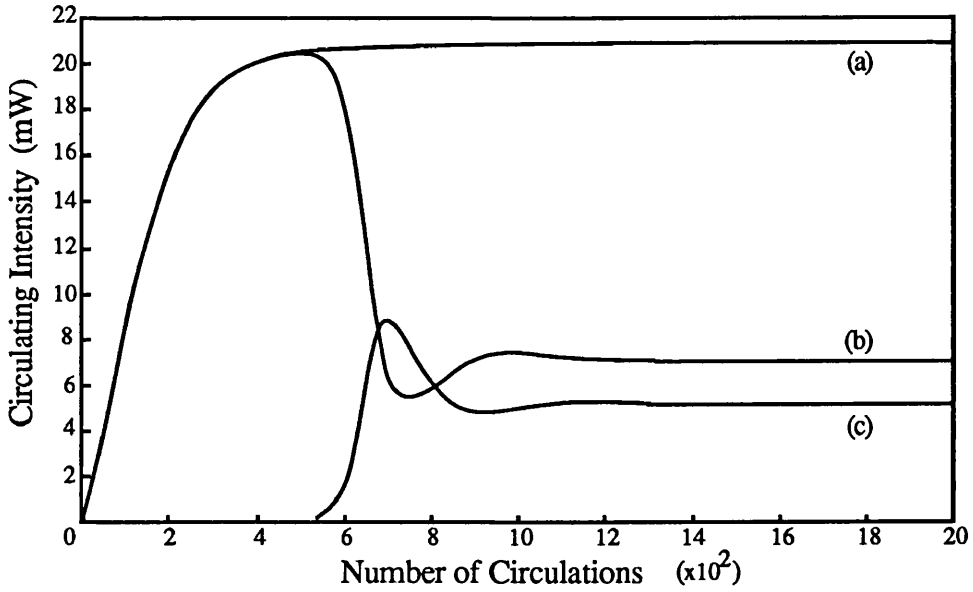

Figure 4.2 Theoretical transient build-up of circulating (a) pump intensity when SBS depletion not taken into account, (b) SBS depletion taken into account and, (c) corresponding Stokes intensity, for an input pump intensity of 208μW

clamped to the threshold level. The transient damped oscillations about the final steadystate value are found to be dependent upon the input pump level, the SBS gain and losses of the ring resonator. The larger the product of input pump and SBS gain the shorter the transient response time. For low input pump-SBS gain products, the circulating pump intensity can reach the non SBS depleted steady state circulating intensity, and remain at this level for many hundreds of loop circulations, before the Stokes power is built up to a sufficient level to begin to significantly depleting the pump and a transient response similar to the one shown follows. This increased transient response time of the SBS depleted resonator as compared to the non SBS depleted resonator, naturally increases the necessary integration time required to obtain a steady state response from the resonator. Curve 4.2(c) demonstrates the corresponding circulating Stokes wave generated for the SBS depleted resonator. Again, it demonstrates a similar transient build-up to that shown by the pump. Note, that the peak in this transient is greater than the steady state value and occurs when the depleted circulating pump first reaches the SBS threshold level. This transient peak cannot be maintained and it settles down to its steady state value. The sum of the SBS depleted circulating pump and Stokes waves do not equal that of the non-SBS depleted pump since modulation depth of the resonator is no longer 100% (as shown in the next section), and some of the pump exits the resonator at port (1). The system of Eqs.4.7-

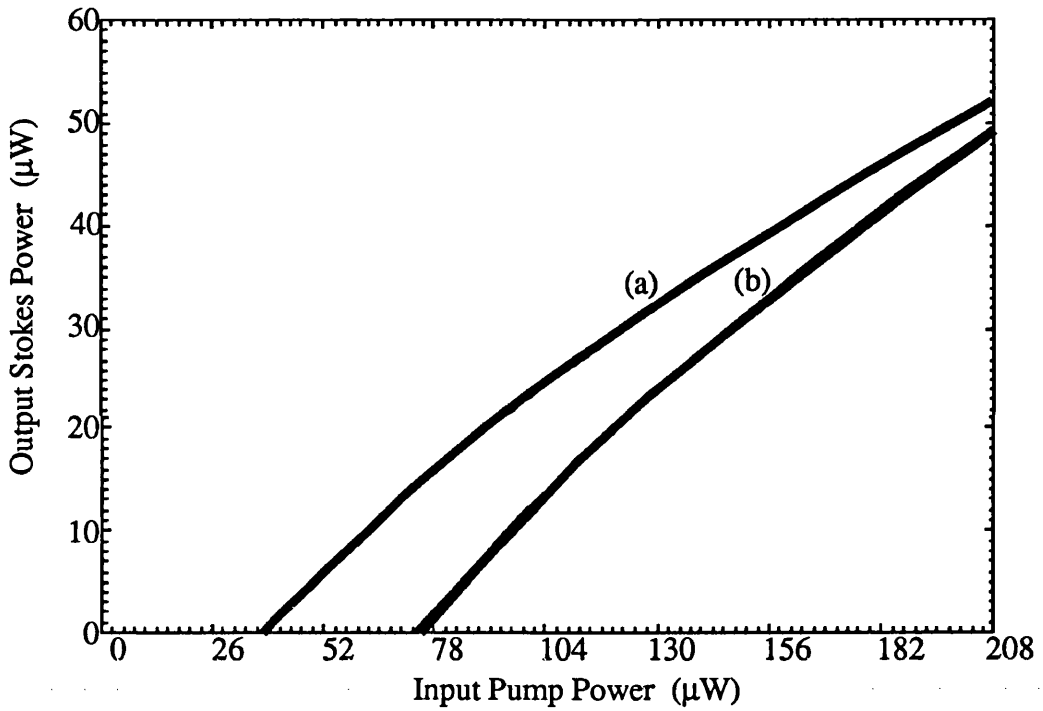

Figure 4.3 Theoretically detected Stokes level at output of 1m resonator, F=314, for (a) the slow axis. $A=0.855\times10^{-11}m^2$ and (b) the fast axis, $A=1.49\times10^{-11}m^2$, as a function of input pump power. $g=4.2\times10^{-11}mW^{-1}$.

4.9 were found to be relatively insensitive (compared to the other parameters) to the initiating Stokes noise level, $P_{S(0)}$, provided it was below 10nW. For higher initial Stokes levels the device demonstrated the expected amplifier type response.

Within the type of York 633nm Bow-Tie polarisation maintaining fibre investigated the core was found to be slightly elliptical and the diameters of the fast and slow axes are 4.36μm and 3.3μm respectively (cf: table 2.2). This indicates that SBS threshold levels for each axis would be expected to be different. Fig. 4.3 shows the threshold nature of the SBS response by plotting the Stokes output power for the resonator of Fig. 4.2 as the input pump power is scanned. The expected response for each polarisation axes is shown and the PM coupler anisotropy parameter h, is assumed to equal 0 dB (although, this generally is not the case), to demonstrate the difference in threshold. The conversion efficiency of the SBS process can also be seen to saturate at higher pump powers.

The optimum loop length for maximising the generation of SBS within the ring can be shown to occur once the linear attenuation of the length of fibre in the loop $2\alpha_o L_{opt}$, is equal to the coupler intensity loss γ_0 [128]. Fig. 4.4, is a plot of the SBS input pump threshold for $\gamma_0=0.008$ and $\gamma_0=0.02$, obtained from the set of Eqs 4.7-4.9. For loop

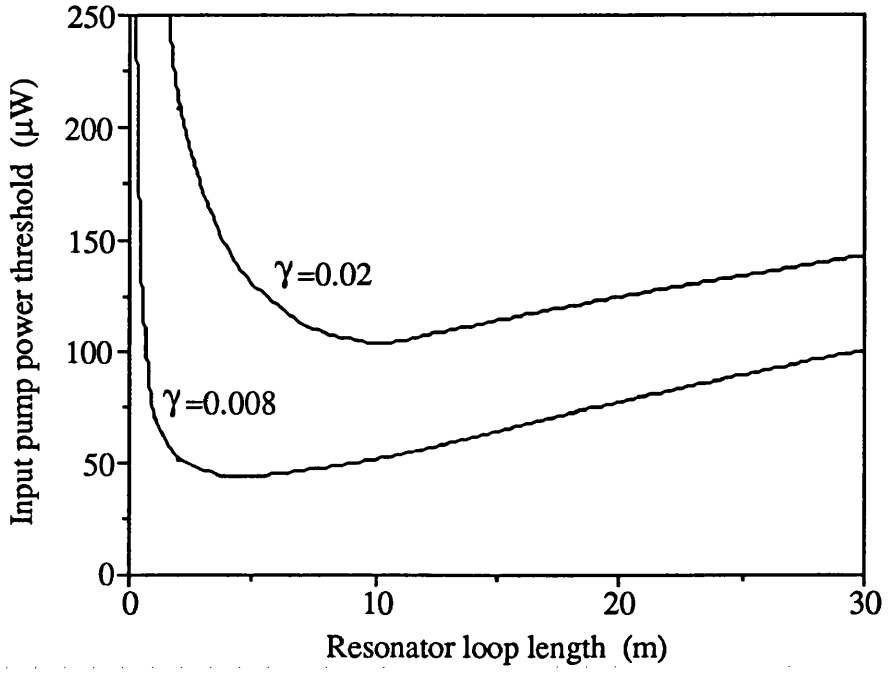

Figure 4.4 Theoretical threshold input pump power as a function of resonator loop length L, with fibre attenuation 8.5dB/km for coupler losses of 0.8% and 2%.

lengths shorter than the optimum, the finesse (and hence P_c) remain roughly constant, being dominated by the coupler losses, while the interaction region decreases, causing the threshold power to rise rapidly. For loop lengths longer than optimum, the finesse (and P_c) decreases, but this is offset by the increase in the interaction region. Hence it is seen to be generally better to chooses loop lengths longer than the optimum, so that the tolerances required in controlling the loop length during fabrication of the ring resonator can be relaxed.

The increase in the level of Stokes power generated, with input pump power, continues until the limit that the level of backwards travelling SBS itself exceeds the SBS threshold level and in turn generates secondary SBS that travels in the same direction as the original pump power. The secondary SBS will be frequency shifted from the original pump by twice the Stokes frequency.

4.1.2. Dependence of Ring Resonator Performance Characteristics upon Resonator Coupling Constant.

The implications of the saturation of the circulating pump power due to SBS in the ring, are intensity dependent variations in the performance characteristics of the device.

The generation of SBS in the ring can be considered as an intensity dependent loss, and the effect of this loss upon the performance characteristic of the resonator depends upon whether the intensity coupling constant is optimised at each new input power or whether it is optimised either at powers above or below SBS threshold and then fixed.

When the resonator coupling constant is adjusted to compensate for the total roundtrip loss, for an input pump power above SBS threshold, then the finesse observed at this input power can be found from Eq.4.3 and is given by,

$$F \approx \frac{\pi P_{c,th}}{P_i} \tag{4.10}$$

where the circulating pump is now clamped to the threshold level. The inverse relationship between the finesse and input power shows how the measured finesse of the device deteriorates rapidly with increases in input powers above the SBS input threshold.

For the case of a fixed coupling constant, both the measured finesse and modulation depth of the device are altered with variations in input power, and this is a direct consequence of the circulating pump power being maintained at the threshold level.

For a general value of intensity coupling constant κ, the circulating and output powers for an isotropic PMRR, with only one eigenstate excited can be shown to be[52],

$$\left|\frac{E_3}{E_1}\right|^2 = \frac{(1-\gamma_o)(1-\kappa)}{(1-\bar{\kappa})^2 + 4\bar{\kappa}\sin^2\left(\frac{\beta L}{2} + \frac{\pi}{4}\right)} \tag{4.11}$$

$$\left|\frac{E_4}{E_1}\right|^2 = \frac{(1-\gamma_o)\left[(\kappa-\bar{\kappa})^2/\kappa + 4\bar{\kappa}\sin^2\left(\frac{\beta L}{2} + \frac{\pi}{4}\right)\right]}{(1-\bar{\kappa})^2 + 4\bar{\kappa}\sin^2\left(\frac{\beta L}{2} + \frac{\pi}{4}\right)} \tag{4.12}$$

where $\bar{\kappa}=\kappa^{1/2}(1-\gamma_0)^{1/2}\exp(-\alpha L)$ and α is the (linear, α_0, and non-linear, gP_SL/A) pump transmission loss through the fibre.

Now, at resonance the output will be non-zero and the maximum circulating power within the loop is given from Eq.4.11 by,

$$\left|\frac{E_3}{E_1}\right|^2_{max} = \frac{(1-\gamma_o)(1-\kappa)}{(1-\bar{\kappa})^2} \tag{4.13}$$

Following the analysis in §2.2.2, by equating Eq.4.11 with $\frac{1}{2}[E_3/E_1]^2_{max}$ to determine the resonator linewidth, one obtains an equation for the finesse exactly the same as Eq.4.2 except that κ_r is replaced by $\bar{\kappa}$,

$$F \approx \frac{\pi\sqrt{\bar{\kappa}}}{1-\bar{\kappa}} \tag{4.14}$$

Re-writing Eq.4.14 as a quadratic of $\bar{\kappa}$, and noting that $\bar{\kappa} < 1$, we can determine the value of $\bar{\kappa}$.

The modulation depth, ς, of the resonator response is defined as the percentage reduction in output level at resonance, as compared to the output level off resonance. Hence from Eq.4.12 we can derive that the modulation depth is given by,

$$\varsigma = \left\{1 - \frac{(\kappa-\bar{\kappa})^2}{\kappa(1-\bar{\kappa})^2}\right\} \times 100\% \tag{4.15}$$

Now, since $\bar{\kappa}$ is known, we can determine the value of κ by re-writing Eq.4.15 as a quadratic in terms of κ. Hence, at powers below the SBS threshold, if α_0 is known, one can determine the value of the coupler intensity loss γ_0 by measuring the finesse and modulation depth. Then once the circulating power is above the SBS threshold level one can determine the non-linear attenuation of the pump, gP_SL/A.

The expected variations in Stokes output, measured finesse and modulation depth with input power can be calculated with the aid of Eqs.4.7-4.9 and Eq.4.14 and Eq.4.15. The case for the coupling constant optimised at powers below and above SBS threshold is illustrated in Fig. 4.5. Optimising the coupling constant at pump powers below SBS threshold, is found to lead to the lowest threshold level. However, optimising the coupling constant at pump powers above SBS threshold, whilst increasing the SBS threshold level, is found to lead to enhanced output Stokes levels.

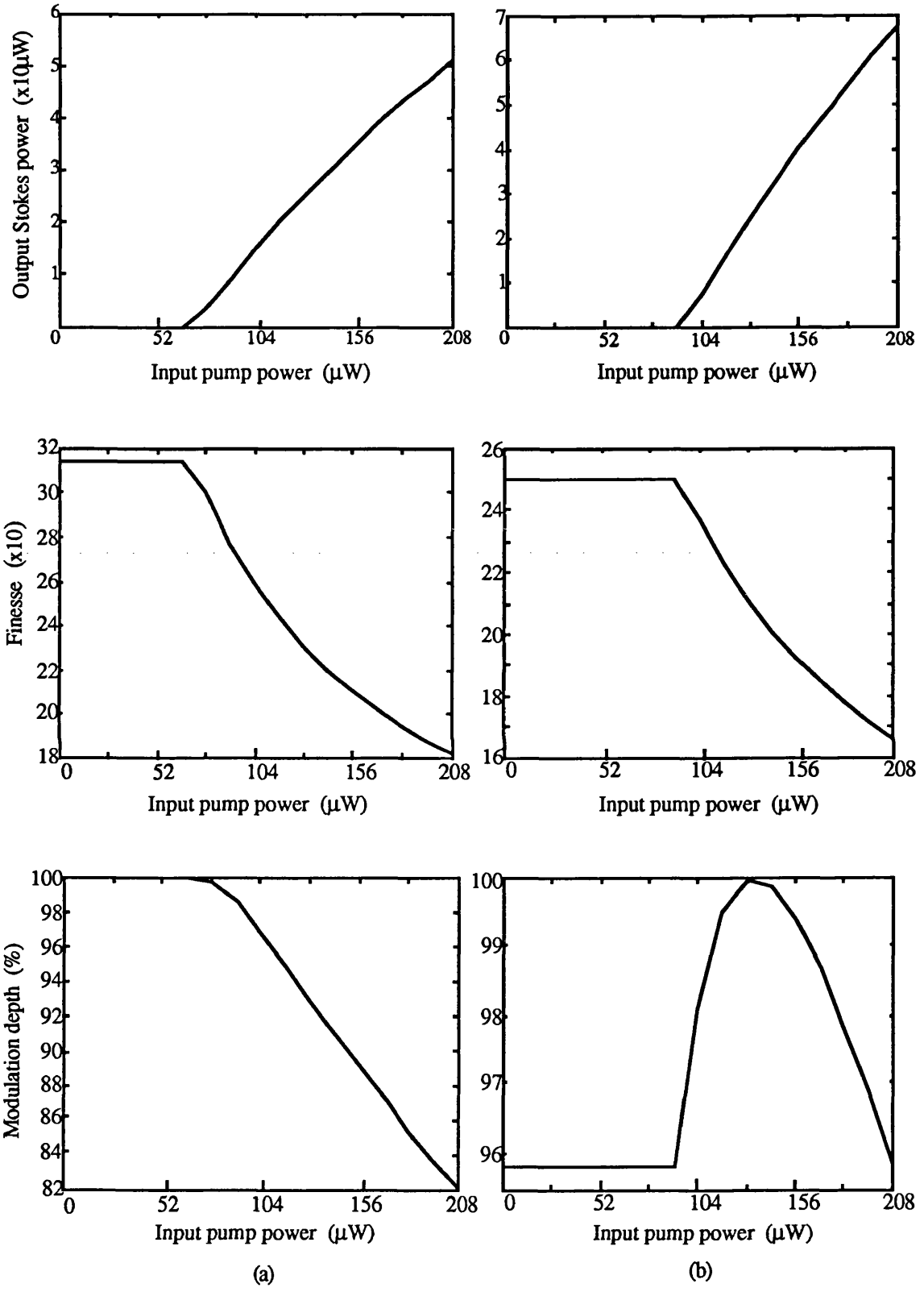

Figure 4.5 Variation in output Stokes level, finesse, and modulation depth, in a 1m PMRR with γ=0.008 and in column (a) coupling constant, k=0.99 optimised below threshold and in column (b) k=0.985 optimised above threshold. Other parameters same as those used in Fig. 4.2.

This can be understood by reference to the theoretical plots on the variation in measured finesse and modulation depth. For both cases, the measured finesse is deteriorated once threshold is exceeded. However, whilst the modulation depth for the first case simply decreases above threshold, for the latter case it actually increases until the loop losses (linear and non-linear) equal the coupling into the loop. Thus, the enhancement of the input pump is improved, and hence the generated Stokes power is increased.

It should be noted that Eq.4.10 is valid only as a first approximation. This is because the non-linear attenuation has implicitly been assumed to be constant for all values of loop phase. However, the circulating pump power decreases as we move away from the resonance dip along the resonance curve and hence the non-linear attenuation is not actually constant. This variation in the Stokes power generated with loop phase is shown in Fig.4.6 (of the experimental section), which represents the Stokes power detected at port 1 as the resonance dip is sinusoidally scanned. In the extreme of high SBS gain there is effectively clipping of the resonance dip, and Eq.4.10 breaks down. However, in the range of pumping employed in the experimental investigations of §.4.2, Eq.4.10 was found to hold quite well. The exact response of the ring resonator to SBS depletion is easily obtained from the set of Eqs.4.7-4.9 slightly modified to take into account loop phase.

4.1.3. Optimum Beamsplitter Ratio.

The choice of splitting ratio of the beamsplitter shown in Fig.4.1, placed at the pump input end of the resonator presents a trade-off between the transmitted input pump power (and hence the amount of Stokes power generated within the ring) and the amount of Stokes power tapped off by the beamsplitter to be detected. From Fig. 4.3, at pump powers outside the saturation regime, the output Stokes level can be seen to be approximated by a straight line with gradient m and crossing the x-axis at the threshold power. If we assume a pump input to the beamsplitter of I_{in}, and a beamsplitter transmission of T and a reflection of 1-T, then the Stokes power tapped off by the beamsplitter can readily be shown to be given by $(I_{in}mT-I_{th})(1-T)$. Differentiating this with respect to T to find the minimum yields,

$$T_{opt} = \frac{1}{2} + \frac{I_{th}}{2mI_{in}} \qquad (4.16)$$

Eq.4.16 which is valid only for $I_{in}T > I_{th}$, suggests that if the input power is expected to be much higher than the threshold power, the splitting ratio should be 50:50 to maximise the amount of tapped Stokes wave.

4.2. Experimental Investigation of SBS Depletion Effects.

4.2.1 Experimental Set-up.

Several ring resonators made of York Bow-Tie 633nm polarisation maintaining fibre were investigated including the 1m loop length device with a demonstrated finesse of better than 600, and the 4.15m loop length device with a finesse of 250 investigated in Chapter 2. The fibre used had a quoted attenuation of 8.5 dB/Km at this wavelength, and refractive index and core diameter parameters as given in table 2.2.

The experimental schematic of Fig. 4.1 was used to investigate SBS lasing in the PMRRs. The source used to characterise the resonator was a single frequency stabilized HeNe laser (λ=0.6328μm). The output power of the device was specified as 0.8mW. The HeNe tube used actually has an output power of 5mW and has 2-3 longitudinal modes separated by 650MHz under its gain curve. By making use of the fact that the polarisation states of alternate longitudinal modes in a HeNe laser are linear and orthogonal, a polariser can be used to filter out only one longitudinal mode. The frequency of this mode is stabilised by monitoring either the ratio of the power in the orthogonal polarisation modes or by monitoring the absolute power level of the chosen lasing mode. Feedback can then be achieved by controlling the laser temperature (and hence cavity length) by means of a heating coil. By slightly modifying the output optics of the HeNe laser and adjusting the feedback electronics to ensure that the desired lasing mode falls under the peak of the HeNe lasing gain curve it is possible to almost double the specified output power to 1.5mW, whilst still ensuring stabilised single frequency operation. This modification gave an output power level, higher than any commercially available stabilised single frequency HeNe lasers. It may be possible to achieve higher single frequency powers by using longer HeNe tubes with much higher gain, and consequently more longitudinal modes. The two neighbouring lasing modes under the peak of the gain curve can then be selected by means of a Fabry-Perot etalon and the laser stabilised in the same fashion as above. Stabilised single frequency output powers of up to 10mW may be achievable with this technique.

A length of the resonator fibre was wrapped around a PZT cylinder and a low rate

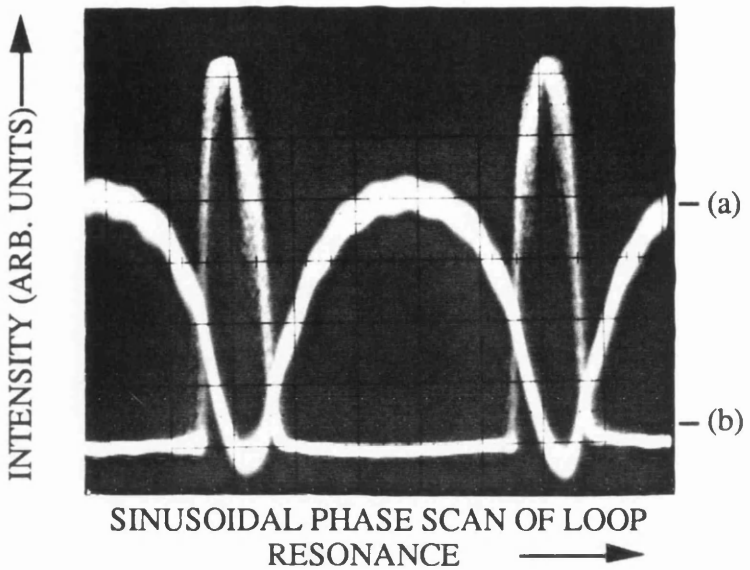

Figure 4.6 Detected backscatter as resonance dip sinusoidally scanned. (a) Resonator output, (b) Backscatter output.

(<50Hz) triangular voltage waveform applied to it to scan the phase response of the device.

The pump light was polarized by a 50dB Glan-Thomson polariser and aligned to one fibre axis, by one of the imaging techniques described in §.2.3. The level of input power was varied by means of attenuation plates at the output of the laser. The resonator response is locked onto resonance by means of the path length control electronics described later in §.4.2.3. A 50:50 beam-splitter was used to tap off the backscattered Stokes wave, which was then observed on a scanning Fabry-Perot etalon.

4.2.2. SBS Lasing in Polarisation Maintaining Fibre Ring Resonators.

As mentioned above SBS lasing only occurs over those regions of the resonance dips in which the circulating pump is above threshold. This is clearly demonstrated in Fig.4.6, which is a photograph of the detected backscatter as the resonator is scanned sinusoidally about its resonance point, and pumped above threshold. Increasing the pump power increases the section over which SBS lasing occurs.

Fig. 4.7 shows the trace recorded from a 7.56 GHz FSR Fabry-Perot etalon used to observe the backscatter in the 4.16m loop length PMRR. The position of the other HeNe laser longitudinal mode is also purposely shown (by slightly misaligning the

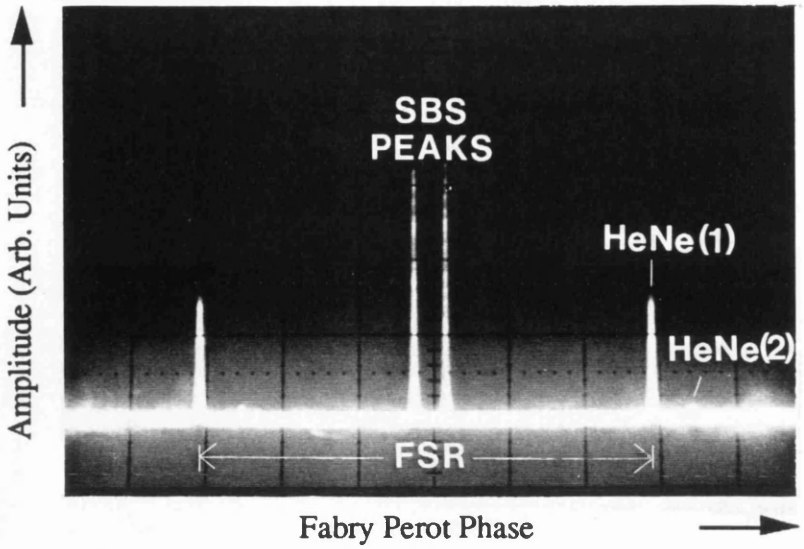

Figure 4.7 Typical Fabry-Perot response showing, pump (HeNe1) and minor orthogonally polarised (HeNe2) laser modes, and the dual SBS peaks generated even in absence of HeNe2. FSR of Fabry-Perot, 7.56 GHz

laser output polariser), but normally this is suppressed by at least 30dB. Surprisingly, two SBS peaks are observed. Typically, only one SBS peak is observed to exist at a time, and mode competition (possibly due to noise, or spontaneous mode locking) leads to the Stokes output jumping between these two SBS peaks. Also, no beat signal was detected on a spectrum analyser, between these two SBS peaks, further suggesting that they do not lase simultaneously. The photograph of Fig.4.7 was obtained by allowing the exposure time to be long enough to record both SBS peaks. The cause of these two SBS peaks is thought to be related to the existence of guided acoustic modes in the PM fibre used, and this is discussed further in §.4.3.

The frequency shifts of the two Stokes waves were found to be different for launch along each polarisation axis (with the polarisation instability suppressed). When the PMRR was pumped with linearly polarised light launched along the fast axes of the fibre, the frequency shifts of the two SBS peaks observed were, 26.32GHz and 26.85GHz (+/-18MHz). When the pump was launched onto the slow axes the corresponding shifts were 26.52GHz and 27.05GHz. The possible acoustic guidance nature of the fibre means that we can no longer directly determine the acoustic velocity of the core material from the simple equation, $\upsilon_a=(\lambda/2n)V_b$, where V_b is the SBS frequency shift, n the refractive index and λ the optical wavelength. However, the

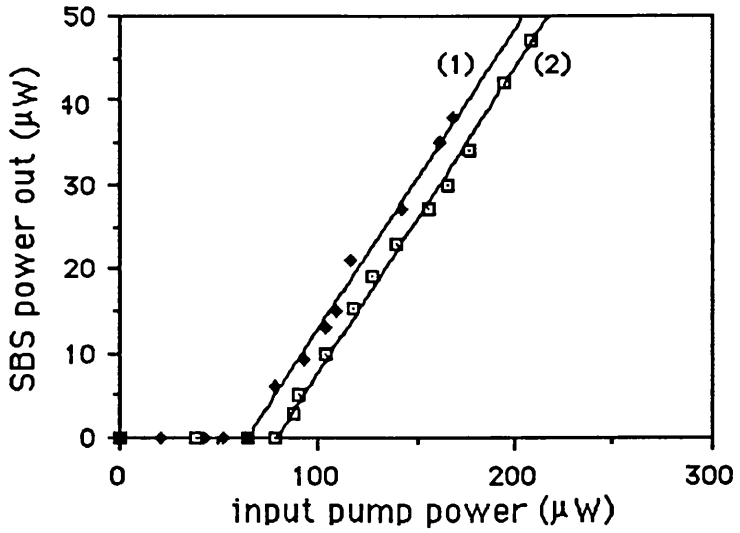

Figure 4.8 Level of SBS output power detected for F values (maximised at low powers) of (1) 330 and (2) 300, with input pump launched along fast axis.

difference in frequency for the dual SBS peaks, of 200MHz generated by pumping along the fast axis or along the slow axis, is a measure of the difference in stress, refractive index and core diameter along each fibre axis. To first order, assuming that the effect of guided acoustic modes can be ignored and that this frequency difference is only due to a difference in refractive index, then this result indicates a refractive index difference between the fast and slow axis of 0.01, which is at least an order of magnitude too large for the York Bow-Tie (HB600-1) fibre used. Hence, a significant proportion of the effect is due to the difference in stress and core diameters of the two fibre axis.

The SBS levels measured on the Fabry-Perot where calibrated by comparison with the 4% far endface Fresnel reflection of the pump power. Fig.4.8 clearly demonstrates the threshold nature of the SBS response and its dependence upon resonator finesse, for the 1m PMRR. The SBS threshold for the resonator with a finesse of 330 is observed to be as low as 65μW, and this is found to be in excellent agreement with the result predicted for a PMRR by Eq.4.6, with $g=4.2\times10^{-11}mW^{-1}$ and launch along the fast axis. With the coupling constant fixed to the values optimised at powers below SBS threshold, a reduction in measured finesse from F=300 to F=210 ,was observed for an increase in input power from 60μW to 220μW as shown in curve (2) in Fig.(4.8).

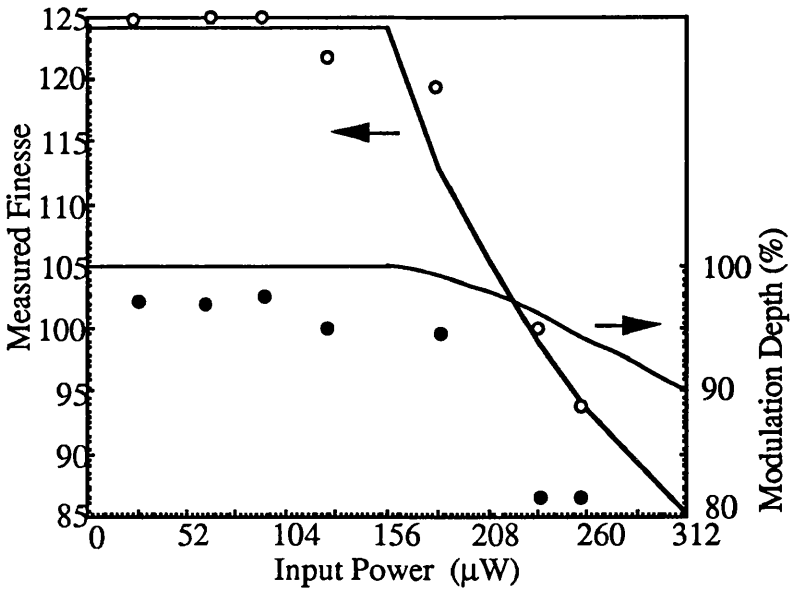

Figure 4.9 Observed variations in measured finesse (open circles) and modulation depth (filled circles) with input power, for a fixed coupling constant optimised at low powers, in a 3m PMRR. Solid lines represent theoretically expected curves.

Fig.4.9 is a plot of the observed variations in measured finesse and modulation depth, for a 3m PMRR with its coupling constant optimised at low input powers. The solid lines represent the theoretical curves expected for launch along the fast axis, with perfectly resonant coupling. The drift in the orthogonal resonant polarisation eigenmode was not stabilised during the measurement of these results, and this led to the discrepancy between the observed and predicted modulation depths. The effect of this polarisation drift upon the finesse was as expected quite small, and these measurements match quite well with the expected variation with input pump.

The finesse value was optimised at an input power below the SBS threshold to F=360 along the slow axis, for the 1m PMRR. The input power was then increased and the coupling constant re-adjusted to account for the additional loss due to SBS at each new input power. The theoretical threshold is 81μW. The measured finesse value, as shown in Fig.4.10 was observed to be degraded to F=240 at P_i=140μW and to F=160 at P_i=195μW, which is in good agreement with the degradation expected from Eq.4.10, (shown above threshold as the solid line in Fig.4.10).

The difference in threshold expected due to the difference in core diameter along each fibre axis is not directly observable as the PM coupler is slightly anisotropic. By measuring the finesse, modulation depth and input pump power at threshold for each eigenstate, and then using Eqs.4.14 and 4.15 to determine the values of $\bar{\kappa}$, κ and γ_o,

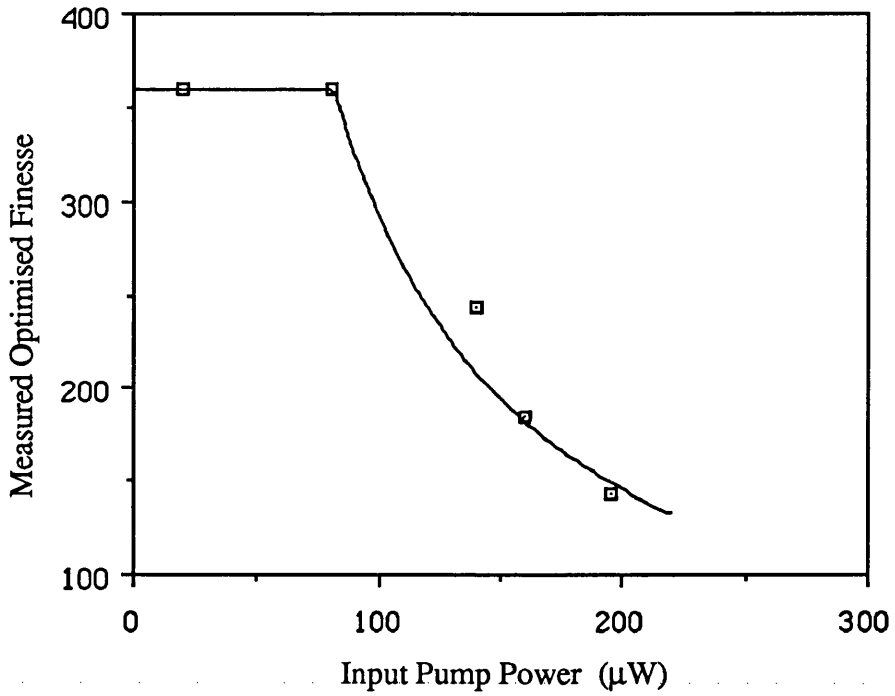

Figure 4.10 Observed variation in the measured finesse with input power, with the coupling constant re-adjusted at each input power for optimum resonance. Solid line corresponds to theory.

the circulating pump power can be determined from Eq.4.13, and differences in threshold noted. The result is still fairly ambiguous as it is dependent upon the coupler loss for each axis, and we can only determine the combined effect of both the differences in core diameter and coupler intensity loss for each axis. However, by taking the ratio of Eq.4.5 for the fast and slow axis, we can obtain a rough approximation to the ratio of the effective areas for each fibre axis. For example in the 3m PMRR, for a particular PM coupler adjustment, the fast axis had a finesse of 93 and a modulation depth of 99%, and input threshold of 143μW. The slow axis had a finesse of 127, a modulation depth of 89% and an input threshold of 130μW. Following the procedure just outlined, the coupler intensity loss for the fast and slow axis at this PM coupler adjustment, is found to be 0.0224 and 0.0271 respectively. This yields, to first order, a ratio between the effective areas along the fast and slow axis of 1.35, which is in good agreement with the data of table 2.2.

4.2.3. Loop Length Control Electronics.

Active length stabilisation techniques are required to keep the device at resonance in order to counteract the random environmentally induced phase perturbations, and

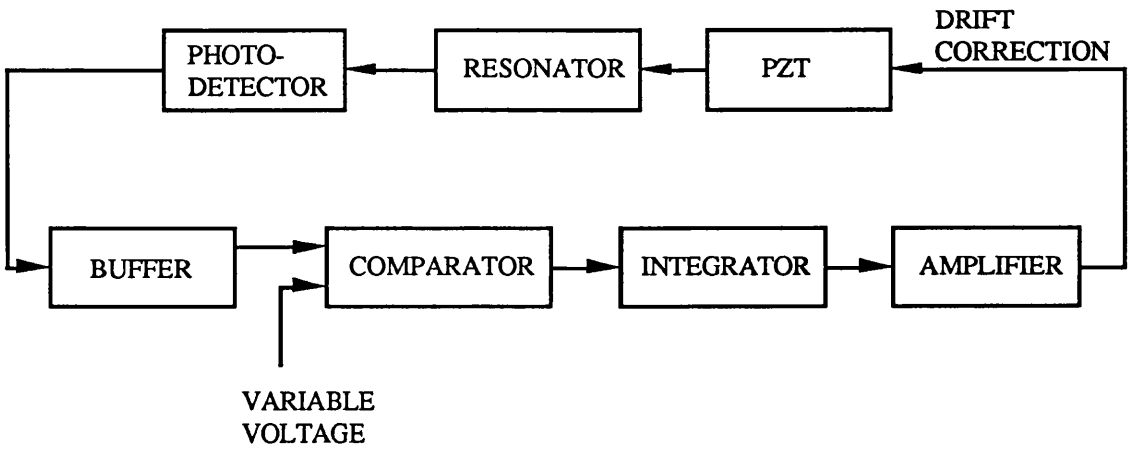

Figure 4.11 Block diagram of 'adjustable lock' loop length stabilisation technique.

maximise the circulating pump intensity. Two methods, which we call the adjustable lock and second harmonic technique were utilised to this end.

In both techniques, the detected output is sent via the feedback electronics to the PZT which is used to adjust the loop length. In the adjustable lock technique shown in Fig.4.11 the dips in the resonator response are assumed to be linear and the detected output is compared to a fixed level which gives the error signal to be supplied to the PZT. The lock-in position on the resonator dip can therefore be determined by the value of the variable DC comparator input. The integrator essentially limits the closed loop response to low frequencies, countering thermal drifts and the amplifier simply serves to suitably scale the error signal supplied to the PZT. Lock positions very close to the resonator dip can be obtained with this technique and the effects of different circulating powers can be investigated. When the resonator is not locked this method automatically scans the response until lock is achieved. The disadvantages of this system is that lock cannot be maintained at the minimum of the dip and the lock position is sensitive to the launch power of the system.

The second harmonic lock-in system is able to lock onto the resonator minimum at the cost of added complexity. The technique relies upon the fact that about the $2m\pi$ operating point the resonator response is approximately parabolic and hence the gradient of the response is a linear function of loop phase. When a small low frequency ac phase variation is applied to the loop, the response of the resonator will contain different amounts of the fundamental signal component, the amplitude of which determines the position on either side of the resonator dip and the phase of which

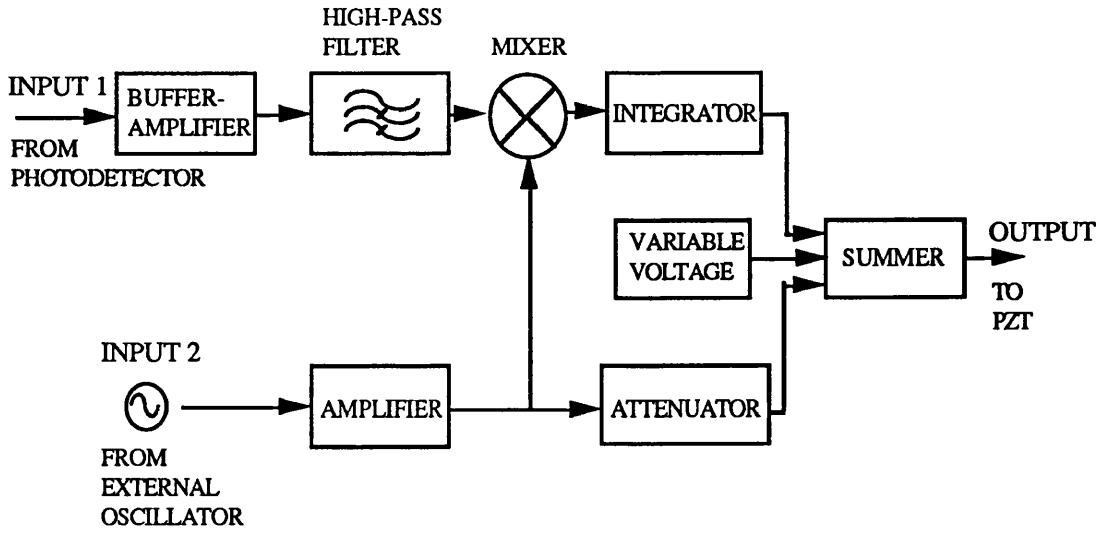

Figure 4.12 Schematic of second harmonic lock-in technique.

determines the sign of the error signal required. The magnitude of the error signal is obtained by simply mixing down the fundamental harmonic component in these waveforms to dc, about the resonance dip the first harmonic content is minimised and the output looks like a full rectified version of the input signal, with the second harmonic content maximised. Fig.4.12 shows the schematic of the second harmonic lock system. The system has two inputs and one output. The input from the photodetector is passed through a buffer-amplifier, which is used to determine the loop gain, and then through an RC high pass filter in order make the system independent of launch powers. The mixer output is passed through the integrator as before and then to the summer, where the suitably scaled ac signal is added, as well as a variable dc voltage. This variable voltage is used to get the resonator back on lock, since if the loop phase is not such that the response is on the dip the system will not have an error signal, and lock has to be initiated manually. Due to noise considerations one would ideally prefer to have the small ac signal applied to the resonator via a different PZT to the one used for the loop stabilisation, however due to the relatively short lengths of the resonators investigated (<5m) this was not possible. For the 3m ring resonator with 1.7m of fibre wrapped around the PZT, the integrators +/- 15V output swing allows +/- 6π rad compensation to thermal drifts. This was sufficient under laboratory conditions to maintain lock with both techniques for over 20mins, provided care is taken to try and minimise the polarisation instability described in Chapter 2.

Fig. 4.13 is a photograph of the 4.15m resonator locked onto resonance. The

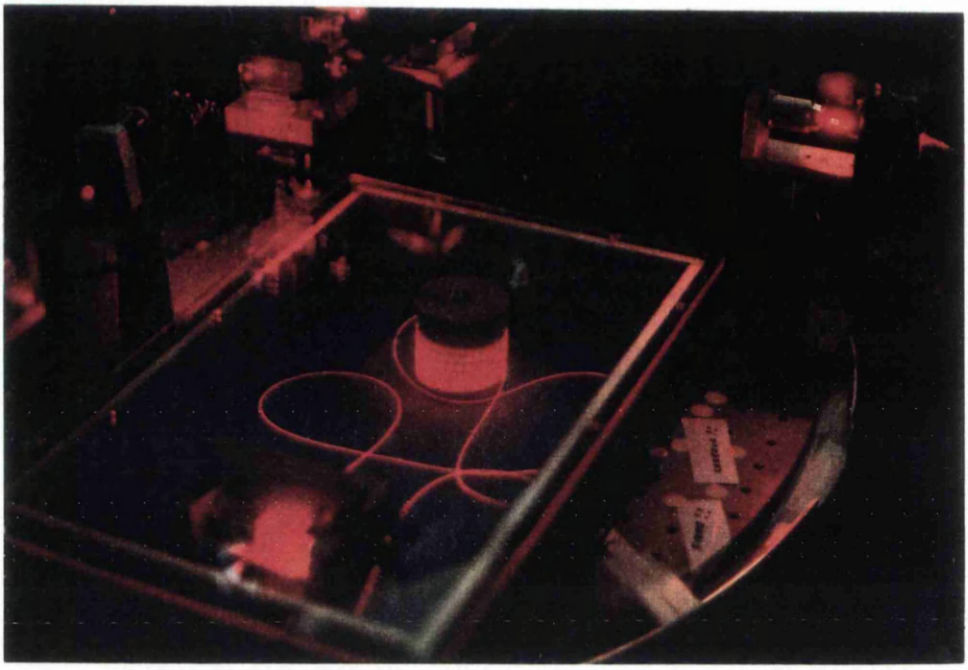

Figure 4.13. Photograph of PMRR locked on resonance, demonstrating large circulating pump power.

resonator loop can be seen glowing clearly, demonstrating the large build-up in circulating pump power that can be achieved.

Such systems as described above can be used to operate the ring resonator as a sensor by adjusting the operating point of the device to be approximately at the mid-point of the peak where the intensity/phase gradient is maximised and the response most linear. Then by monitoring the drift correction signal applied back to the PZT, the value of the measurand causing the drift can be determined[1].

4.3 Guided Acoustic Modes in PM Fibre.

The observation of multiple SBS peaks on a Fabry-Perot étalon may be caused by one of the following effects; (1) Anti-Stokes generation; (2) Higher order Stokes generation; (3) Stimulated scattering in both the core and cladding; (4) Interaction of the scattered wave with the HeNe laser; (5) Seeding effects due to the second orthogonal laser mode and (6) Acoustic guidance property of the optical fibre. When the backscatter was observed on a Fabry-Perot étalon, with an FSR of 300MHz (instead of 7.56GHz as in Fig.4.7), the SBS peaks were not symmetrically positioned about the pump frequency, nor were they in the positions expected by effect (2). Also the dual peaks were observed even at pump powers just above SBS threshold. This negates the

possibility of effects (1) or (2) explaining the dual SBS peaks observed in Fig.4.7. The fact that both SBS peaks do not resonate simultaneously, and that the major concentration of pump power is in the core (whilst the SBS peaks were observed to have the same intensity) negates the possibility of effect (3) explaining the dual peaks. The possibility of effect (4) is negated by the fact that the Stokes waves generated lie outside the gain bandwidth of the HeNe laser cavity. Seeding effects of the second orthogonal HeNe laser mode as in effect (5) are also improbable in our experiments because of the low level of this mode, the frequency selectivity of the PMRR and the fact that both SBS peaks were observed to have the same polarisation as the main pump. This finally leaves the most probable explanation of the observed dual peaks as being due to effect (6), the acoustic guidance nature of the fibre.

The approximate composition of the 633nm York HiBi fibre used is as follows[129]. The core is made of SiO_2 doped with 6mol% GeO_2 and has an effective diameter of 3.3μm for the slow axis and 4.36μm for the fast. The cladding is SiO_2 with approximately 0.25mol% F and 0.75mol% P_2O_5 dopant. Since the guided optical field does not extend far beyond the core, the composition of the highly doped stress-inducing bow regions is not relevant. This gives a core density, ρ_1, of 2288g/cm^2, a longitudinal acoustic velocity, V_{L1}, of 5679ms^{-1}, and a shear acoustic velocity, V_{S1} of 3590ms^{-1}. The cladding density,ρ_2, longitudinal acoustic velocity, V_{L2}, and shear acoustic velocity, V_{S2}, are approximately the same as that of pure SiO_2, ie, 2202g/cm^2, 5944ms^{-1} and 3749ms^{-1} respectively[130]. This case can be approximated to first order by a recent analysis presented by Jen, *et. al.*[131-133], which was successfully used to interpret the experimental results of Shibata *et. al.*[133]. Jen *et. al.* investigated the acoustic properties of an optical fibre with $V_{L1}<V_{L2}$, $\rho_1\approx\rho_2$, and $V_{S1}\approx V_{S2}$. Such a fibre is found to support longitudinal acoustic modes $L_{n,m}$, governed by the same mathematical formulation as that used to describe weakly guided linearly polarised optical $LP_{n,m}$ modes, in a step index fibre[134]. The shape of the SBS gain curve is now determined by the interaction between the optical pump and the guided acoustic modes. By considering the overlap integral between the electromagnetic HE_{11} mode and the guided acoustic modes, only the pair of longitudinal acoustic modes $L_{0,m}$ and $L_{2,m}$, are found to give rise to Brillouin gain, and these thus primarily determine the shape and bandwidth of the SBS gain. The longitudinal L_{01} mode has zero cut-off frequency, and the longitudinal modes $L_{0,m+1}$ and $L_{2,m}$ (m>1) have equal cut-off frequencies. This last pair of modes have a similar dispersion curve and to good approximation we need

consider only the dispersion curve of the $L_{0,m}$ modes. The dispersion equation for the $L_{0,m}$ modes is given by[134],

$$\frac{UJ_1(U)}{J_0(U)} - \frac{WK_1(W)}{K_0(W)} = 0 \tag{4.17}$$

where J and K are Bessel and modified Bessel functions respectively, and

$$U = \omega a\left(\frac{1}{\upsilon_{L1}^2} - \frac{1}{\upsilon^2}\right)^{1/2} \tag{4.18}$$

$$W = \omega a\left(\frac{1}{\upsilon^2} - \frac{1}{\upsilon_{L2}^2}\right)^{1/2} \tag{4.19}$$

where $\omega=2\pi F$ (F=acoustic frequency), a is the core radius, and υ_{L1} and υ_{L2} are the phase velocities of the core and cladding. Following the treatment given, we can calculate the relationship between the acoustic phase velocity and the normalised frequency, given by the product of the sound frequency and the core radius. Fig.4.14 is a plot of the dispersion curve calculated using the above analysis for the York Bow-Tie fibre used in the PMRRs. The relationship between the acoustic velocity υ, and the SBS frequency shift is $\upsilon=(\lambda/2na)(Fa)$. The factor of 2 takes into account that for efficient opto-acoustic coupling the acoustic propagation constant should be twice the optical propagation constant. The two curves in Fig.4.14 are drawn according to this relation for n=1.465, λ=633nm, and a core radius of 2.18μW along the fast axis and 1.65μW along the slow axis. The filled circles represent the data points corresponding to the slow axis (SBS frequency shifts of 26.52GHz and 27.05GHz), and the open circles to the fast axis (SBS frequency shifts of 26.32GHz and 26.85GHz).

The FSR of the 4.16m PMRR is 48MHz, so one would expect the resonator to be able to resonate near all the peaks in the SBS gain generated by the interaction with the guided longitudinal modes. However, the experimental results and the calculated response using Eq.4.17 appear only to be approximately correlated. The analysis predicts 3 SBS peaks to be observed along the slow axis and 4 along the fast axis. The intensity of the $L_{0,m}$ modes is expected to decrease for increasing m, as these modes

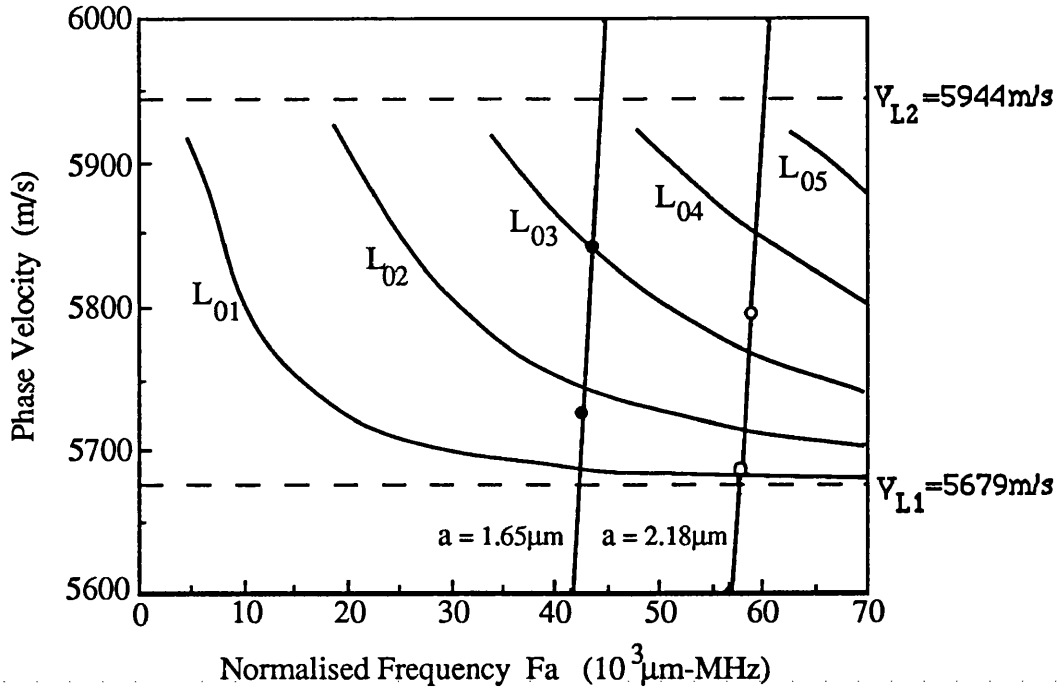

Figure 4.14 Phase velocity dispersion curves of L_{0m} modes calculated from Eq.4.17, and experimentally observed phase velocities measured from Brillouin shifts detected at output of PMRR.

are not as well confined within the core as the lower order modes. The experimental results fall within the boundary set by the core and cladding longitudinal acoustic velocities, and show the expected downward trend in phase velocity with increasing normalised frequency. The discrepancy between the analysis and the experimental results, is most likely due to the stringency required in meeting the assumptions that $\rho_1 \approx \rho_2$, and $V_{S1} \approx V_{S2}$. The analysis of Eq.4.17 can therefore only be expected to give a general trend for the York Bow-Tie fibre used. A more detailed analysis of these variations should be the subject of future work. It should be noted that Fujikura Panda fibre also has a Ge-doped SiO_2 core and SiO_2 cladding, and is also expected to guide acoustic waves.

4.4 Effects of SBS Depletion Upon PMRR Operation.

The depletion effects and guided acoustic wave effects described above have serious consequences upon the performance characteristics of the PMRR. The main results also apply in general to the ordinary single mode fibre ring resonators as well, the principal difference being that the SBS gain is halved and there are no significant variations in core radius, with fibre axis.

The variations in finesse and modulation depth of the ring resonator with input pump, lead to large scale factor and dynamic range variations which would be unacceptable for most sensor applications. The modulations in the dynamic response of the resonator over many hundreds of cycles also increases the required system integration time, and competition near threshold leads to excess noise via the Kerr effect, and this is still an open research issue. Therefore, in general, if the maximum finesse/modulation depth combination is to be obtained from the resonator then the input pump power has to be limited to below threshold levels, with the consequent increase in shot noise. The intensity dependent SBS depletion of the pump also leads to the interesting observation of the fibre resonator having a non-reciprocal finesse and modulation depth, when the input pump powers in each direction are different (and at least one of them above SBS threshold). This could lead to scale factor and sensitivity problems in resonator fibre optic gyroscopes, if the splitting ratios of the input coupler launching light into each direction varies over time.

In PMRRs the situation is further complicated by the drift in the resonator eigenstates with loop phase. This leads to a drift in the circulating pump power whose variation with loop phase is similar to the variation in transmitted intensity (except that the intensity transmission minima become circulating intensity maxima). The circulating pump power variation can be obtained by plotting only the last three terms of Eq.2.26. The stabilisation schemes outlined in §2.3.3 can be used to reduce the drift in the resonator eigenstates. The occurrence of SBS depletion effects are therefore seen as disadvantages in resonator sensor systems, and if greater use is to be made of state of the art fibre resonators, with their even lower SBS lasing thresholds, then techniques to suppress SBS need to be investigated, and these are considered in the next section.

4.5 Methods for Suppressing Stimulated Brillouin Scattering in Ring Resonators.

In attempting to suppress the onset of SBS lasing in fibre ring resonators, the problem needs to be approached on two levels. First the fibres material characteristics need to be optimised to increase the SBS threshold. Secondly, schemes compatible with ring resonator operation need to be developed to reduce the SBS lasing thresholds. The material considerations that need to be taken into account have already been outlined in §.3.2.3. In this section the fibre parameters that can be optimised to reduce

SBS are first discussed, and then two novel suppression techniques suitable for use in ring resonators with coherent cw input are investigated. There have been only two other SBS lasing suppression techniques reported in the literature and these are included for completeness and comparison.

From §.4.3 the first criterion that should be met is to ensure that the fibre does not guide acoustic modes. This can easily be avoided by choosing fibres which have acoustic velocities faster in the core material than in the cladding material. Single mode fibres with larger effective core diameters, to reduce the pump intensity, can be made by adjusting the core/cladding refractive indices. However, this would make the fibre more weakly guiding, and incompatible with standard fibres operating at those wavelengths. The SBS threshold can be doubled by forming the resonator out of single mode non-polarisation preserving fibre, however this then re-introduces the need for active polarisation control.

Shelby *et. al.* have recently reported two methods for increasing the SBS threshold in all fibre ring resonators[135,136]. The first technique is based upon modulating the SBS gain bandwidth by applying a sinusoidal temperature gradient along the length of the fibre, and the second technique is based upon incorporating a Faraday isolator within the fibre ring. The disadvantage of the first scheme is that because there is only a slight variation in the SBS bandwidth with temperature in glass, a temperature gradient of 200° had to be applied to raise the SBS threshold only by a factor of 3. In the second technique with the in-line fibre isolator, the ring resonator studied was constructed from York LB-600 low birefringence fibre and had a cavity free spectral range of 15.89MHz. The polariser was constructed from a polished half coupler within the fibre loop with a birefringent material contacted upon it such that one polarisation continued to be guided while the other was efficiently guided out of the fibre. On leaving the polariser the fibre then entered the Faraday rotator, which consisted of twenty-four 10cm straight fibre segments inside the bore of a 1-KG solenoid. Half wave plates where placed between the fibre segments to enable precise control of the phase retardation. The fibre isolator was reported to have a rejection ratio of approximately 200. The resonator had a finesse of 100 and with the magnet turned off the input SBS threshold was found to be 0.25mW of input light. With the magnet turned on the input threshold was raised to over 20mW, which corresponds to over 600mW circulating in the ring. The increase in the threshold circulating power is given by[136],

$$\frac{\Delta P_c}{P_c}=\frac{\log T_B}{\log(\kappa.\exp(-2\alpha_o L))} \qquad (4.20)$$

where P_c is the intensity circulating in the cavity at the stimulated Brillouin threshold with no isolation, ΔP_c is the increase in threshold due to the isolator, T_B is the transmission of the isolator in the reverse direction. Thus we can see that high suppression ratios can be achieved. However, this method is limited in that the resonator can only be operated uni-directionally, which renders it unusable for gyroscope applications, and the need for bulky in-line faraday rotators makes it impractical for such things as hydrophone use.

In order to improve the ease of implementing SBS reduction schemes, we proposed the two novel schemes described below.

(1) In the first method, we require that the resonator cavity has a free-spectral-range larger than the characteristic Brillouin gain bandwidth of the optical-fibre used. Then by carefully selecting the pump frequency so as to ensure that the pump and Brilluoin backscatter cannot resonate simultaneously, the SBS threshold is conveniently suppressed upto such a circulating power level that the non-linear gain on a single pass is so high such that the fibre loop acts as a travelling wave amplifier and the cavity effects are diminished. It is now the combination of SBS bandwidth and loop length that determine the viability of this scheme for a particular application. The cavity loop length considerations were summarised in Fig.4.4. Reducing the loop length to below the optimum length does not have much effect upon the resonator finesse, but does have a significant effect upon the sensitivity of the resonator and thus it would be advantageous to work at longer wavelengths where the Brillouin linewidth is narrower allowing larger cavity lengths to be utilised. For example at 1.55μm the Brillouin linewidth for pure silica core fibres is $\Delta\nu_B$=16MHz[137], implying that the maximum loop length at this wavelength that can be used for this technique is only of the order of 3m. Such limitations upon loop length may prove prohibitive in some applications, where the potential benefit in improved signal to noise ratio (due to increased launch powers) is overidden by the reduced device sensitivity to the measurand (due to the reduced loop lengths).

The predicted SBS suppression using this technique can be very high, and is governed by an equation analogous to Eq.4.20, with the only difference being that T_B

is replaced by the amount of SBS resonating simultaneously with the pump, which can readily be found from Eq.4.12. For example in a PMRR with λ=1.55μm, $\Delta\nu_B$=16MHz, a fibre attenuation of 8.5dB/Km, a loop length of 3m (FSR=67MHz) and a finesse of 200, the maximum suppression of the SBS threshold using this method is by a factor of over 240 (achieved when the SBS gain curve falls exactly between two resonances). The major advantage of this method is its simplicity and that it allows dual directional operation. As the critical parameter for this method is the Brillouin linewidth, materials should be chosen to give the minimum value of this linewidth at the operating temperature and wavelength, and care must be taken during the manufacture of the fibre to ensure that the intrinsic Brillouin gain is not broadened by inhomogeneities along the fibre length. A disadvantage of this technique for use in silica based fibre ring resonators operating at 633nm is that the short cavity lengths required (<1m) require loop phase modulators with greater phase modulation per unit length.

If the pump wave frequency is such that it does resonate simultaneously with the SBS wave, in such a short resonator, then the SBS threshold may actually be reduced This is because the lifetime of the acoustic wave is now longer than the time required for a single transit of the ring by the pump, and hence it is possible that the acoustic wave will be re-pumped before it has a chance to decay, thereby increasing its lifetime and hence decreasing the threshold. The longer phonon lifetime should also lead to a narrower SBS linewidth.

(2) In the second SBS suppression scheme we note from §.3.2.2 that, if we have a coherent pump spectrum made of discrete frequency components separated by more than the SBS linewidth, the SBS threshold will not be exceeded, provided that no spectral mode exceeds the 'single longitudinal mode SBS threshold'. We can utilise this technique in ring resonators in the following manner. By launching such a multimode laser into the resonator, ensuring that the power in no individual mode exceeds the SBS threshold, we can operate the resonator at higher powers, in a seemingly single mode fashion, provided that the laser mode spacing is an exact multiple of the resonator free-spectral-range and that the beat frequency between modes is larger than the coherent detection bandwidth. We can ensure that the mode spacing is an exact multiple of the resonator free-spectral-range either by varying the length of the pump laser cavity, or by the use of Bragg cells. If more than two modes are to be used then we also require that no two laser modes are separated by exactly twice the Brillouin frequency shift in

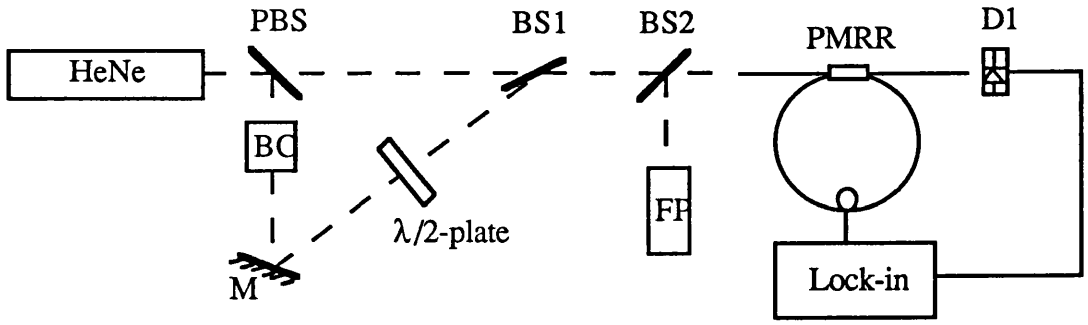

Figure 4.15 Experimental schematic used to investigate SBS suppression. PBS, polarising beam splitter; M, mirror; BC, Bragg cell; BS1 & BS2; 50:50 and 90:10 beamsplitters respectively.

order to dismiss the possibility that the Stokes mode associated with one laser mode could act as an anti-Stokes mode for a different laser mode. The use of this technique in a 4.15m PMRR operated at 633nm was investigated. The two longitudinal modes of the laser were utilised and their amplitudes made equal by centralising them under the pump laser gain curve. Fig.4.15 shows the experimental schematic used to implement the suppression technique.

The resonator was adjusted to a finesse of 127 with a modulation depth of 88%, and the Bragg cell was used to ensure that the mode spacing is an integer multiple of the cavity free-spectral-range. The half wave plate was required in order to make both beams polarised in the same direction The dual beam frequency spacing was able to be adjusted to within 10KHz compared with a full width half maximum for the resonator of 378KHz. This was limited by the resolution observable on the transfer function of the resonator, and leads to a maximum variation of circulating power between both beams (assuming equal launch power) of under 3%. However, the reduction in the efficiency of the Bragg cell away from its designed operating driving frequency, and the difficulty of launching both beams efficiently via a single set of launch optics led to the ratio of beam powers launched of approximately 2.5:1. Measurements where first taken of the SBS threshold for a single beam (the squares in Fig.4.16), and then the threshold level was measured for a dual beam with the above power ratio launched, with the frequency spacing between the modes of 790MHz, (the diamonds in Fig.4.16). If we assume that the Brillouin gain bandwidth is enlarged by the acoustic guidance properties of the fibre, to approximately 577MHz, then with a maximum frequency separation of 790MHz and a power separation ratio of 2.5:1 the new gain for the SBS process will from Eq.3.20, now be 0.815 times the gain for a single beam.

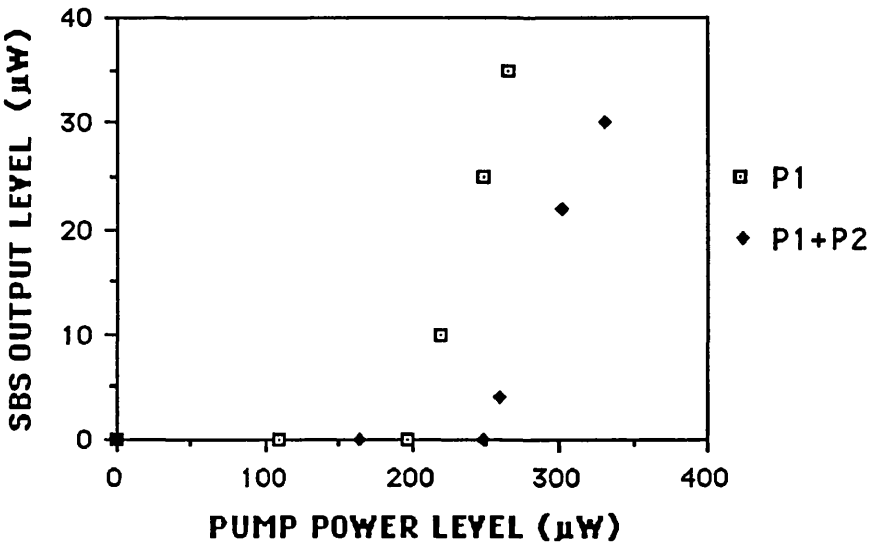

Figure 4.16 Suppression of SBS threshold with ratio P1:P2 of 2.5:1 .

This would predict that the threshold for a single, measured as 195µW should now become 240µW, which is in excellent agreement with the obtained experimental results. This result further supports the model of dual beam pumping given by Lichtman, *et. al*[89]. Hence, the principle of SBS suppression in ring resonators with this technique is demonstrated. The disadvantages of this system are obviously that in order to increase the permitted power level by a factor of n, we need a multimode laser with n modes and perhaps even n Bragg cells. Both of the previous two suppression schemes proposed have the significant advantage of being bi-directional, and not requiring additional components in the fibre loop.

It should be noted that the effects of various ASK, PSK and FSK modulation schemes upon the SBS gain, outlined in §.3.2.2, are generally not applicable in the ring resonator, because of the relatively long integration time required by the resonator. Once the threshold for SBS lasing is increased, other weaker non-linear phenomenon will eventually become apparent, such as optical bistability and FWM[136].

4.6 Conclusions.

The continued improvements in the fabrication of optical fibre ring resonators has led to the onset of non-linear stimulated Brillouin scattering effects occurring within the devices for input pump powers as low as 65µW. These low input SBS lasing

thresholds are easily surpassed in modern optical systems, and the effects of SBS generation upon the device performance characteristics need to be considered in future system designs. The major feature of the onset of SBS lasing is that the circulating pump power becomes clamped at steady state to the threshold circulating pump power. The transient response of this pump depletion has been investigated and found to last for up to several hundred loop transit cycles, thus necessitating longer detector integration times. The transmission response of the fibre resonator shows a strong sensitivity to variations in input pump powers above SBS threshold. The nature of these variations in the measured finesse and modulation depth of the device is governed by the set of Eqs.4.7-4.9. Inclusion of the phase variation in the ring resonator fully describes the transmission response of the device with input power. For low SBS gains the model and experiments show that to good approximation the variations in measured finesse and modulation depth can be described in terms of a mismatch between the resonators coupling constant and the loop losses. These variations are therefore dependent upon the input pump power at which the resonator coupling constant was optimised. For high SBS loop gains, as would be possible with higher pump powers and/or special low threshold optical fibres, the model predicts that 'clipping' of the resonance dip occurs and the measurement of a finesse for the device is no longer appropriate.

The SBS depletion effects were experimentally demonstrated in several high finesse PMRRs. Dual SBS peaks apparently due to the acoustic guidance properties of the fibre used were observed, and the observations compared to an approximate theory used to model the acoustic modes. Their observation demonstrates a difference between SBS in bulk and guided wave systems, and also highlights the need to consider the acoustic properties of the materials used in the fibre composition.

The increased optical backscatter due to the SBS process can lead to stability problems in some laser sources, and the resonator performance variations with pump power, leads to non-reciprocal resonator responses when the device is pumped in both directions with at least one direction pumped above the SBS threshold level. These effects cause significant scale factor drifts in sensor applications, and in order to avoid these problems the device needs to be operated below SBS threshold. In order to suppress the onset of SBS lasing so as to increase the allowable input power levels (and hence improve signal to noise ratios) two novel SBS suppression techniques were proposed and one of them experimentally demonstrated. Both schemes have the significant advantages of not requiring additional components within the fibre resonator and of allowing dual directional operation.

Chapter 5

ACTIVE AND PASSIVE FIBRE-OPTIC RING RESONATOR GYROSCOPES

The previous chapters dealt with the fibre-optic ring resonator in an applications independent manner. This chapter now extends that work, to examine specifically the use of these devices to form fibre-optic ring resonator gyroscopes. Fibre-optic gyroscopes utilise the Sagnac effect[138], in which two waves propagating in opposite directions around a loop interferometer experience an optical path length difference proportional to the rotation rate relative to an inertial frame.

The detection of rotation rate is an important parameter for inertial navigation systems. Potential applications would be found in space flight, aircraft, robotics, oil well logging, and provided the cost can be brought low enough - automobiles. The requirements for inertial navigation can be fairly stringent. The pointing accuracy needed to fly a 3000km route in 3hrs and arrive within 1km of the destination means that rotation rates as low as 0.01 deg/hr must be measurable, whilst for operational maneuvers in tactical aircraft, rotation rates as high as 1000 deg/sec must be measured to approximately 5 ppm accuracy. This represents a dynamic range of 10^8. In order to achieve such inertial grade sensitivity and long term stability, it is important that the characteristics of the device are thoroughly understood in order to eliminate or minimise any potential error sources.

Various optical configurations have been developed to implement the Sagnac effect for rotation sensing. The chapter begins with a description of the Sagnac effect, and a comparison between these various gyroscope technologies. Both active and passive

implementations of the resonant fibre optic gyroscope (RFOG), are investigated. The drift characteristics of passive RFOGs fabricated with polarisation maintaining fibre are examined with the aid of the analysis developed in Chapter 2. The magnitude of this drift is calculated for both the cases of isotropic and highly anisotropic PMRRs[16]. Next, the use of stimulated Brillouin scattering to form one of the first solid state active fibre gyroscopes is demonstrated[22,23]. Such an SBS gyroscope has significant advantages over conventional approaches, and these, as well as the design criteria that need to be followed in such gyroscopes are established and discussed. A novel method is also presented to eliminate the frequency lock-in effect present at low rotation rates in the SBS gyro.

5.1 The Sagnac Effect.

A rigorous analysis of the Sagnac effect involves expressing Maxwell's equations in a rotating (hence accelerating) frame of reference, using the formalisms of General Relativity[2]. However, the analysis is complex and a less rigorous algebraic treatment that gives the same result is provided by the kinematic model[139]. The kinematic model of the Sagnac effect starts by considering a hypothetical circular interferometer of radius **R** in a vacuum as shown in Fig.5.1. Light is injected at a point P_i, and propagates in both directions around the loop. When the interferometer is at rest in an inertial frame of reference the path lengths of the counterpropagating waves are equal, and since light travels at the same speed c, in both directions around the loop, both arrive back at the point of injection P_i after a time $\tau=2\pi R/c$. When the interferometer begins to rotate relative to this inertial frame at an angular velocity Ω, the injection point moves through an angle $\Omega\tau$ during the propagation time τ. The time difference between the arrival of the two waves at the new position of the injection point P_i', is now given to first order in $R\Omega/c$ by,

$$\Delta\tau = 2\pi R\left(\frac{1}{c-R\Omega} - \frac{1}{c+R\Omega}\right) = \frac{4A\Omega}{c^2} \tag{5.1}$$

where $A=\pi R^2$ is the enclosed area of the interferometer. For continuous waves this time difference results in a phase shift $\Delta\phi_S$ given by,

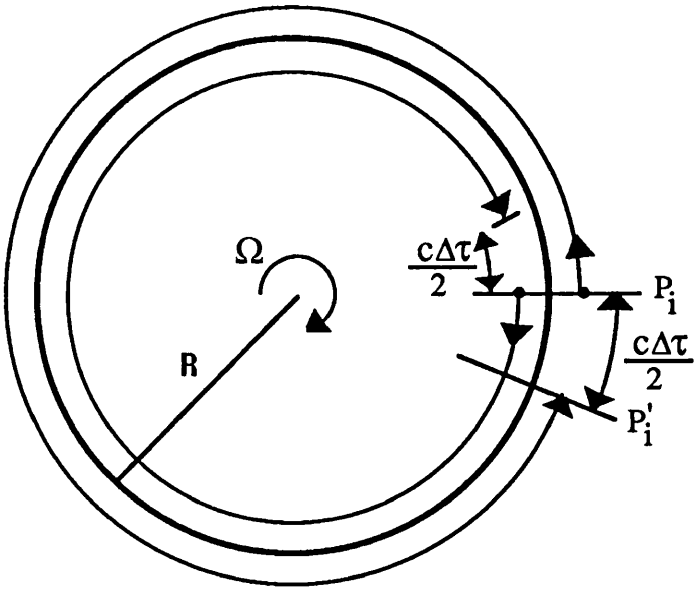

Figure 5.1. Schematic of rotating Sagnac interferometer showing path length difference of $c\Delta\tau$ between the counterpropagating waves.

$$\Delta\phi_s = \omega\Delta\tau = \frac{4A\omega}{c^2}\Omega = \frac{8\pi A}{\lambda c}\Omega = \frac{2\pi LD}{\lambda c}\Omega \qquad (5.2)$$

where λ is the vacuum wavelength, L is the loop length and D is the loop diameter. Eq.5.2 gives the Sagnac phase shift associated with one transmission around a loop of radius **R** in a vacuum. If the two counterpropagating optical waves are collected again at the injection point and interfered at a detector, an interference pattern is formed whose fringe pattern varies with rotation rate in accordance with the phase shift given by Eq.5.2. Thus, by measuring the change in this fringe pattern, the Sagnac phase shift, $\Delta\phi_S$, and hence the rotation rate, Ω, can be determined.

The sensitivity of the Sagnac phase shift can be improved by increasing the number of turns around the loop. This leads to the right hand side of Eq.5.2 being multiplied by a factor N, where N is the number of turns. This is in fact the approach adopted by the interferometric fibre-optic gyroscope (IFOG) where the low loss of optical fibres is utilised to form long loop lengths and hence enhanced sensitivities.

When the guiding structure under consideration is a resonant cavity as in the case of ring laser gyroscopes (RLGs) and both passive and active resonator fibre-optic gyroscopes (RFOGs), it is often advantageous to view the path length difference as leading to a frequency difference Δf_S, between the counterpropagating resonant

frequencies in the cavity. Defining the optical perimeter of the circular cavity as $P=n2\pi R$, this frequency shift is given by $\Delta f_S/f_O = c\Delta\tau/P$ where f_O is the resonant frequency of the non-rotating cavity. Using Eq.5.1 we have,

$$\Delta f_s = \frac{c\Delta\tau}{P} f_0 = \frac{4A}{\lambda P}\Omega = \frac{D}{\lambda n}\Omega \tag{5.3}$$

We see in this case that since the oscillation frequency in each direction is determined by the path length in that direction the differential frequency Δf_S can be obtained in the RLG and active RFOG by beating the output of each lasing direction at a detector. In the case of the passive RFOG this difference in counterpropagating resonant frequencies must be measured by means of an external laser. The factor relating the rotation rate to the beat frequency (in the RLG and RFOG) or the phase difference (in the FOG) is commonly known as the scale factor S, of the gyroscope.

The above treatment of the Sagnac effect is based upon different path lengths leading to different times of flight around the loop. An equivalent interpretation can be obtained by considering the different doppler shift in the counterpropagating directions caused by the moving injection point and the optical path length remaining the same.

5.2 Comparison of Gyroscope Technologies.

In order to appreciate the role played by RFOGs in gyroscope technologies, it is beneficial to compare the various techniques for measuring the Sagnac phase shift shown in Fig.5.2. The approaches are split between active and passive techniques. In the active approach two counterpropagating waves oscillate in a resonant cavity, which contains an active gain medium. The presence of this gain medium within the cavity forces the counterpropagating waves to oscillate at different frequencies with rotation in response to the Sagnac effect. The active approach can be implemented in the form of RLGs or active RFOGs. The RLG is the most mature of the optical gyroscope technologies, and already provides navigation functions in commercial passenger aircraft such as the Airbus A310 and the Boeing 757 and 767. RLGs capable of detecting rotation rates over a range 10^{-3} to 10^{4} ^{0}/hr have been demonstrated, with performance close to the quantum noise limit[140]. The active approach has the advantages of a frequency readout of rotation rate, and an ideally linear scale factor.

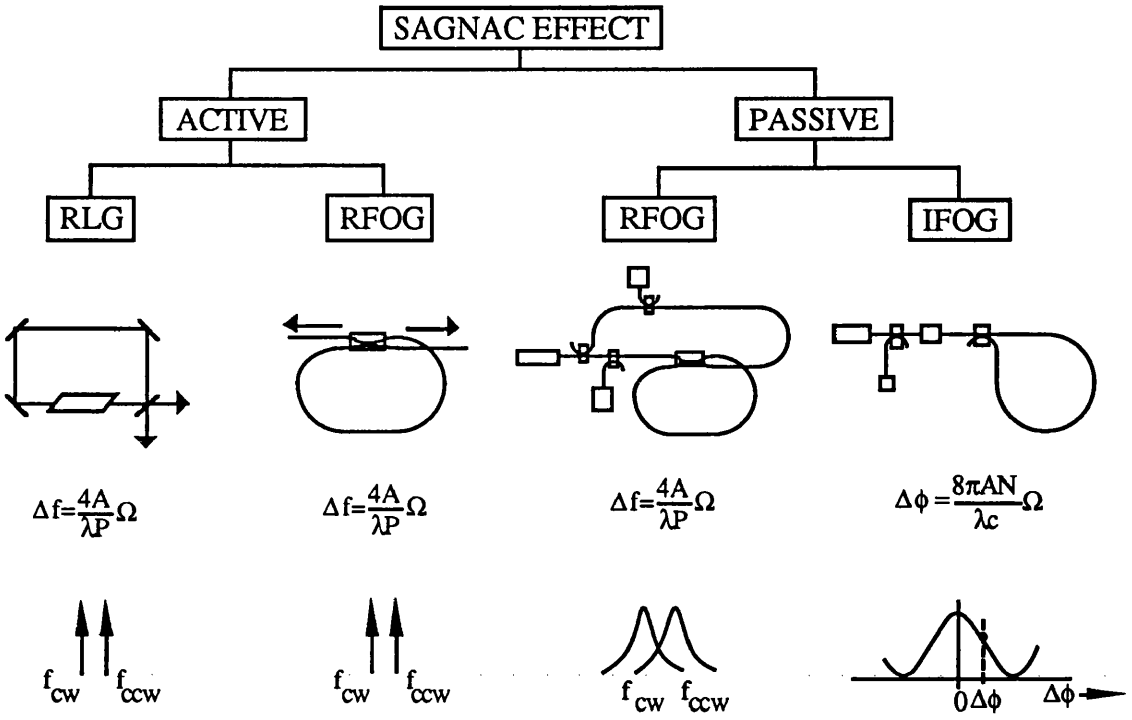

Figure 5.2 Techniques for measuring the Sagnac effect, showing conventional passive RFOG categories and the recently demonstrated active RFOG (SBS gyroscope) category.

During the development of the RLG three major error sources have been found and extensively reported[141,142] that can make Eq.5.3 invalid. These are the null-shift error, mode locking and a dependence of the scale factor upon rotation rate. Of these the most serious is the mode locking effect. Mode locking (also known as frequency lock-in) leads to the frequency difference in the RLG vanishing for small but non-zero input rotation rates, and is caused by weak coupling, due to backscattering, between the otherwise independent travelling waves. Much of the RLG development work has gone into minimising the sources of backscatter within the ring. Lock-in ranges as low as 30 deg/hr can now be obtained with total scatter losses less than 1ppm[143]. Techniques for avoiding lock-in have been based upon either alternating bias approaches (dithering), which attempt to average the lock-in region over positive and negative bias cycles to zero[144], or differential laser gyro approaches[145], which effectively bias their response away from lock-in regions. Scale factor stability in the RLG is usually addressed by fabricating the cavity with special ultra-low thermal expansion materials, and piezo feedback. Scale factor variations due to variations in the refractive index must also be addressed. State of the art RLG's typically exhibit scale factor linearities of 10ppm[146].

A major drawback of the RLG is its cost, with a typical inertial grade 3-axis device costing several tens of thousands of pounds.

A potentially much simpler, low cost device is the SBS gyro discussed in §5.4. This device is a solid state fibre gyro that uses the stimulated Brillouin scattering effect to provide gain within the fibre cavity. The frequency lock-in effect still occurs in this device and techniques similar to the ones developed for the RLG can be applied to this gyro as well.

The passive approach can be divided into IFOG and passive RFOG categories. The IFOG has received much attention and has recently been chosen to perform Attitude and Heading Reference System (AHRS) functions for a new regional airliner program[147]. The IFOG is based upon the use of low loss optical fibre to form Sagnac interferometers with long loop lengths. Because of the extremely small Sagnac phase shifts to be measured (typically of the order of 10^{-6} of a radian) loop lengths of several kilometers are typical and the so called minimum reciprocal configuration IFOG[2], shown in Fig.5.2 has been developed. This configuration ensures reciprocal operation by placing a spatial filter and polariser at the input to the interferometer, and using only the reciprocal port of the fibre loop coupler. Because of the reciprocal nature of the device and sinusoidal scale factor (cf. Fig.5.2), a bias scheme is required to operate the device in the most linear region of the response curve. All three functions of beamsplitting, phase modulator and polariser can be performed on a single integrated-optics gyro chip, further reducing costs, and closed loop operation of the IFOG is also commonly implemented in order to stabilise and linearise the scale factor, although this has the disadvantage of significantly complicating the associated electronics. The IFOG has not yet reached the performance levels of the RLG although compact (500m length of polarisation maintaining fibre coiled into 10cm diameter) versions have demonstrated 0.1°/hr bias stability, and 100ppm scale factor linearity[148]. The major sources of error are, direct dynamic environmental effects, Rayleigh backscattering, the optical Kerr effect, and the Faraday effect[149-153]. The effects of Rayleigh backscattering, which can interfere with the counterpropagating waves changing their amplitudes and phases in an unpredictable manner, can be reduced by using the combination of polarisation maintaining fibre, a low coherence source and suitable bias scheme. The broadband source can also help to raise the threshold for stimulated Brillouin scattering and reduce the noise from the optical Kerr effect, where non equal circulating intensities can lead to non-reciprocal propagation constants. The use of polarisation maintaining fibre also

helps to eliminate noise due to the Faraday effect provided twist is avoided in the fibre. Present emphasis in FOG research is upon scale factor stability. The use of doped fibre sources are therefore currently of great interest because of their high power, broadband output and wavelength stability[154].

The passive RFOG though first demonstrated in 1977, has only recently been receiving increasing interest. It is potentially much cheaper than the IFOG because all else being equal, a fibre loop of length L_T in an RFOG of finesse F, has the same sensitivity as a FOG of length $(F/\pi)L_T$, and as demonstrated previously F can be quite large. The rotation rate output of the device can be made in terms of the resonant frequencies of each counterpropagating wave, although this is not intrinsically supplied as in the RLG and SBS gyroscope. Also, because the active laser medium is not within the cavity it does not inherently suffer from lock-in. A form of electronic lock-in has been observed in some closed loop detection schemes used in the RFOG but these can readily be avoided[155]. A major advantage of the passive RFOG is that the shorter fibre lengths required, greatly reduce volume, and direct dynamic environmental effects upon the gyro response. Because of the resonant nature of the device, coherent sources are required and this leads to a series of unwanted associated problems. As shown in chapter 4, the onset of non-linear effects occur at much lower thresholds than in the FOG, where the spectral densities of the sources are often 7 orders of magnitude lower than those suitable for a resonator. The onset of stimulated Brillouin scattering can lead to excess noise and sets an absolute limit upon the RFOG performance. The methods outlined in §4.5 can be used to reduce its effect. The resonant enhancement of the circulating power also leads to a more stringent requirement upon the equalisation of the input intensities, in order to control errors introduced by the Kerr effect, and this forms a significant immediate problem for the RFOG. Compensation schemes based upon intensity modulation at an integer multiple of the round trip cavity delay time have been investigated[156]. A scheme which actually makes use of the Kerr effect to dramatically increase the rotation sensitivity of the RFOG has also been proposed[157]. In this scheme the RFOG is biased to operate at the side of the resonance dip, where the phase sensitivity is greatest. Rotating the RFOG then leads to the circulating intensity increasing in one direction and decreasing in the other. This in turn changes the refractive index in each direction via the Kerr effect, thereby enhancing the Sagnac effect. Enhancement factors of over 100 have been theoretically predicted. Another major consequence of the use of a coherent source is that Rayleigh backscattering is

also significant, and this is further enhanced by the resonator action[158]. Fibre end reflections can also cause significant response distortions, but these can be reduced by suitable modulation schemes outside the cavity[159]. There are thus still several open research issues in the RFOG that need to be addressed before the RFOG matches the performance of the other gyro schemes.

5.3 Drift in Passive Polarisation Maintaining Fibre Ring Resonator Gyroscopes.

Recently the use of PMRRs for passive RFOG applications has been receiving increasing attention because of the potential for reduced system complexity and their reduced sensitivity to the Faraday effect. In this section we examine a potential source of drift in the passive RFOG due to polarisation instability in PMRRs, as characterised in Chapter 2.

Due to reciprocity, the excitation of the unwanted eigenstate in a polarisation maintaining ring resonator, is not in itself necessarily a problem for PMRR gyroscope applications, provided that the eigenstates are identically excited in both directions. However, in practice there is always some mismatch between the states of polarisation exciting each resonator direction, and therefore the shape distortion of the major resonance due to the presence of the minor resonance is different in each direction. As outlined in chapter 2, even when one attempts to launch on a principal fibre axis there is still a small component of the orthogonal fibre polarisation excited as well. Due to the finite accuracies of alignment at the input polarisers, this excitation of orthogonal field components is not necessarily the same, and the difference in the birefringence of the two input lead fibres, due to environmental changes, thus leads to polarisation states of different ellipticity exciting the PMRR. The resonance drift, $\Delta\omega_d$, is caused by this unequal excitation of the eigenstates. $\Delta\omega_d$ is defined as the differential phase shift of the resonance point between the two counterpropagating fields in the absence of rotation. For simplicity we initially consider the case of a PMRR in the absence of non-orthogonality. The general expression of transmission is then given by Eq.2.31. Letting $x=\beta L$ and differentiating Eq.2.31 with respect to x yields,

$$\frac{dI_4}{dx} = \frac{P_1A_1}{2}\frac{\sin(x+a_1)}{\left[1+A_1\sin^2\left(\frac{x+a_1}{2}\right)\right]^2} + \frac{P_2A_2}{2}\frac{\sin(x+a_2)}{\left[1+A_2\sin^2\left(\frac{x+a_2}{2}\right)\right]^2} \qquad (5.5)$$

where $a_j=(\pi/2+\theta_j)$ and use has been made of the identity sin(b)=2sin(b/2)cos(b/2).

For nearly perfect excitation of eigenstate 1, $x+a_1\approx 0$ at overall resonance, thus $\sin(x+a_1)\approx(x+a_1)$ and the $\sin^2(..)$ term in the denominator can be dropped. We can thus write,

$$\frac{dI_4}{dx}=\frac{P_1A_1}{2}(x+a_1)+\frac{P_2A_2}{2}\frac{\sin(x+a_2)}{\left[1+A_2\sin^2\left(\frac{x+a_2}{2}\right)\right]^2} \tag{5.6}$$

$$=\frac{P_1A_1}{2}(x+a_1)+\frac{P_2A_2}{2}.g(x+a_2)$$

By equating Eq.5.6 to zero we can now determine the resonance (operating) point of the PMRR in that direction. If we assume that in one direction around the PMRR that eigenstate 1 is perfectly excited (ie that $P_2=0$) then $x=-a_1$ is the resonance point for that direction. If in the opposite direction we assume that a small component of the second eigenstate is also excited, then the new resonance point for that direction is given from Eq.5.6 by,

$$x'=-a_1-\frac{P_2A_2}{P_1A_1}.g(x'+a_2) \tag{5.7}$$

The drift, which is the difference in the resonance points of both directions is then,

$$\Delta\omega_d=\frac{P_2A_2}{P_1A_1}.g(x'+a_2)=\frac{P_2}{P_1}\left(\frac{F_2}{F_1}\right)^2.g(x'+a_2) \tag{5.8}$$

where use has been made of Eq.2.37 for A_j (j=1,2) close to 1 (i.e. large finesse) to obtain the last equation. Note that since x' varies from $-a_1$ by only a small quantity, we can re-write the argument of the function g(..) for small drifts as $g(a_2-a_1)$, which demonstrates important result that the drift will change as the separation between the eigenstates varies with fibre birefringence.

We can further determine the maximum drift by determining the maximum value of the function $g(\sigma)$, where σ replaces $x'+a_2$ and is the overall phase delay.

Differentiating $g(\sigma)$ with respect to σ, and equating to zero yields the equation,

$$\cos(\sigma)[1+A_2\sin^2(\sigma/2)] - A_2\sin^2(\sigma) = 0 \tag{5.9}$$

Using the identities $\sin^2(\sigma/2)=(1-\cos\sigma)/2$ and $\sin^2(\sigma)=1-\cos^2(\sigma)$, Eq.5.9 reduces to a quadratic equation in $\cos(\sigma)$ with the solution,

$$\cos(\sigma) = \frac{1}{2}\sqrt{9+\frac{4}{A_2}+\frac{4}{A_2^2}} - \frac{1}{A_2} - \frac{1}{2} \tag{5.10}$$

For large values of finesse, A_2 is also large. The term $4/A_2^2$ in Eq.5.10 can be dropped, and the square root can be approximated as $\sqrt{9+4/A_2} \approx 3 + 2/(3A_2)$. Thus Eq.5.10 becomes $\cos(\sigma) \approx 1-2/(3A_2)$. Further, σ is small for high finesse and hence $\cos(\sigma) \approx 1- \sigma^2/2$. Equating the preceding two expressions for $\cos(\sigma)$ gives the approximate solution to Eq.5.10 as,

$$\sigma_0 \approx \frac{2}{\sqrt{3A_2}} \approx \frac{\pi}{\sqrt{3}F_2} \tag{5.11}$$

This leads to a maximum value $g(\sigma_0)\approx\pi/3F_2$, and hence the maximum drift is given by,

$$\Delta\omega_{dmax} \approx \frac{\pi}{3}\frac{P_2}{P_1}\frac{F_2}{F_1^2} \tag{5.12}$$

The variation in drift with loop birefringence was calculated for the case of a PMRR with a finesse of 100 and no anisotropy (h=0dB). For one direction the polarisation state was assumed perfectly linear along the x axis and for the other direction a -30dB component was also present on the y axis. The results are plotted in Fig. 5.3 for a PMRR with a polarisation isolation ratio of {a} infinity {b}33dB and {c} 25dB. The upper line in each case corresponds to the maximum ellipticity of the mismatched input and the lower one to the minimum ellipticity. The precise ellipticity as mentioned above

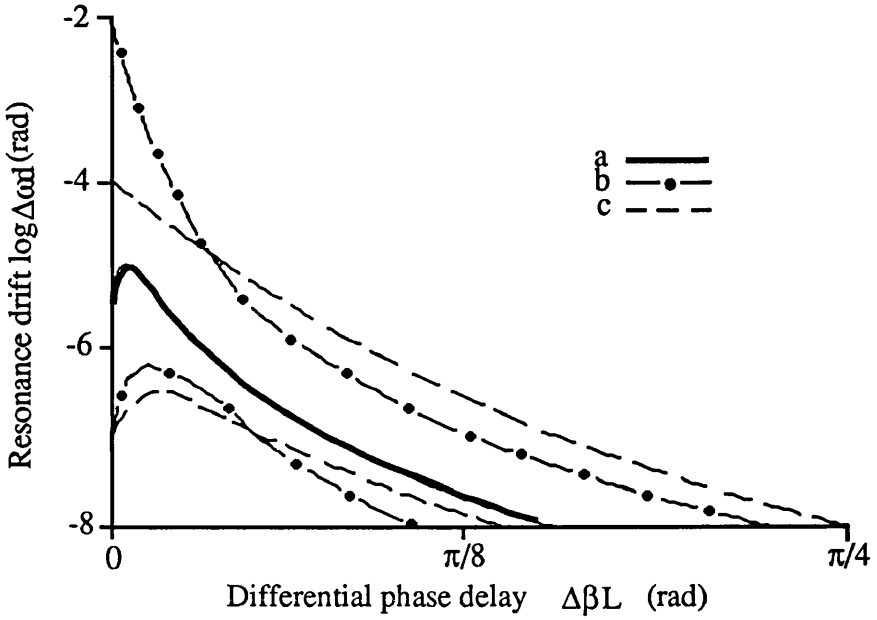

Figure 5.3. Resonance drift of a PMRR gyroscope (F=100, h=0dB). The isolation ratio is (a) ∞ (b) 33dB and (c) 25dB. The upper and lower lines in (b) and (c) correspond to the maximum and minimum ellipticities of the mismatched inputs.

will be sensitive to the lead birefringence, and the exact projection of the input onto the cavity eigenstates will therefore also change. Clearly in the presence of cross talk the drift is seen to increase significantly. It is interesting to note that the drift is larger for the case of the higher isolation ratio (33dB). Recalling Fig. 2.10, when $\Delta\beta L=0$, both eigenstates are equally excited but their phase separation decreases with the level of isolation, therefore the two resonance dips overlap to a greater extent and the resonance drift is enhanced. For the PMRR under consideration (F=100), the drift is maximised for a polarisation isolation ratio of 33dB and reduces thereafter. Also, when the two resonance points are well separated, the effect of the second eigenstate upon the resonance point in the transmission response of the first eigenstate is minimised. Fig.2.10 also suggests that a gyroscope detection system locked onto the resonance dip of eigenstate 1 could face signal fading when $\Delta\beta L$ changes sign, since in this case eigenstate 2 becomes the major resonance dip.

In chapter 2 solutions to reduce the polarisation instability were suggested. The effectiveness of the solutions based upon the introduction of a large anisotropy parameter, as for example in the case of the nematic liquid crystal placed between the coupler blocks, for reducing the drift in gyroscope applications is now discussed. If we consider the case of the same PMRR as in the previous case but now with an

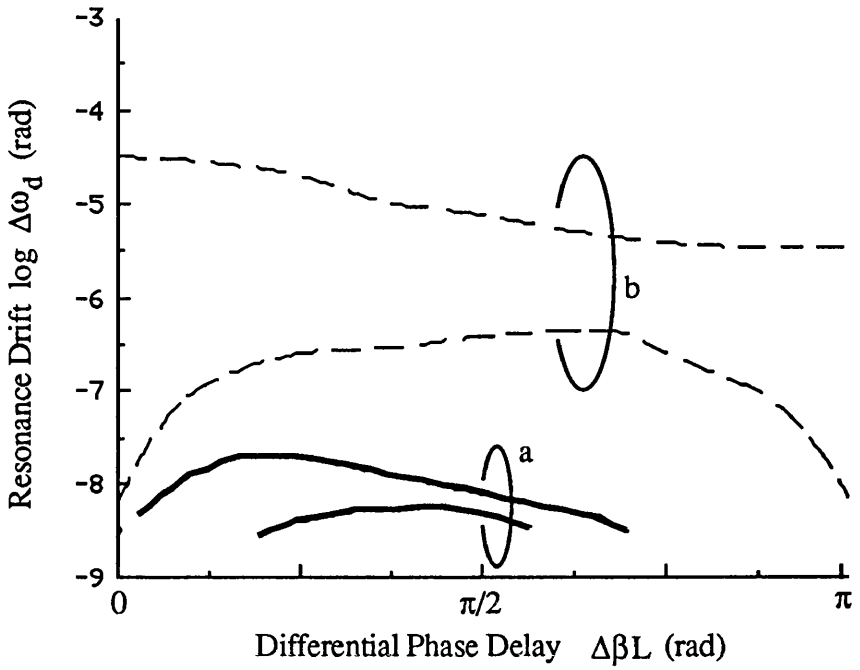

Figure 5.4. Resonance drift for the same PMRR as in Fig. 5.4, but h=-10dB. In curve (a) the non-orthogonality term of Eq.2.26 is neglected and in curve (b) it is included.

anisotropy parameter of h=-10dB and a polarisation isolation ratio of 25dB, the plot of Fig. 5.4 is obtained. Fig. 5.4 (a) shows the hypothetical drift neglecting the non-orthogonality term in Eq.2.26. This curve can be considered as the drift in an ideal PMRR, with zero cross-talk, the eigenstates of which exhibit vastly different finesses. The drift is now several orders of magnitude reduced, indicating that decreasing the finesse of the unwanted eigenstate can be a useful tool to increase the tolerance of the mismatch between the two input polarisation states. However, in the presence of cross-talk, the appearance in the non-orthogonality term in Eq.2.26 is the price to pay for the suppression of the unwanted resonance. Although this term is very small ($<10^{-3}$), its sharp variation close to the major resonance point can still be the cause of significant drift, as shown in Fig. 5.4 (b) which was calculated using the full Eq.2.26. In applications where extreme phase sensitivity is required, the benefit of introducing anisotropy in the resonator cavity is eliminated by the fact that the polarisation eigenstates become non-orthogonal, indicating that the isolation level between the fibre modes is still a crucial parameter in such systems.

Noting that the resonance drift is minimised when the eigenstates are well seperated, and recalling from §2.2.3.1 that this can be achieved by the introduction of a $\pi/2$ coupling point within the cavity (either by a $\pi/2$ effective misalignment at the

coupler or a $\pi/2$ splice within the fibre loop). The eigenvectors of such a resonator are approximately right and left circular polarisations and the eigenstates vary little with loop birefringence. When such a resonator with a $\pi/2$ coupler misalignment was modelled as the RFOG gyro, with one direction perfectly excited with right circular polarisation and the other direction excited with right handed elliptically polarised light with an ellipticity ξ, of 0.998 (i.e. a -30dB difference between the components along the fast and slow components) the gyro drift was found to be less than 10^{-9} rads, which was the minimum reliable drift measurable on the computer system used to model the response. This result is encouraging, but it should be noted that in practice it may be difficult to fabricate isotropic $\pi/2$ misaligned couplers and hence the use of a fibre splice within the loop may be more practical to achieve the $\pi/2$ polarisation coupling. Another significant advantage of this scheme can be derived from the fact that the resonator eigenstates are left and right circular polarisation states. If both directions are pumped with say left circularly polarised light, then any scattering in the loop will be right circular, and this will not resonate simultaneously with the left circularly polarised light as it corresponds to a different eigenmode. Thus the resonant backscatter should be greatly reduced, further reducing the gyroscope error due to Rayleigh backscatter effects.

A gyro drift analysis based upon a PMRR formed by splicing two PM couplers together with small polarisation axes misalignment has been reported by Hotate *et. al.*[54] The effect of polarisers placed at the input leads was found to suppress the drift at mutual resonance, but again the non-orthogonality of the eigenvectors (now taking into account the polarisers) was similarly shown to lead to a larger average drift.

5.4 Stimulated Brillouin Scattering All-Fibre Ring Resonator Gyroscope

This section now investigates the use of RFOGs to form active gyroscopes. In view of the discussion of § 5.2, it would be desirable to combine the favourable aspects of RLGs with those accrued from the use of optical fibres. Several active fibre ring laser gyroscope schemes have been proposed. These include those based upon the use of doped optical fibres[160], stimulated Raman scattering[161] and stimulated Brillouin scattering[162,163]. Of the schemes proposed, those based upon the use of stimulated Brillouin scattering (SBS) appeared to be the most promising, as it was proposed that since the generated counterpropagating Stokes waves were derived from distinct

counterpropagating acoustic waves, the gain medium would be distinct for each direction and the problem of lock-in would would be eliminated. It was also proposed that mode-pulling errors would also be reduced.

Initial attempts to demonstrate the SBS gyroscope proved unsuccessful[163,52], primarily because of limitations in the quality of the ring resonators and/or the suitability of available sources. Progress in the development of optical fibre components and fabrication technology now means that high quality all fibre ring resonators can regularly be made.

In this section the demonstration of such a fibre optic SBS gyroscope is reported. The operational theory of the SBS gyroscope is first described, and some of the design considerations required are emphasised. Experimental investigations into the use of both PMRRs and ordinary single mode fibre resonators for this application are then discussed. The lock-in effect is still found to occur in this type of gyroscope. A novel solution to avoid the effect of lock-in at low rotation rates in the SBS gyroscope is also presented. Finally, areas requiring further research for this type of gyroscope are outlined.

5.4.1 Operation of SBS Gyroscope.

The operation of the SBS gyroscope can best be understood by reference to Fig.5.5. The output of a single frequency source is coupled into both directions of an optical fibre ring resonator. The resonator has a finesse F, assumed for the moment to be identical in each direction, and an SBS lasing threshold for the circulating pump power of $P_{c,th}$. The input pump powers for the clockwise and counterclockwise directions are also assumed identical, $P_{i,cw}=P_{i,ccw}$. One direction is then maintained on resonance by means of feedback electronics.

Considering first the response of the resonator in the absence of rotation, both pumps will resonate at the same position f_o. This pump excites a possible SBS spectrum downshifted in frequency, determined (in straight lengths of fibre) only by the fibre composition, structure and pump wavelength. However, since the SBS now occurs in a cavity the filter response of the resonator means that only those SBS frequencies that can resonate simultaneously with the pump frequency will be selected. Further, because of mode competition and phase matching, those SBS components that lie nearest to the resonance dip of the response curve will be preferentially selected. The

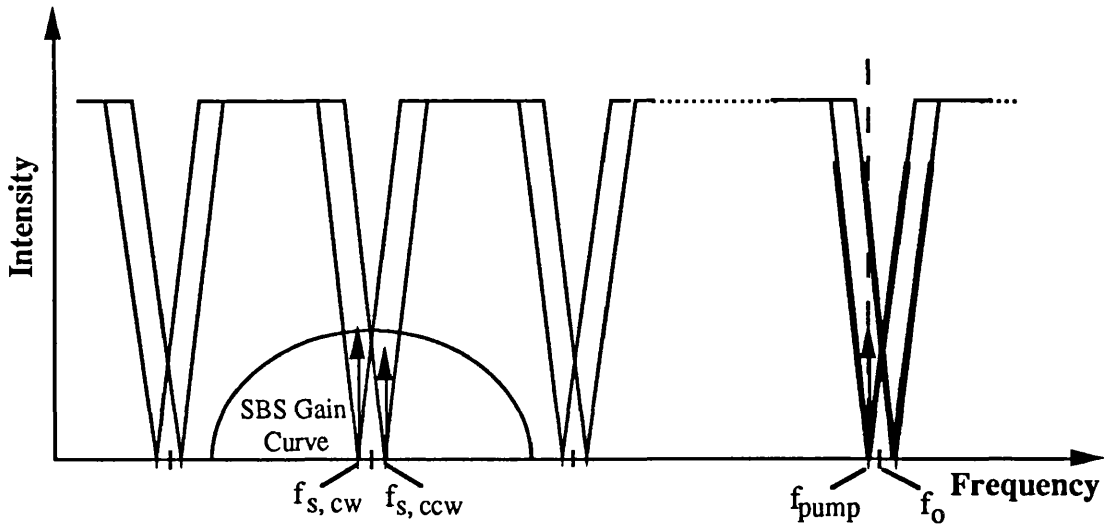

Figure 5.5 Response curve of ring resonator in the presence of rotation, showing effect of single frequency pump locked to clockwise direction of resonator response. f_{pump} is the pump frequency, f_o, the resonant pump frequency at rest, $f_{s,cw}$ and $f_{s,ccw}$ are the clockwise and counterclockwise Stokes frequencies.The thick lines represent portion of resonator response above SBS threshold for that input pump.

linewidth of the SBS generated will, as in conventional lasers, be much narrower than the width of the ring resonator, because of the gain experienced by the SBS waves, and is also inversely related to the pump power[72]. This linewidth will therefore set the resolution limit of the SBS gyroscope.

There are several considerations that need to be taken into account when choosing the cavity length of an SBS gyroscope. The optimum fibre loop length that minimises the input pump power required to obtain SBS threshold is satisfied when the coupler loss is equal to the fibre loss (cf: Fig.4.4). It is preferable however to have loop lengths exceeding the optimum value rather than lower values, because the SBS threshold for the input pump power increases much more rapidly in the latter case. However, in order to avoid the possibility of the counterpropagating SBS waves resonating at an integer multiple of 2π apart, thus creating a null shift bias, it is necessary to ensure that the cavity free spectral range is chosen such that only one resonance dip falls under the SBS gain curve. Additional care is then required to ensure this resonance dip falls near the frequency for peak SBS gain. For silica fibre at 633nm the SBS bandwidth is approximately 100MHz, and so the maximum fibre loop length that meets this condition is 2m. At longer wavelengths the SBS bandwidth is significantly reduced and thus larger loop lengths are then allowed. Another major advantage of ensuring that only one resonator response mode falls under the SBS gain curve is that the problems

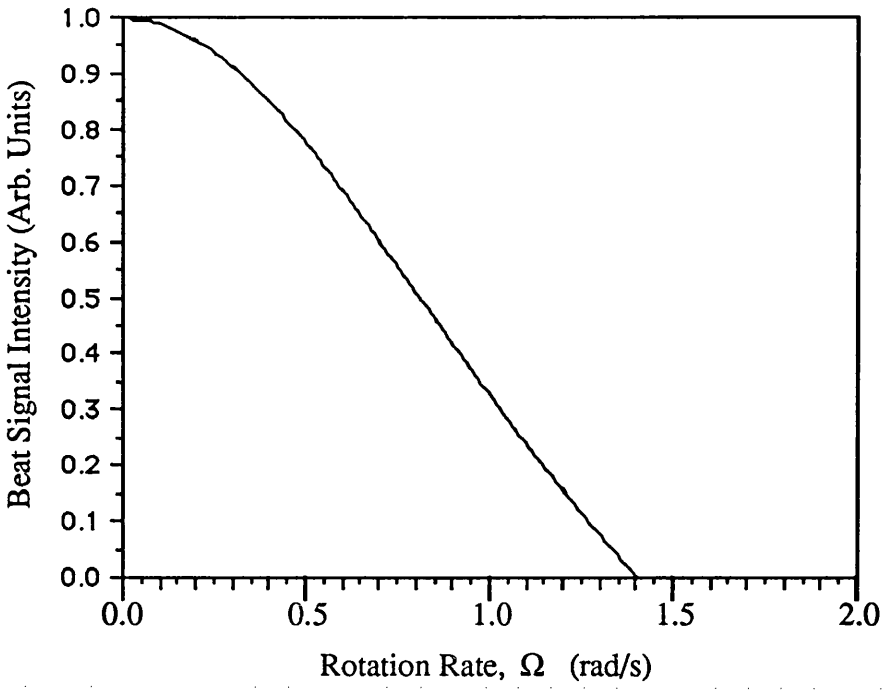

Figure 5.6 Variation of SBS beat signal with rotation rate, for a 2.3m resonator with finesse of 200 and an input pump of 400μW.

of spontaneous mode locking of the SBS lasers is avoided (cf. § 3.4), the occurrence of which would be unacceptable for stable gyroscope applications.

Now, in the presence of rotation, the resonance conditions for the clockwise and counterclockwise waves are shifted as shown in Fig.5.5, and determined by Eq.5.3. The SBS waves track the resonance dips for the reasons outlined above, and hence the SBS lasing frequencies generated also shift. It is the beat between these two SBS frequencies that gives us an indication of rotation rate. Note that typically the rotationally induced resonance shift is small, and hence the variation in the SBS gain over this region is also small and can be ignored.

However, because the resonator is locked to resonance by loop length control electronics, only one direction can be maintained accurately on resonance. The pump in that direction will continue to resonate the pump at the bottom of the resonator response curve, but the counterpropagating pump will now, be shifted off resonance, as shown. Only pump waves resonating in a portion of the resonance curve (thick lines in Fig 5.5, cf. Fig.4.6) will be above SBS threshold, and hence as the pump wave in one direction moves away from resonance, the amount of SBS generated will decrease and the signal level will also decrease, until finally when these portions of the resonator response curve no-longer overlap, the signal is lost, placing a limit upon the rotation rate

detectable by this detection scheme. The variation in the signal intensity is in itself quite tolerable, as it is only the beat frequency that provides the information. Hence, we see that the SBS gyroscope is fairly insensitive to variations in the input pump power levels, provided they do not fall below the power level required to give the necessary SBS linewidth (determined by the gyroscope resolution specified), or above the threshold for higher orders of SBS to be generated. For SBS power levels away from saturation, the SBS power generated by the resonant clockwise pump, can be approximated to first order by the equation of the straight line given by (cf Fig 4.8),

$$\left(\frac{P_{i,cw}F}{\pi} - P_{c,th}\right)\xi = P_{s,cw} \tag{5.13}$$

where ξ is a factor that describes the conversion efficiency of the additional input pump power above threshold. For the counterclockwise direction the pump is shifted off resonance with rotation and hence, for that direction we have,

$$\left(\frac{(1-\gamma_b)(1-\kappa)P_{i,ccw}}{(1-\bar{\kappa})^2 + 4\bar{\kappa}\sin^2\left(\frac{\beta L}{2}+\frac{\pi}{4}+\frac{8\pi A}{\lambda c}\Omega\right)} - P_{c,th}\right)\xi = P_{s,ccw} \tag{5.14}$$

where use has been made of Eq.4.8 and Eq.5.2, and we have ignored the optical Kerr effect. The product of Eqs.5.13 and 5.14, along with other system parameters such as beamsplitter ratios/losses and detector configurations gives the measured SBS beat signal intensities as a function of rotation rate. This is illustrated in Fig.5.6 for a 2.3m single-coil single-mode fibre resonator (8 dB/Km fibre loss at 633nm) with an optimised finesse of 200, a core diameter of 5μm, and a Brillouin gain of $4.2\text{x}10^{-11}$ mW^{-1}, pumped at 400μW input power in each direction. Eq.5.14 demonstrates that the beat signal disappears when the rotation rate is such that the terms within the brackets are equal. In the example of Fig.5.6, where the input threshold is 200μW, corresponding to a circulating pump threshold power of 12.77mW, this occurs for rotation rates in excess of 8 deg/s. The corresponding maximum SBS beat frequency obtained is 108KHz. Typically in more practical SBS gyroscopes, the fibre loop would be wrapped in small coils and the scale factor would be consequently reduced, and this

would increase the maximum detectable rotation rate. This upper limit can also be increased by increasing the input pump power, which has the effect of further increasing the portion of the resonance curve that is above threshold, upto the limit that higher orders of SBS are generated.

The advantages of this detection scheme are that it requires only one set of lock-in electronics and allows for the possibility of investigating the possible enhancement of the Sagnac effect in ring resonators, due to the optical Kerr effect[157]. However, the main disadvantage of this scheme as outlined above, is that it places a limitation upon the maximum detectable rotation rate. A dual lock-in set of electronics that keeps both counterpropagating pump directions in resonance, using frequency shifters at the inputs can be used to overcome this limitation, but the possible Sagnac enhancement effect is then no longer implementable.

5.4.2 Experimental Investigations of SBS Gyroscopes.

The schematic arrangement of Fig. 5.7 was set up on a rotation table, and used to investigate the viability of the SBS gyroscope. A 1.4mW single longitudinal mode HeNe laser (λ=633nm) was used as the pump source. Pump light was coupled to both directions of the ring resonator by means of the 50/50 beamsplitter, BS1. Bragg cells

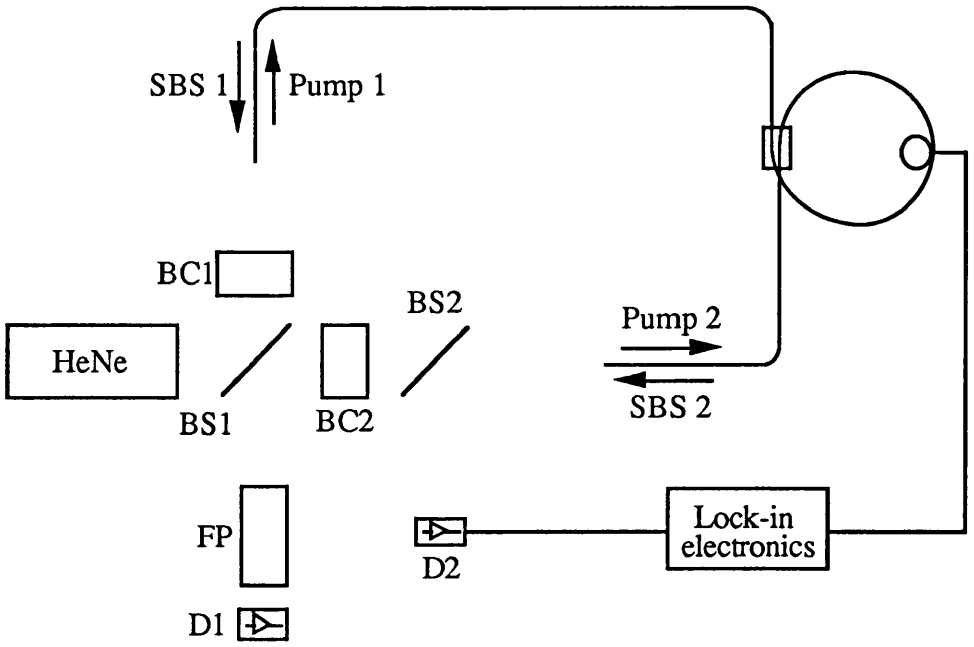

Figure 5.7 Schematic of experimental system used to investigate viability of SBS gyroscope. BC1 & BC2: Bragg cell, BS1: Beamsplitter (50/50 splitting ratio), BS2 (90/10 splitting ratio), FP: Fabry-Perot, D1 & D2: Detectors.

BC1 and BC2 were placed between BS1 and the input to each end of the resonator. They served the dual purpose of providing a rotation bias for the system and isolating the pump laser. The loop is stabilised at resonance for one direction by means of BS2 and the loop length control electronics. The outputs of the counterdirectional SBS lasers formed are coupled at BS1 and passed through a Fabry-Perot to filter out the pump and then detected by detector, D1.

The initial experiments were with a York HB600-1 PMRR. The resonator had a finesse of 240 and a loop length of 4.16m. The polarisation instability, was minimised by ensuring the phase separation of the resonator eigenmodes was $(2n+1)\pi$.

The resonator was pumped with linearly polarised light launched onto the fast axis, in both directions using the imaging technique outlined in § 4.2.1. The launch can be easily optimised by performing the following procedure. First the light transmitted through BS1 is launched into one end of the resonator. An objective lens, chosen to be as closely mode matched to the fibre output as possible first is aligned with the principal axis of the reflected port of BS1, and then translated perpendicularly, out of the way, so as not to interrupt the reflected laser beam. The output from the other fibre-end is then also aligned to the principal axis of the reflected pump light, and this compensates for any variations in fibre cleave angle. At this stage some light is found to be launched even in the absence of a launch objective lens. The previously aligned objective lens is then translated back to its former position, and the only further alignment required is to translate the fibre endface to the focal point of the lens. Only very slight adjustment is then required to optimise the launch power in this direction. This method is then repeated for the light roughly launched on the transmitted port of BS1. As well as ensuring that the launch power is maximised in that direction, this technique has the important benefit of ensuring that both outputs of the resonator are perfectly spatially combined at BS1, as everything has been aligned with the pump laser principal axis from the beginning.

With the onset of SBS lasing, two SBS peaks are again observed in each lasing direction of the PMRR as described before in Chapter 4 (cf. Fig.4.7). The Fabry-Perot helps to ensure that a beat signal is only detected at D1 when the same SBS peak is generated in each direction, by filtering out the unwanted SBS peaks. A small variable rotation bias can be applied via the Bragg cells, by driving them at different frequencies, thus allowing low frequency noise due to launch vibrations, which could mask the SBS beat frequency, to also be avoided.

5.4.2.1. Lock-In Effect in SBS Gyroscopes.

The experimental schematic of Fig. 5.8 is useful in determining the presence of mode locking in the SBS gyroscope. If the dual SBS lasers formed are uncoupled, then the SBS signal amplitude detected at D1 is expected to be of the form,

$$|E_B| = A(1-a\cos\omega_m)[\cos(\omega_p+\omega_a+2\omega_1) + b\cos(\omega_p+\omega_a+2\omega_2) + c(1+b)\cos(\omega_p+\omega_a+\omega_1+\omega_2)] \quad (5.15)$$

where A is a proportionality constant. The first term in brackets takes into account the effect of fibre end-face reflections at the fibre lead after BC2, which has the effect of creating a beat detected by D2, and is equal to the difference frequency between the frequency of BC1 and BC2, $\omega_m = |\omega_1-\omega_2|$. This beat is then faithfully fed back by the feedback electronics and leads to the amplitude modulation of the SBS components. This effect was observed experimentally for values of ω_m that fall within the low pass bandwidth of the feedback electronics. However, for larger values of ω_m the effect appeared negligible and the corresponding value of the constant a is then small. This effect, which can be the source of a form of electronic lock-in, can be removed by the addition of a phase modulator placed on one of the input leads of the resonator[155]. This has the effect of frequency shifting the beat by integer multiples of the phase modulator frequency, and these can then be removed by appropriate filtering. The Fabry-Perot simplifies the analysis, as only the SBS terms need be considered at D1. The first and second terms in the second set of brackets, represent the counterdirectional oscillating frequencies of the direct SBS1 and SBS2 terms. Note the $2\omega_j$ (j=1,2) component, due to the generated SBS components experiencing the effects of the Bragg cells twice (once indirectly by the shift in the pump frequency and then again on its way to D1. The final term represents the effect of fibre end-face reflections of the SBS components, and thus the constant c is correspondingly small. The intensity spectrum expected for the case of decoupled SBS lasers derived from Eq.5.15, has frequency components at integer multiples of ω_m. In the absence of feedback and endreflections there is no component at ω_m, and a strong component (proportional to b) at $2\omega_m$. The presence of these effects however leads to first order to a small component proportional to (c-a) appearing at ω_m, a slight reduction in the intensity of the second harmonic, and

the appearance of a third and fourth harmonic proportional to a and a^2 respectively. However, the main spectral component is still at the second harmonic.

For the case of the circulating SBS components being locked in frequency to each other, and not tracking the resonance split with rotation (actual or rotation bias due to differential Bragg cell frequencies), the expected signal amplitude at D1 is,

$$|E_B| = A(1-a\cos\omega_m)[\cos(\omega_p+\omega_a+\omega_1) + b\cos(\omega_p+\omega_a+\omega_2) + c(1+b)\cos(\omega_p+\omega_a+\omega_1+\omega_2)] \quad (5.16)$$

The intensity spectrum of Eq.5.16 in the absence of the electronic feedback and end-reflection effects now leads only to the appearance of a strong component at ω_m. The inclusion of these effects leads to the slight reduction in the first harmonic component, and the appearance of small components at both $2\omega_m$ and $3\omega_m$. By monitoring the spectrum detected at D1, we can therefore determine if mode locking is present.

When the experiment was performed a strong component at the fundamental was observed and a much smaller second harmonic component also. The amplitude of the first harmonic was found to vary with rotation rate, as would be expected in a passive gyroscope. The SBS gyroscope thus also demonstrates frequency lock-in. The experiment was repeated with the feedback electronics switched off, and the resonator maintained on lock by means of manually adjusting the PZT voltage. The small second harmonic component was still present, and is therefore due only to the effect of end-reflections and linear fibre backscatter. The lock-in effect is therefore optical, and not affected by the loop length control electronics. In order to counter the proposition[163,164] that the SBS frequencies can only change with rotation, by competition near threshold, the experiment was repeated with the SBS lasers both pumped near threshold. Still, no rotation signal was observed.

The total amount of SBS generated when the ring was lasing in both directions was also found to be greater (by as much as a factor of 2) than the sum of the SBS generated by each lasing direction independently. To investigate this further, the fibre end-face at the input to Pump 1 was polished at an angle to reduce the end-reflection at this lead. A beamsplitter BS3 similar to BS2 was then placed between BC1 and the fibre endface to tap a portion of SBS1. The intensity of SBS1 was measured first for uni-directional and then dual-directional SBS lasing. This procedure was repeated with BS3 now between BS2 and the other (unpolished) fibre end to measure SBS2. The

intensity of the SBS with dual directional lasing was found to increase in both cases. The effect of the end-reflections was quantified by adjusting first pump1 to be larger than pump2 and noting the percentage increase in the dual directional SBS lasing (as compared to the sum of the uni-directional lasing), and then repeating this measurement for pump2 larger than pump1. The effect of having unequal pumps is that the pump with the greater intensity, will reach a circulating SBS lasing threshold before the other pump. This generated backward SBS wave will then be partially reflected at the fibre end-face that forms the input to its corresponding pump, and will then re-enter the fibre loop, hence seeding the opposite direction. The greater the back-reflection of the Stokes, the greater the efficiency of SBS generation in the opposite direction. This was indeed found to be the case, with the percentage increase in dual directional SBS intensity being greater when pump2 was larger than pump1. Note, that this also experimentally demonstrates for the first time the feasibility of the SBS ring laser as an in-line fibre amplifier. The resonator would be pumped in one direction, and the signal shifted in frequency from the pump, by the phonon frequency would be input at the other end. An advantage of the type of fibre amplifier is that it only requires a low power pump source. A major disadvantage, in common with all cavity amplifiers is that the bandwidth of the signal to be amplified is limited by the response time of the resonator.

5.4.2.2 Reduction in Lock-In Effect in SBS Gyroscopes.

The lock-in range in the 633nm PMRR was larger than 30deg/s, which was the maximum rotation rate tested, whereas in the 1.15μm single mode (non-polarisation preserving) SBS fibre gyroscope investigated by the MIT group[23], the lock-in range was approximately 1deg/s. This is due to the fact that the scattering at this higher wavelength is much less than at 633nm.

A novel method for overcoming the problem of lock-in is to resonate the counter-propagating SBS lasers at frequencies that are separated by greater than the SBS gain bandwidth, ideally by a factor of 5 greater (cf. §3.2.2 and 4.5), and that are also an integer multiple of the cavity free spectral range. This ensures that the SBS generated in one direction cannot seed the counterpropagating SBS direction, and therefore the SBS lasers are uncoupled. Such a lock-in reduction scheme is only feasible in SBS and Raman type gyroscopes, since as the phonon frequencies are fixed the actual Stokes

frequencies which experience SBS gain can be shifted by shifting the pump frequency. In conventional RLG's, the gain curve is fixed in frequency space by the atomic transitions of the material used. Such an experiment with the Bow-Tie PMRR fibre resonator was not practicable because of its greatly extended SBS gain profile (cf § 4.2 and 4.3).

A 633nm resonator made of non-polarisation preserving fibre and core/cladding parameters chosen so as not to guide acoustic waves was thus fabricated. The resonator has a loop length of 2.3m and a demonstrated finesse of approximately 1000. However the coupler positioners used in our system were too coarse to keep this high finesse value stable over long periods of time. The fibre is expected to have an SBS gain bandwidth of approximately 100MHz. The frequency difference of the pumps launched into each direction of this resonator was adjusted to equal one cavity free spectral range (87.14MHz). Fibre polarisation controllers were placed at the input leads of the single mode resonators in order to efficiently excite only one cavity eigenmode. The rotation experiment was then repeated. As expected only one SBS peak was now observed in this resonator. The total SBS power generated with dual directional lasing was also found to be equal to the sum of the SBS power generated by unidirectional lasing, a good indication that lock-in is now absent. With the Fabry-Perot removed Fig. 5.9(a) shows that below SBS threshold a second harmonic component of Bragg cell 1 is found due end-reflections and Rayleigh scattering, is detected at D1. Figures 5.8(b) and (c) show the SBS beat frequency for an increasing uncalibrated rotation rate. The magnitude of the observed SBS beat frequency with rotation rate is also of the order of that expected by Eq.5.3. The potential enhancement of the Sagnac effect via the Kerr effect[157] is however not readily noticeable in our experiments. The SBS beat signal was found to be unstable in amplitude and this is thought to be probably due to the electronics used to stabilise the loop at resonance.

It should be noted, that whilst this lock-in reduction scheme eliminates the effect of lock-in for the detection scheme used, if the dual frequency method is used to keep both pump directions on resonance, then lock-in will again occur when the rotation rate is high enough, to make the corresponding gain curves overlap again. A more pressing problem with this lock-in reduction scheme is the possible non-reciprocity arising from the use of non-identical pump frequencies in each lasing direction. In terms of the generated SBS waves, the clockwise and counterclockwise waves are separated by one free spectral range, and the total differential round trip phase delay is therefore 2π,

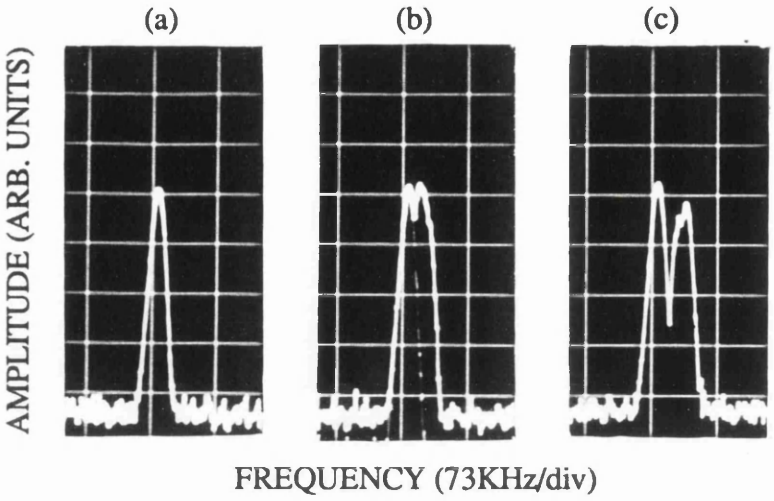

Figure 5.8 Detected response on spectrum analyser showing (a) 2nd harmonic of BC2, zero rotation and (b), (c) SBS beat frequency for increasing rotation rates.

which can be expressed in the absence of rotation by,

$$\phi_{cw} - \phi_{ccw} = 2\pi nL\left(\frac{1}{\lambda_{cw}} - \frac{1}{\lambda_{ccw}}\right) = 2\pi \tag{5.17}$$

where λ_{cw} and λ_{ccw} are the corresponding SBS vacuum wavelengths, L is the resonator length and n is the refractive index, assumed over the small frequency difference (<90MHz) to be identical for each direction. The temperature sensitivity of this phase difference can be found by differentiating Eq.5.17 with respect to temperature,T, to give,

$$\frac{d}{dT}(\phi_{cw} - \phi_{ccw}) = 2\pi nL\left(\frac{1}{\lambda_{cw}} - \frac{1}{\lambda_{ccw}}\right)\left(\frac{1}{L}\frac{dL}{dT} + \frac{1}{n}\frac{dn}{dT}\right) \tag{5.18}$$

The term (1/L)dL/dT represents the thermal expansion coefficient of the optical fibre and for silica fibres this equals $5\times10^{-7}/^{o}C$. The corresponding value of the change in index with temperature dn/dT is much larger and equals $1\times10^{-5}/^{o}C$. Generalising Eq.5.18 to show the variation in phase difference as a function of change in temperature from the initial temperature at which the initial phase difference was set to 2π, and dropping the thermal expansion term gives,

$$\phi_{cw} - \phi_{ccw} = 2\pi + \frac{2\pi}{n}\frac{dn}{dT}\Delta T \qquad (5.19)$$

The second term on the RHS of Eq.5.19 represents the phase error. This phase error is independent of the loop length L, and is only dependent upon the differential loop phase delays. This error can be quite large. For a ΔT of 1°C and n=1.45, the corresponding phase error given by Eq.5.19 is 43μrad. From Eq.5.1 this non-reciprocal phase shift corresponds to an error in our single mode resonator (A approx. 29cm^2) of 80deg/hr. This value ofcourse scales directly with the scale factor. The use of this lock-in reduction scheme may therefore only be applicable in low cost low performance guidance schemes, such as AHRS and automobile navigation.

An open research topic is the role that phase conjugation of the SBS wave could play upon the performance of the SBS gyroscope. It is possible that if a high fidelity phase conjugate SBS wave is generated, then the lock-in reduction scheme described above would be insensitive to the differential loop phase due to different frequencies, and the resulting phase error would be zero. Phase conjugation would render the device insensitive to reciprocal effects, but still sensitive to non-reciprocal effects[2,165]. The portions of SBS not phase conjugated would simply lead to a source of drift noise in this SBS gyro configuration. The combination of the decoupled SBS gain curves and phase conjugate counterdirectional Stokes waves makes this lock-in reduction scheme very attractive, and warrants further research.

5.6 Conclusions.

The use of the RFOG, in both passive and active fibre gyroscope embodiments has been investigated. Passive RFOGs made with polarisation maintaining fibre exhibit a drift in their resonance positions with loop birefringence, whenever the loop eigenmodes are not identically excited in both directions. This drift can be quite severe, and methods to suppress it were investigated. The viability of drift reduction schemes based upon increasing the anisotropy factor h, to reduce the finesse and modulation depth of the unwanted eigenmode, were examined and it was found that the increase in the non-orthogonality of the eigenvectors counteracts the potential reduction in drift. The use of isotropic $\pi/2$ polarisation coupling points within the fibre cavity is predicted to successfully minimise the gyro drift as the resonant eigenstates are then well seperated. The levels of resonant scatter within such a resonator are also expected to be

substantially reduced.

One of the first solid state active fibre gyroscope based upon stimulated Brillouin scattering has also been demonstrated, and its design criterion outlined. Experimental results demonstrated the presence of frequency lock-in in RFOGs fabricated either with polarisation maintaining fibre or with single mode fibre. The frequency lock-in was due to backscattering and end-reflections seeding the counterpropagating SBS laser. This also experimentally demonstrates for the first time the viability of the fibre resonator as an in-line narrow-band fibre amplifier. The extended SBS gain bandwidth in the Bow-Tie polarisation maintaining fibre resonator investigated led to that device having a much larger lock-in range. A novel technique for reducing the effects of lock-in in the SBS gyroscope based upon the frequency seperation of the clockwise and counterclockwise SBS gain curves was also proposed and successfully demonstrated.

Chapter Six

DISCUSSION AND CONCLUSIONS

This dissertation investigated both theoretically and experimentally the polarisation properties of ring resonators made with polarisation maintaining fibre (PMRRs), and the effects of stimulated Brillouin scattering upon device performance.

The characteristics of practical ring resonators made with polarisation maintaining fibre were modelled by evoking the Jones Matrix formalism and an expression was derived that completely characterised the polarisation response of the PMRR. The unavoidable presence of a finite amount of polarisation mode cross coupling was shown to lead to the eigenvectors of the ring becoming dependent upon the loop birefringence. Cavity anisotropy in terms of polarisation loss or coupler coupling coefficient was further shown to lead to the two resonant eigenstates of the loop becoming non-orthogonal. This non-orthogonality leads to the eigenstates becoming interdependent. For constant polarisation state inputs, the intensity transmission response of the resonator shows strong variations with loop birefringence, especially when the loop birefringence is an integer multiple of 2π. In both the cases of isotropic and anisotropic cavities, in the presence of polarisation cross-talk, the phase separation between resonant eigenstates is not a linear function of loop birefringence. A minimum phase separation between the resonant eigenstates was shown to exist, which for the case of an isotropic cavity was equal to twice the effective misalignment angle.

The tolerance required in the polarisation cross-talk levels to minimise the polarisation instability were shown to be impractical, with even a polarisation cross-talk level of -35dB leading to significant resonance distortions for resonators with finesse

values over 100. Such strong variations in the resonator transmission response render the device unsuitable for most applications, and necessitate the need for suitable solutions. Several methods were shown theoretically to be feasible for suppressing the polarisation instability. These include the use of 90^0 coupler misalignment angles; 90^0 fibre splices within the loop; large anisotropic loop losses; and large anisotropic coupler coupling coefficients. The latter technique was successfully implemented with the aid of a nematic liquid crystal placed between the coupler half blocks to demonstrate the first reported polarisation stabilised PMRR. These techniques dramatically improve the stability of the resonator response and restore the suitability of the device for most applications.

Limitations in the maximum achievable sensitivity of the fibre ring resonator set by the onset of stimulated Brillouin scattering were also researched. These effects had not been previously considered and are increasingly important, as the finesse values of state of the art fibre ring resonators continue to improve. A PMRR with a finesse of 600 and a single mode fibre resonator with a finesse of 1000 has already been fabricated within the UCL laboratories. Depletion of the circulating input wave due to the SBS process was shown to lead to saturation of the steady state circulating intensity at the lasing threshold. This leads to increased response integration times, significant intensity dependent variations in the transmission characteristics, and a potentially non-reciprocal resonator response. The variations in the transmission characteristics of the device can be modelled to first order as variations in the finesse and modulation depth of the device, although for strong depletion effects this approximation breaks down and effectively 'clipping' of the resonance notches occurs.

The threshold for SBS lasing in a 1m PMRR with a finesse of 330 was observed to be only 65μW. Such low SBS thresholds place a constraint upon the signal to noise ratios obtainable from the device and the effects of SBS depletion therefore need to be considered as a potential limitation by future system designers. Two novel suppression techniques for increasing the SBS threshold level for stimulated Brillouin lasing within the ring resonator were investigated. The first method was based upon filtering of the pump and Stokes waves, and the second was based on mutually resonating multiple independent pumps. This latter technique was also experimentally demonstrated for the first time in a ring resonator. Both methods allow dual directional operation of the resonator (which is important for gyroscope applications) and avoid the requirement of additional components within the resonator device. On an applications front, the

feasibility of the use of the stimulated Brillouin scattering process in fibre ring resonators to form in-line-amplifiers was also demonstrated for the first time. Guidelines were given on the various material parameters that need to be considered in the choice of suitable optical fibre used for fabricating the devices. The occurrence of guided acoustic waves within the optical fibres was also examined and shown to lead to an extended stimulated Brillouin gain profile.

The characterisation and stabilisation/suppression techniques outlined above should aid future fibre ring resonators to be operated without the need for active polarisation control and with improved sensitivity over an increased dynamic range.

The characterisation work was further extended by investigating the ring resonator fibre-optic gyroscope (RFOG) as a specific resonator application. Both active and passive implementations of the RFOG were demonstrated. The analysis developed for modelling the polarisation maintaining fibre ring resonator was used to predict the suitability of the device for gyroscope applications, where extreme phase sensitivity is required. A gyroscope drift dependent upon loop birefringence was shown to occur whenever the excitation of the resonator eigenstates was not identical in both cavity directions. The drift in the resonance condition with loop birefringence was plotted and it was shown that the reduction expected in the resonance stability by the use of strongly anisotropic couplers was counteracted by the non-orthogonality of the resonator eigenstates. The use of 90^0 misaligned couplers was however predicted to substantially reduce the gyroscope drift as well as reduce the level of resonant backscatter.

The onset of stimulated Brillouin lasing at relatively low input thresholds was used to experimentally demonstrate one of the the first solid state ring laser gyroscopes. Such a gyroscope possesses many advantages over its contemporaries, both on technical and economic grounds. The basic design criterion required for this gyroscope were outlined, the most important parameter being the cavity free spectral range. This has to be suitably adjusted to avoid spontaneous mode locking and null-shift errors. Despite earlier predictions[67], frequency lock-in was shown to occur in this new gyroscope. A novel method for avoiding the frequency lock-in effect was then proposed and successfully demonstrated.

Recommendations and Future Work

Experimental demonstrations need to be performed for the various PMRR stabilisation schemes proposed, in order to further evaluate their suitability. It is expected that the use of anisotropic coupling as opposed to anisotropic loss will be preferable due to the reduced eigenstate non-orthogonality in this case, but this needs to be further quantified.

More work needs to be done on stimulated Brillouin suppression techniques in ring resonators, and the Stokes wave filtering technique in particular appears promising and should be experimentally evaluated.

The effects of the passive RFOG gyroscope drift reduction schemes also need to be further investigated, especially the use of a 90^0 polarisation coupling point within the cavity. The demonstration of the stimulated Brillouin scattering gyroscope is also expected to stimulate many new research topics. The fibre SBS gyroscope offers significant advantages over its bulk-optic RLG rival. It should be much cheaper, more reliable and simpler to implement. The all-fibre design would provide low weight, rugged construction as well as optimisation of the gyroscope shape. The primary areas that need to be further studied are: (1) A full investigation of the guided acoustic wave properties of optical fibres, (2) The relationship between reciprocity and phase conjugate fidelity in the proposed lock-in reduction scheme and (3) The interaction with other non-linear effects, especially with a view to characterising and possibly enhancing the sensitivity of the device to Sagnac phase. Points (2) and (3) are particularly important. The presence of a well phase conjugated Stokes wave in the SBS gyroscope would allow the possibility of an effective low drift frequency lock-in reduction scheme, and the combination of the SBS and Kerr effects could lead to significant enhancements in the scale factor of the SBS gyroscope.

The precise polarisation instability effects, similar to those described in § 5.3 upon the SBS selection process also needs to be considered. The free-spectral-range of each eigenstate is effectively slightly different and so the drift in resonance point at the SBS frequencies will be different to those at the pump frequencies.

REFERENCES

[1] L. F. Stokes, M. Chodorow, and H. J. Shaw, "Sensitive all-single mode fibre resonant ring interferometer", *J. Lightwave Technol.*, **LT-1**, 110 (1983).

[2] In "*Fibre-optic rotation sensors & related technologies*", Edited by S. Ezekiel, H. J. Arditty, Publ. Springer-Verlag (Berlin, Heidelberg, New York) 1982.

[3] S. A. Newton, "Optical fibre delay line signal processing", PhD Dissertation, Ginzton Laboratory, Stanford University, Jan. (1984).

[4] S. A. Newton, R. S. Howland, K. P. Jackson, and H. J. Shaw, "High speed pulse train generation using single mode fibre recirculating delay lines", *Elect. Lett.*, **19**, 756 (1983).

[5] D. Jong, K. Hotate, "Frequency division multiplexing of optical fibre sensors using an optical delay loop with a frequency shifter", *Appl. Opt.*, **28**, 1289 (1989).

[6] S. Tai, K. Kyuma, K. Hamanaka, and T. Nakayama, "Applications of fibre optic ring resonators using laser diodes", *Optica Acta*, **33**, 1539 (1986).

[7] Y. Ohtsuka, "Analysis of a fibre optic passive loop resonator gyroscope: Dependence on resonator parameters and light source coherence", *J. Lightwave Technol.*, **LT-3**, 378 (1985).

[8] B. Lamouroux, B. Parde, and A. Orszag, "Polarisation effect in optical fibre ring resonators", *Opt. Lett.*, **7**, 391 (1982).

[9] R. J. Mears, M. P. Varnham, D. N. Payne and A. J. Barlow, "Polarisation control in resonant ring fibre gyroscopes", Proc. Optical Fibre Sensors, OFS-88 (Stuttgart, Germany), 1988.

[10] K. Iwatsuki, K. Hotate, and M. Higashiguchi, "Eigenstate of polarisation in a fibre ring resonator and its effect in an optical passive ring resonator gyro", *Appl. Opt.*, **25**, 2606 (1986).

[11] M. Tur, B. Moslehi, and J. W. Goodman, "Theory of laser phase noise in recirculating fibre optic delay lines", *J. Lightwave Technol.*, **LT-3**, 20 (1985).

[12] K. Iwatsuki, K. Hotate, and M. Higashiguchi, "Effect of Rayleigh backscattering in an optical passive ring resonator gyro", *Appl. Opt.*, **23**, 3916 (1984).

[13] K. Iwatsuki, K. Hotate, and M. Higashiguchi, "Kerr effect in an optical passive ring resonator gyro", *J. Lightwave Technol.*, **LT-4**, 645, (1986).

[14] K. Hotate, M. Murakami, "Drift of an optical passive ring resonator gyro caused by the Faraday effect", Proc. Optical Fibre Sensors, OFS-88, (New Orleans, USA), **FBB6**, 405, (1988).

[15] Z. Ioannidis, R. Kadiwar, and I. P. Giles, "Polarisation mode coupling in high birefringence optical fibre ring resonators", *Opt. Lett.*, **14**, 520 (1989).

[16] Z. Ioannidis, R. Kadiwar, and I. P. Giles, "Polarisation effects in highly birefringent fibre ring resonators", Proc. Optical Fibre Sensors, OFS-89, Paris, France, Sept. 18-20, 1989. Editors H. J. Arditty, J. P. Dakin, and R. Th. Kersten, Publishers Springer-Verlag.

[17] (a) I. P. Giles, M. Farhadiroushan, A. Kerr, M. N. Zervas, and R. Kadiwar, "Polarisation maintaining optical fibre components for advanced sensor systems", EFOC/LAN-88, Amsterdam, The Netherlands, June 29-July 1, 1988; (b) C. Y. Yue, J. D. Peng, Y. B. Liao, and B. K. Zhou, "Fibre ring resonator with finesse of 1260", *Elect. Lett.*, **24**, 621 (1988)

[18] R. Kadiwar, P. Bayvel, I. P. Giles, "Stimulated Brillouin Scattering in polarisation maintaining ring resonators", *Proc.* Society of Photo-Instumental Engineers, SPIE, Fibre Optics & Lasers, **985**, Boston, USA, (1988).

[19] R. Kadiwar, I. P. Giles, "Effects of stimulated Brillouin scattering on the performance of polarisation maintaining fibre ring resonators", *Opt. Lett.*, **14**, 332 (1989).

[20] P. Bayvel, J. Halley, R. Kadiwar, and I. P. Giles, "Theoretical and experimental investigation of all fibre single mode Brillouin lasers", *IEE* European Conference On Communications, ECOC-88, Brighton, UK, Sept. 11-15 1988.

[21] I. P. Giles, R. Kadiwar, and Z. Ioannidis, "Stimulated Brillouin scattering in polarisation maintaining all fibre ring resonators",*IEE* European Fibre Optic Communications and Local Area Networks symposium, EFOC/LAN-89, Amsterdam, The Netherlands, 1989

[22] R. Kadiwar, I. P. Giles, "Optical fibre Brillouin ring laser gyroscope", *Elect. Lett.*, **25**, 1729 (1989).

[23] S. P. Smith, F. Zarinetchi, and S. Ezekiel, "Fibre optic ring laser gyroscope", Proc. Optical Fibre Sensors, OFS-89, Paris, France, 1989, Post-deadline paper TU-10.6.

[24] E. J. Bachus, R. P. Braun, and B. Strebel, "Polarisation maintaining single mode fibre resonator", *Elect. Lett.*, **19**, 1027 (1983)

[25] G. Sanders, N. Demma, G. Rouse, and R. B. Smith, "Evaluation of polarisation maintaining fibre resonator for rotation sensing applications", Proc. Optical Fibre Sensors, OFS-88, New Orleans, USA, **FBB7-1**, 409 (1988).

[26] J. Noda, K. Okamoto, and Y. Sasaki, "Polarisation maintaining fibres and their applications", *J. Lightwave Technol.*, **LT-4**, 1071 (1986).

[27] A. J. Barlow, D. N. Payne, M. R. Hadley, and R. J. Mansfield, "Production of single mode fibres with negligible intrinsic birefringence and polarisation mode dispersion", *Elect. Lett.*, **17**, 725 (1981).

[28] S. C. Rashleigh, M. J. Marrone, "Polarisation holding in elliptical core birefringent fibres", IEEE *J. Quant. Elect.*, **QE-19**, 1515 (1982).

[29] R. B. Dyott, P. F. Schrank, "Self locating elliptically cored fibre with an accessible guiding region", *Elect. Lett.*, **18**, 980 (1982).

[30] R. D. Birch, D. N. Payne, and M. P. Varnham, "Fabrication of polarisation maintaining fibres using gas phase etching", *Elect. Lett.*, **18**, 1036 (1982).

[31] (a) V. Ramaswamy, R. H. Stolen, M. D. Divine, and W. Pliebel, "Birefringence in elliptically clad borosilicate single mode fibres", *Appl. Opt.*, **18**, 4080 (1979); (b) S. C. Rashleigh, M. J. Marrone, "Polarisation holding in a high birefringence fibre", *Elect. Lett.*, **18**, 326 (1982).

[32] N. Shibata, Y. Sasaki, K. Okamoto, and T. Hosaka, "Fabrication of polarisation maintaining and absorption reducing fibres", *J. Lightwave Technol.*, **LT-1**, 38 (1983)

[33] S. B. Poole, J. E. Townsend, D. N. Payne, M. E. Fermann, G. J. Cowle, R. I. Laming, and P. R. Morkel, "Characterisation of special fibres and fibre devices", *J. Lightwave Technol.*, **LT-7**, 1242 (1989).

[34] M. P. Varnham, D. N. Payne, and J. D. Love, "Fundamental limits to the transmission of linearly polarised light by birefringent optical fibres", *Electon. Lett.*, **20**, 55 (1984).

[35] F. M. Sears, "Cross polarisation limits in polarisation maintaining fibres and measurements", *Proc.* IEE European Conference On Communications, ECOC-87, Barcelona, Spain, 239 (1987).

[36] R. A. Bergh, G. Kotler, and H. J. Shaw, "Single mode fibre optic directional coupler", *Electon. Lett.*,**16**, 260 (1980).

[37] T. Ozeki and B. S. Kawasaki, "New star coupler compatible with single multimode fibre data links", *Electon. Lett.*, **12**, 151 (1976).

[38] S. K. Sheem and T. G. Giallorenzi, "Single mode fibre optical power divider: Encapsulated etching technique", *Opt. Lett.*, **4**, 29 (1979).

[39] B. K. Nayar, and D. R. Smith, "Monomode polarisation maintaining fibre directional couplers", *Opt. Lett.*, **8**, 543, (1983).

[40] W. Pleibel, R. H. Stolen, and S. C. Rashleigh, "Polarisation preserving coupler with self aligning birefringent fibres", *Electon. Lett.*, **19**, 825 (1983).

[41] I. Yokohama, K. Chida and J. Noda, "Low excess loss conditions of polarisation maintaining fibre couplers", *Appl. Opt.*, **27**, 4807 (1988).

[42] S. L. A. Carrara, B. Y. Kim, and H. J. Shaw, "Elasto-optic alignment of birefringent axes in polarisation holding optical fibre", *Opt. Lett.*, **11**, 470 (1986).

[43] M. J. Marrone, C. A. Villarruel, N. J. Frigo, and A. Dandridge, "Internal rotation of the birefringence axes in polarisation holding fibres", *Opt. Lett.*, **12**, 60 (1987).

[44] C. Chen and W. K. Burns, "Polarisation characteristics of single mode fibre couplers", IEEE *J. Quant. Elect.*, **QE-18**, 1589 (1982).

[45] A. W. Snyder and A. Stevenson, "Anisotropic fibre couplers with non-aligned optical axes", *J. Lightwave Technol.*, **LT-6**, 450 (1988).

[46] M. S. Yataki, D. N. Payne, and M. P. Varnham, "All fibre polarising beamsplitter", *Electon. Lett.*, **21**, 249 (1985).

[47] A. W. Snyder and A. J. Stevenson, "Polarisation splitters and birefringent couplers", *Electon. Lett.*, **21**, 75 (1985).

[48] A. W. Snyder and A. J. Stevenson, "Polished type couplers acting as polarising beam splitters", *Opt. Lett.*, **11**, 254 (1986).

[49] E. Shafir, A. Hardy and M. Tur, "Polarisation maintaining fibre couplers with misaligned birefringent axes", *Electon. Lett.*, **24**, 754 (1988).

[50] W. Shurcliff, "*Polarised Light - Production and Use*", Harvard University Press, (1962).

[51] R. Azzam, and N. Bashara, "*Ellipsometry and polarised light*", North-Holland Publishing Co., (1977).

[52] L. F. Stokes, "Single mode optical fibre resonator and applications to sensing", PhD dissertation, Stanford University, 1983.

[53] M. Takahashi, S. Tai, and K. Kyuma, "Nondestructive measuring technique for misaligned angle in polarisation maintaining fibre coupler", *Elect. Lett.*, **25**, 600 (1989).

[54] K. Hotate, K. Takiguchi, and M. Murakami, "Bias of an optical passive ring resonator gyro due to the misalignment of the polarisation axis in the resonator formed by polarisation maintaining fibre", Proc. Optical Fibre Sensors, OFS '89 (Paris, France), Mo-4-2, 94 (1989).

[55] H. G. Jerrard, "Transmission of light through birefringent and optically active media: the Poincaré sphere", *JOSA*, **44**, 634 (1954).

[56] M. P. Varnham, D. N. Payne, R. D. Birch and E. J. Tarbox, "Single polarisation operation of highly birefringent bow-tie optical fibres", *Elect. Lett.*, **19**, 246 (1983).

[57] M. Corke, A. D. Kersey, K. Liu, and D. A. Jackson, "Remote temperature sensing using polarisation preserving fibre", *Elect. Lett.*, **20**, (1984).

[58] A. Arie, and M. Tur, "The effects of polarisation control on the transfer function and the phase induced intensity noise of a fibre optic recirculating delay line", *J. Lightwave Technol.*, **LT-6**, 1566 (1988).

[59] Personal communication with Dr Stuart Robinson, GEC Hirst research Laboratories, Wembly, London.

[60] Z. K. Ioannidis, P. M. Radmore and I. P. Giles, "Phase modulation in all fibre ring resonator sensor", Proc. Optical Fibre Sensors, OFS '88, **ThBB3-1**, (New Orleans, USA), 1988.

[61] M. N. Zervas, "Non-linear and resonance effects in fibre optic components", PhD dissertation, University Collage London, London University (1989).

[62] M. P. Varnham, D. N. Payne, A. J. Barlow and E. J. Tarbox, "Coiled birefringent fibre polarisers", *Opt. Lett.*, **9**, 306 (1984).

[63] R. C. Youngquist, L. F. Stokes, and H. J. Shaw, "Effects of normal mode loss in dielectric waveguide directional couplers and interferometers", *IEEE J. Quantum Elect.*, **QE-19**, 1888 (1983).

[64] M. Zurn and R. Ulrich, "Elasto optic loss modulation in side polished fibre", *Elect. Lett.*, **24**, 829 (1988).

[65] K. O. Hill., B. S. Kawasaki, and D. C. Johnson, "CW Brillouin laser", *Appl. Phys Lett.*, **28**, 608 (1976).

[66] I. Bar Joseph, A. Dienes, A. Friesem, E. Lichtman, R. Waarts and H. Yaffe, "Spontaneous mode locking of single and multi mode pumped SBS fibre lasers", *Opt. Comm.*, **59**, 296 (1986)

[67] P. J. Thomas, H. M. van Driel, G. I. A. Stegman, " Possibility of using an optical fibre Brillouin ring laser for inertial sensing ", *Appl. Opt.*, **19**, 1906 (1980).

[68] N. Bloembergen, and Y. R. Shen, "Quantum theoretical comparison of non-linear susceptibilities in parametric media, lasers and Raman lasers", *Phys. Rev.*, **133**, A 37 (1964).

[69] M. V. Bergot, M. C. Farries, M. E. Fermann, L. Li, L. J. Poyntz-Wright, P. St. J. Russell, and A. Smithson, "Generation of permanent optically induced second-order non-linearities in optical fibres by poling", *Opt. Lett.*, **12**, 585 (1988).

[70] K. Kaiser, and M. Mair, "Stimulated Rayleigh, Brillouin and Raman spectroscopy", in *Laser Handbook*, vol. 2, ch. E2, 1078, F.T. Arecchi and E.O. Schultz-Dubois, Eds. North Hollands publishing Co. Amsterdam,. (1972).

[71] Chiao, Townes and Stoicheff, "Stimulated Brillouin scattering and coherent generation of intense hypersonic waves", *Phys. Rev. Lett.* **12**, 592 (1964).

[72] C. L. Tang, "Saturation and spectral characteristics of the Stokes emmision in the Stimulated Brillouin process", *J. Appl. Phys.* **37**, 2945 (1966).

[73] N. M. Kroll, "Exitation of hypersonic vibrations by means of photoelastic coupling of high-intensity light waves to elastic waves", *J. Appl. Phys.* **36**, 34 (1965).

[74] V. S. Starunov, and I. L Fablinskii, "Stimulated Mandel'shtam-Brillouin scattering and stimulated entropy (temperature) scattering of light", *Soviet Phys* USPEKHI, **12**, 463 (1970).

[75] Y. R. Shen, in "*The principles of non-linear optics*", publ: Wiley-Interscience, 187 (1984).

[76] A. Yariv, "Quantum theory for parametric interactions of light and hypersound", *IEEE J. Quantum Electron.*, **QE-4**, 28 (1965).

[77] E. P. Ippen, and R. H. Stolen, "Stimulated Brillouin scattering in optical fibres", *Appl. Phys. Lett.*, **21**, 539 (1972).

[78] L. Brillouin, "Diffusion de la lumiere et des rayon x par un corps transparent homogene", *Annales de Physique* (Paris), **17**, 88 (1922).

[79] L. Mandelshtam, *Zh. Russ. Khim. Obschestva* **58**, 381 (1926)

[80] J. Stone, and Chraplyvy, "Spontaneous Brillouin noise in long distance high bandwidth optical fibre transmission", *Elect. Lett.*, **19**, 275 (1983).

[81] K.O Hill, D.C Johnson, and B. S. Kawasaki, " CW generation of multiple Stokes and anti-Stokes Brillouin shifted frequencies ", *Appl. Phys. Lett.*, **29**, 185 (1976).

[82] K. O Hill, B. S Johnson, B. S. Kawasaki, and R. I. MacDonald, "CW three wave mixing in single mode fibres ", *J. Appl. Phys.*, **49**, 5098 (1978).

[83] J. A. Bucaro, and H. D. Dardy, " High temparature Brillouin scattering in fused quartz", J. *Appl. Phys.*, **45**, 5324 (1974).

[84] P. Narum, M. D. Skeldon, and R. W. Boyd, " Effect of laser mode structure on stimulated Brillouin scattering", IEEE *J. Quantum Electron.*, **22**, 2161 (1986).

[85] Y. E. D'yakov, " Exitation of stimulated light scattering by broad spectrum pumping ", *Soviet Phys. JETP Lett.*, **11**, 243 (1970).

[86] G. C. Valley, " A review of stimulated Brillouin scattering excited with a broad band pump laser ", *IEEE J. Quantum Electron.*, **QE-22**, 704 (1986).

[87] D. Cotter, " Suppression of stimulated Brillouin scattering during transmission of high power narrowband laser light in monomode fibre ", *Elect. Lett.*, **18**, 638 (1982).

[88] M. Tsubokawa, S. Seika, T. Nakashima, N. Shibata, " Suppression of SBS in a single-mode fibre by an acousto-optic modulator ", *Elect. Lett.*, **22**, 473 (1986).

[89] E. Lichtman, A. A. Friesem, R. G. Waarts, and H. H. Yaffe, "Stimulated Brillouin scattering exited by two pump waves in single-mode fibres ", *J. Opt. Soc. Am. B.*, **4**, 1397 (1987).

[90] R. Mullen, R. .C. Lind, and G. Valley, " Observations of stimulated Brillouin scattering gain with a dual spectral-line pump ", *Opt. Comm.*, **63**, 123 (1987).

[91] Y. Aoki, K. Tajima, " Stimulated Brillouin scattering in a long fibre exited with a multimode pump laser ", *J. Opt. Soc. Am. B.*, **5**, 358 (1988).

[92] Peronal communication with DR D. Cotter, BTRL, Martelsham Heath, Ipswich Suffolk, 1P12 4JN, UK (1989).

[93] Y. R. Shen, Chapter 14, in "*The principles of non-linear optics*", publ: Wiley-Interscience, (1984).

[94] E. Lichtman, R. G. Waarts, and A. A. Friesem, " SBS exited by a modulated pump wave in single-mode fibres ", *J. Lightwave Technol.*, **LT-7**, 171, (1989).

[95] A. Bolle, G. Grosso, B. Daino, " Brillouin gain curve dependance on frequency spectrum of PSK-Modulated signals ", *Elect. Lett.*, **25**, 2 (1989).

[96] A. Hadjifotiou, and G. A. Hill, " Suppression of SBS by PSK modulation for high power optical transmission ", *IEE Proc.*, **133**, Pt. J, 256 (1986).

[97] E. I. Ippen, and R. H. Stolen, "Stimulated Brillouin scattering in optical fibres" *Appl. Phys. Lett.*, **21**, 539 (1972).

[98] R. H. Stolen, "Polarisation effects in fibre Raman and Brillouin Lasers", *IEEE J. Quantum Electron.*, **QE-15**, 1157 (1979).

[99] T. Horiguchi, M. Tateda, N. Shibata, and Y. Azuma, "Brillouin gain variation due to a polarisation state change of the pump or Stokes fields in standard single mode fibres ", *Opt. Lett.*, **14**, 329 (1989).

[100] M. D. Levenson, R. M. Shelby, and A. Aspect, "Generation and detection of squeezed states of light by nondegenerate four wave mixing in an optical fibre" *Phys. Rev. A.*,**32**, 1550 (1985).

[101] L. Hwa, J. Schroeder, and X. Zhao, "Intrinsic Brillouin linewidths and stimulated Brillouin gain coefficients in glasses studied by inelastic light scattering", *J. Opt. Soc. Am. B*, **6** 833 (1989).

[102] J. Schroeder, M. Fox-Bilmont, B. G. Pazol, V. Tsoukala, M. G. Drexhage, O. H. Elbayoumi, "Rayleigh and Brillouin scattering in heavy metal flouride glasses Intrinsic Rayleigh scattering", *Opt. Eng.*, **24**, 697 (1985).

[103] Y. Azuma, N. Shibata, T. Horiguchi, and M. Tateda, "Wavelength dependence of Brillouin gain spectra for single mode optical fibres", *Elect. Lett.*, **24**, 250 (1988).

[104] W. Heinicke, G. Winterling, "The temperature dependance of SBS in quartz", *Appl. Phys. Lett.*, **11**, 231 (1967).

[105] R. Vacher, J. Pelous, "Behaviour of thermal phonons in amorphous media from 4 to 300K", *Phys. Rev. B*, **14**, 823 (1976).

[106] Y. Aoki, S. Kishida, and K. Washio, "Stable cw backward Raman amplification by stimulated Brillouin scattering suppression ", *App. Opt.*, **25**, 1056 (1986).

[107] R. H. Stolen, and J. E. Bjorkholm, "Parametric amplification and frequency conversion in optical fibres ", *IEEE J. Quantum Electron.*, **18**, 1062 (1982).

[108] R. H. Stolen, M. A. Bosh, and C. Lin, "Phase matching in birefringent fibres" *Opt. Lett.*, **6**, 213 (1981).

[109] R. H. Stolen, and C. Lin, " Self-phase modulation in silica optical fibres ", *Phys. Rev. A.*, **17**, 1448 (1978).

[110] Silberberg,Y., and Bar-Joseph,I., "Optical instabilities in a non-linear Kerr medium", *J. Opt. Soc. Am. B.*, **1**, 662 (1984).

[111] T. .C. Rich, and D. A. Pinnow, "Evaluation of fibre optical waveguides using Brillouin spectroscopy", *Appl. Opt.*, **13**, 1376 (1974).

[112] R. Vacher, and L. Boyer, "Brillouin scattering: A tool for the measurement of elastic and photoelastic constants", *Phys. Rev. B*, **6**, 639 (1972).

[113] J. Schroeder, " Brillouin scattering and pockels coefficients in silicate glasses ", *J. Non-Crystalline Solids*, **40**, 549 (1980).

[114] N. Lagakos, J. A. Bucaro, and R. Hughes, "Acoustic sensitivity predictions of single mode optical fibres using Brillouin scattering", *Appl. Opt.*, **19**, 3668 (1980).

[115] B. Y. Zel'dovich, V. I. Popovichev, V. V. Ragul'skii, and F. S. Faisullov, "On the relationship between wavefronts of reflected and exciting light in stimulated Brillouin scattering", *JETP Lett.*, **15**, 109 (1972).

[116] D.A Rockwell, and C. R. Giuliano, "Coherent coupling of laser gain media using phase conjugation", *Opt. Lett.*, **11**, 147 (1986).

[117] M. Valley, G. Lombardi, and R. Aprahamian, "Beam combination by SBS", *J. Opt. Soc. Am. B*, **3**, 1492 (1986).

[118] T. Loree, D. Watkins, T. Johnson, N. Kurnit, and A. Fisher, "Phase locking two beams by means of seeded Brillouin scattering", *Opt. Lett.*, **12**, 178 (1987).

[119] Dolgopolov, "Experimental investigation of the feasability of application of the wavefront reversal phenomenon in SMBS", *Sov. Phys.JETP*, **49**, 458 (1979).

[120] N. A. Olsson, and J. P. van der Ziel, "Cancellation of fibre loss by semiconductor laser pumped Brillouin amplification at 1.5μm", *Appl. Phys. Lett.*, **48**, 1329 (1986).

[121] C. G. Atkins, D. Cotter, D. W. Smith, and R. Wyatt, "Application of Brillouin amplification in coherent optical transmission", *Elect. Lett.*, **22**, 556 (1986).

[122] A. R. Charaplyvy and R. W. Tkach, "Narrowband tunable optical filter for channel selection in densely packed WDM systems", *Elect. Lett.*, **22**, 1084 (1986).

[123] N. A. Olsson, and J. P. van der Ziel, "Charecteristics of a semiconductor laser pumped Brillouin amplifier with electronically controlled bandwidth", *J. Lightwave Technol.*, **LT-5**, 147 (1987).

[124] R. V. Johnson, and J. H. Marburger, "Relaxation oscillations in stimulated Raman and Brillouin scattering", *Phys. Rev. A*, **4**, 1175 (1971).

[125] I. Bar-Joseph, A. A. Friesem, E. Lichtman, and R. G. Waarts, "Steady and relaxation oscillations of SBS in single mode optical fibers", *J. Opt. Soc. Am. B*, **10**, 1606 (1985).

[126] D. T. Hon, "Pulse compression by SBS", *Opt. Lett.*, **5**, 516 (1980).

[127] G. B. Hocker, "Fibre optic acoustic sensors with composite structure: an analysis", *Appl. Opt.*, **18**, 3679 (1979).

[128] L. F. Stokes, M. Chodorow, and H. J. Shaw, "All-fibre stimulated Brillouin ring laser with submilliwatt pump threshold", *Opt. Lett.*, **7**, 509 (1982).

[129] Personal communication - Louis Poyntz Wright, Southampton University.

[130] P. Andreatch, and H. J. McSkimin, "Pressure dependence of ultrasonic wave velocities and elastic stiffness moduli for a TiO_2-SiO_2 glass (Corning 7971)", *J. Appl. Phys.*, **47**, 1299 (1976).

[131] C.K.Jen, and J. E. B. Oliveira, "Backward collinear acousto-optic interactions", Proc. Society of Photo-Instrumental Engineers, SPIE Laser Applications, (Boston, USA), 987-22 (1988).

[132] C. K. Jen and N. Goto, "Backward collinear guided wave acousto optic interactions in single mode fibres", *J. Lightwave Technol.*, **LT-7**, 2018 (1989).

[133] N. Shibata, R.Waarts, and R.Braun, "Brillouin gain spectra for single mode fibres having pure silica, GeO_2-doped, and P_2O_5-doped cores", *Opt. Lett.*, **12**, 269 (1987).

[134] D. Gloge, "Weakly guiding fibres", *Appl. Opt.*, **10**, 2252 (1971).

[135] M. D. Levenson, R. M. Shelby, A. Aspect, M. Ried and D. F. Walls, "Generation and detection of squeezed states of light by nondegenerate four wave mixing in an optical fibre", *Phys. Rev. A.*, **32**, 1550 (1985).

[136] R. M. Shelby, M. D. Levenson and S. H. Perlmutter, "Bistability and other effects in a nonlinear fibre optic ring resonator", *J. Opt. Soc. Am. B.*, **5**, 347 (1988).

[137] D. Heinman, D. S. Hamilton and R. Hellwarth, "Brillouin scattering measure on optical glasses, *Phys. Rev. B.*, **12**, 6583 (1979).

[138] G. Sagnac, "L'ether lumineux demontre par l'effet du vent relatif d'ether dans un interferometre en rotation uniforme", *C. R. Acad. Sci.*, **95**, 708 (1913).

[139] E. J. Post, "Sagnac effect", *Rev. Mod. Phys.*, **39**, 475 (1967).

[140] J.R.Wilkinson, "*Ring Lasers*", Publ. Pergamon Press Ltd., 1987

[141] R.A. Patterson, B. Ljung, and D. A. Smith, *Proc.* Society of Photo-Instrumental Engineers, SPIE, **487**, 78 (1984).

[142] F. Aronowitz, in "*Laser Applications*", edited by M. Ross, Publ. Academic Press, New York, 113-200 (1971).

[143] W. Chow, J. Gea-Banacloche, L. Pedrotti, V. Sanders, W. Schleich, M. Scully, "The ring laser gyro", *Rev. Mod. Phys.*, **57**, 61 (1985).

[144] F. Aronowitz, in "*Laser Inertial Rotation Sensors*", edited by S. Ezekiel and G. Knausenberger, Society of Photo-Instrumental Engineers, SPIE, 1978.

[145] W. Chow, Proc. Society of Photo-Instrumental Engineers, SPIE **487**, 30 (1984).

[146] J. Killpatrick, "The GG1308 ring laser gyroscope", *Gyroscope Symposium*, Stuttgart, Germany (1989).

[147] Honeywell has been selected to manufacture a fibre gyro based AHRS for the Dornier 328 program in Germany.

[148] H. C. Lefevre, "Evolution of the fibre optic gyroscope", Proc. Proc. Optical Fibre Sensors, OFS-89, Paris, France, Sept. 18-20, 1989. Editors H. J. Arditty, J. P. Dakin, and R. Th. Kersten, Publishers Springer-Verlag.

[149] D. M. Shupe, "Thermally induced nonreciprocity in the fibre optic interferometer", *Appl. Opt.*, **19**, 654 (1980).

[150] K. Hotate and K. Tabe, "Drift of an optical fibre gyroscope caused by the Faraday effect: influence of the Earth's magnetic field", *Appl. Opt.*, **25**, 1086 (1986).

[151] K. Hotate and K. Tabe, "Drift of an optical fibre gyroscope caused by the Faraday effect: Experiment", *J. Lightwave Technol.*, **LT-5**, 997 (1987).

[152] S. Ezekiel, J. L. Davis, and R. W. Hellwarth, "Observation of intensity induced nonreciprocity in a fibre optic gyroscope", *Opt. Lett.*, **7**, 457 (1982).

[153] C. C. Cutler, S. A. Newton, and H. J. Shaw, "Limitation of rotation sensing by scattering", *Opt. Lett.*, **5**, 488 (1980).

[154] P. R. Morkel, "Erbium doped fibre superfluorescent source for the fibre gyroscope", Proc. Optical Fibre Sensors, OFS-89, Paris, France, Sept. 18-20, 1989. Editors H. J. Arditty, J. P. Dakin, and R. Th. Kersten, Publishers Springer-Verlag.

[155] F. Zarenetchi, and S. Ezekiel, "Observation of lock-in behaviour in a passive resonator gyroscope", *Opt. Lett.*, **11**, 401 (1986).

[156] K. Iwatsuki, K. Hotate, and M. Higashiguchi, "Kerr effect in an optical passive ring resonator gyro", *J. Lightwave Technol.*, **LT-4**, 645 (1986).

[157] A. E. Kaplan, and P. Meystre, "Enhancement of the Sagnac effetct due to nonlinearly induced nonreciprocity", *Opt. Lett.*, **6**, 590 (1981).

[158] K. Iwatsuki, K. Hotate, and M. Higashiguchi, "Effect of Rayleigh backscattering in an optical passive ring resonator gyro", *Appl. Opt.*, **23**, 3916 (1984).

[159] M. Takahashi, S. Tai, and K. Kyuma, "Effect of reflections on the drift charecteristic of a fibre optic passive ring resonator gyroscope", *J. Lightwave Technol.*, **LT-8**, 811 (1990).

[160] B. S. Gorovaya et. al., *Sov. J. Quantum Electron.*, **7**, 521 (1971).

[161] M. Nakazawa, "Synchronously pumped fibre Raman gyroscope", *Opt. Lett.*, **10**, 193 (1985).

[162] V. Vali and R. W. Shorthill, "Stimulated Brillouin scattering ring laser gyroscope", *U.S. Patent No.* 4159178, 1976.

[163] P. J. Thomas, H. M. van Driel, and G. I. A. Stegeman, "Possibility of using an optical fibre Brillouin ring laser for inertial sensing", *Appl. Opt.*, **19**, 1906 (1980).

[164] P. J. Thomas, N. L. Rowell, H. M. van Driel, and G. I. Stegeman, "Normal acoustic modes and Brillouin scattering in single mode optical fibres", *Phys. Rev. B.*, **19**, 4986 (1979).

[165] I. McMicheal, P.Beckwith and P. Yeh, "Phase conjugated multi-mode fibre gyro", *Opt. Lett.*, **12**, 1023 (1987).

LIST OF PUBLICATIONS

The following is a chronological list of my publications,

[1] I. P. Giles, M. Farhadiroushan, A. Kerr, M. N. Zervas, and R. Kadiwar, "Polarisation maintaining optical fibre components for advanced sensor systems", EFOC/LAN-88, Amsterdam, The Netherlands, June 29-July 1, 1988

[2] R. Kadiwar, P. Bayvel, I. P. Giles, "Stimulated Brillouin Scattering in polarisation maintaining ring resonators", *Proc*. Society of Photo-Instumental Engineers, SPIE, Fibre Optics & Lasers, **985**, Boston, USA, (1988).

[3] P. Bayvel, J. Halley, R. Kadiwar, and I. P. Giles, "Theoretical and experimental investigation of all fibre single mode Brillouin lasers", *IEE* European Conference On Communications, ECOC-88, Brighton, UK, Sept. 11-15 1988.

[4] R. Kadiwar, I. P. Giles, "Effects of stimulated Brillouin scattering on the performance of polarisation maintaining fibre ring resonators", *Opt. Lett* ., **14**, 332 (1989).

[5] Z. Ioannidis, R. Kadiwar, and I. P. Giles, "Polarisation mode coupling in high birefringence optical fibre ring resonators", *Opt. Lett.*, **14**, 520 (1989).

[6] Z. Ioannidis, R. Kadiwar, and I. P. Giles, "Polarisation effects in highly birefringent fibre ring resonators", Proc. Optical Fibre Sensors, OFS-89, Paris, France, Sept. 18-20, 1989. Editors H. J. Arditty, J. P. Dakin, and R. Th. Kersten, Publishers Springer-Verlag.

[7] I. P. Giles, R. Kadiwar, and Z. Ioannidis, "Stimulated Brillouin scattering in polarisation maintaining all fibre ring resonators",*IEE* European Fibre Optic Communications and Local Area Networks symposium, EFOC/LAN-89, Amsterdam, The Netherlands, 1989

[8] R. Kadiwar, I. P. Giles, "Optical fibre Brillouin ring laser gyroscope", *Elect. Lett* ., **25**, 1729 (1989).

[1] To clarify the argument at the bottom of p40 we note that: In York Bow-Tie fibres, the core geometry leads to the elliptical shape of the output, but it is the refractive index difference between the fast and slow axes that leads to the different mode confinements and hence different core intensities for linearly polarised light launched along the fast or slow axes.

[2] The analysis of guided acoustic waves in optical fibres presented in §4.3 (pp.88-91), follows that presented by Jen, *et. al.*[132]. It is based upon the approximation that for weakly guiding acoustic waveguides the mathematical form of the dispersion equation for the *lowest* order longitudinal acoustic modes $L_{0,m}$ is identical to that of the *lowest* order linearly polarised ($LP_{0,m}$) optical modes, of weakly guiding optical waveguides. It is erroneously stated, both in a recent paper by Jen[166] and in the text of this thesis (p89) that in general the acoustic $L_{n,m}$modes have the same form as the optical $LP_{n,m}$ modes. In fact the general dispersion equation for the acoustic $L_{n,m}$ modes is given by,

$$\frac{UJ_n'(U)}{J_n(U)} - \frac{WK_n'(W)}{K_n(W)} = 0 \qquad \text{A.1}$$

where

$$UJ_n'(U) = UJ_{n-1}(U) - nJ_n(U) \qquad \text{A.2}$$

$$WK_n'(W) = -WK_{n-1}(W) - nK_n(W) \qquad \text{A.3}$$

This clearly reduces to a form similar to that of LP modes only for n=0. As the acoustic $L_{0,m}$ modes were the only ones plotted in fig.4.14, the results of that plot are still valid.

Arguments based upon the use of EM wave analogies to acoustic waves can be quite misleading. The particle displacement function used to derive the guided acoustic wave equation is expressed in terms of both a scalar and a vector potential, which when decoupled describe the propogation of longitudinal and shear waves respectively in the medium. In general however the longitudinal and shear waves couple when reflected from an interface between different media. The difficulty then arises that in acoustics only 3 of the elastic field components are independent, whereas in optics only 2 of the electromagnetic field components are independent. As a consequence only those acoustic waves described by the decoupled vector wave equation (eg the torsional and radial-axial shear waves) have direct EM wave analogies (TE and TM waves respectively). The particle displacements of these acoustic waves are identical in form to the polarisation of the optical modes. However, the similarity between the dispersion equations for the lowest order acoustic longitudinal waves (which involves the use of the scalar potential of the particle displacement function) and the lowest order linearly polarised optical waves *does not* imply that the longitudinal acoustic waves are linearly polarised (which would ofcourse be an obvious contradiction!).

[166] C. Jen, J. Oliveira, N. Goto, K. Abe, "Role of guided acoustic waves in single mode optical fibre design", *Electron Lett.*,**24**, 1419 (1988).